CHARACTERIZATION, MODELING AND DYNAMIC IMPLEMENTATION OF TERFENOL-D PARTICULATE COMPOSITES

A Thesis

Presented in Partial Fulfillment of the Requirements for

the Degree Master of Science in the

Graduate School of The Ohio State University

By

Anthony Mortensen, B.S.

* * * * *

The Ohio State University

2005

Master's Examination Committee:

Dr. Marcelo J. Dapino, Adviser

Dr. Mark E. Walter

Approved by

Adviser

Graduate Program in

Mechanical Engineering

ABSTRACT

The combination of smart materials with a binder to form composites has been investigated for the possibility of improving performance and functionality. This thesis examined the combination of Terfenol-D, ball-milled powder to a soft epoxy vinyl ester resin with the particles magnetically aligned during casting. These composites were characterized with quasistatic testing to measure strain, induction, and magnetization as a function of magnetic field for volume fractions of less than 10% and a 50% rod. The later rod was applied to a hybrid Terfenol-D/PMN-PT Tonpilz broadband transducer originally designed to operate from excitation of a monolithic Terfenol-D rod and an electrostrictive PMN-PT stack, that was characterized in a previous project [12]. In a previous study this hybrid design successfully extended the bandwidth to a lower frequency compared to a single element, and a composite rod was tested for dynamic performance in the same transducer. The impedance and head velocity was measured for the transducer with varying magnetic bias, dynamic magnetic field, composite preload and for two different magnetic circuit designs. The composite extended the bandwidth but the response was much less than achieved with a monolithic rod in the previous study. A linear model to describe the system was developed from classical mechanical vibrations to characterize the physical response, electroacoustics theory of transduction to couple the electrical and mechanical regimes, and the linear constitutive relations for piezomagnetic and piezoelectric material justified by operating the material within a biased, low signal range. The model determined the impedance of each active element, the head mass velocity, and was capable of finding material properties from the dynamic electrical impedance data. A clear resonance

of the composite impedance could not be measured while loaded in the transducer to obtain properties dynamically. Properties from static testing of the composite were utilized in the model which describes the data well after making some justifiable modifications.

To my late grandmother, Pearl Brookhart

ACKNOWLEDGMENTS

I would like to thank my advisor, Dr. Marcelo J. Dapino, for his support, guidance and insight throughout this project. Without his advice and patient editing, this thesis would not be possible. I would also like to thank the other half of my defense committee, Dr. Mark E. Walter, for listening to my project and for his support with testing throughout the year.

The project required fabrication, so Gary Gardner and Keith Rogers were very helpful in times of immediate need. Joe West provided help with miscellaneous electrical issues throughout the project. A huge thanks to David Nosse for moral support and an infinite amount of ideas (*a few good*) for the duration of the project. LeAnn Faidley and Aayush Malla taught me almost everything I know about the lab that i didn't have to learn on my own.

My family was very supportive throughout my education along with all my friends. I would like to thank my previous education from the University of Pittsburgh at Johnstown and all of the professors that helped me get to Ohio: Jerry Samples, James Bandstra, Gregory Dick, Robert Martinazzi, and Professor Malmgren.

VITA

November 17, 1980	Born - Harrisburg, PA
May 2003	B.S. Mechanical Engineering Tech., University of Pittsburgh at Johnstown
2003-present	Graduate Research Assistant, Ohio State University

PUBLICATIONS

Proceedings Publications

A.P. Mortensen, M.J. Dapino, "Hybrid polymer matrix Terfenol-D composite/PMN-PT transducer in mechancial series configuration". *Proceedings of SPIE Smart Structures and Materials*, Paper # 5761-91, San Diego, Ca, March 2005.

FIELDS OF STUDY

Major Field: Mechanical Engineering

Studies in Smart Materials and Structures: Dr. Marcelo J. Dapino

TABLE OF CONTENTS

Page

LIST OF TABLES

LIST OF FIGURES

Figure **Page**

CHAPTER 1

INTRODUCTION

The evolution of technology creates a continual need for more advanced sensors capable of higher efficiencies, more bandwidth, greater motion and robustness. Smart materials have made a lot of these advances possible over the past few decades. Smart materials exhibit a characterizable change in physical properties and macroscopic response when activated by an electrical field, magnetic field, stress, or heat. In this thesis the use of magnetostrictive particle composites to improve various limitations of monolithic material will be examined, along with the use of multiple smart materials to achieve enhanced velocity response in a broadband underwater transducer. To place the research in context, an overview of magnetism, magnetic properties, and magnetostriction is presented below. In Chapter 2 the design of a mold with a magnetic circuit and the fabrication of a soft epoxy magnetostrictive composite is examined. A dynamic model to characterize complex smart material systems is presented in Chapter 3. Design and testing of a a broadband hybrid magnetostrictive/electrostrictive transducer is discussed in Chapter 4. Results from the quasistatic testing of Terfenol-D particle composites, dynamic response of a composite in the hybrid transducer, and correlation of the model to the dynamic data is presented in Chapter 5. Chapter 6 finishes with the conclusions and future work of this project.

1.1 Principles of Magnetics

1.1.1 Magnetic Field and Magnetic Induction

A magnetic field is one of the primary concepts of magnetics and produced by the motion of an electric charge across a current carrying conductor as shown in Fig 1.1. A permanent magnet also produces a field from the orbital motions and spins of electrons within the material. A force on current carrying conductors and permanent magnets is produced by a magnetic field and is the principle of operation that allow electric motors to do work. The strength of a magnetic field H is often defined in units of Amperes per meter where a current of 1 ampere traveling through a straight 1 meter conductor produces a field of $\pi/4$ A/m at a radial distance of 1 meter [19]. In a medium, a magnetic field creates a response or magnetic induction B.

The presence of a magnetic field creates a magnetic flux that is capable of aligning iron filings along the flux path. Magnetic flux is measured in Weber, where 1 Weber is the amount of flux that when reduced to zero in one second produces and electro magnetic field of one volt across a one turn conductor coil that the flux passes through. Magnetic induction is also known as flux density and can be defined in units of Weber per meter square, where one Weber/m^2 is equal to 1 Tesla. The Tesla is defined such that the induction of one tesla generates a force of 1 Newton per meter on a conductor carrying a current of 1 ampere perpendicular to the direction of induction.

Magnetic induction and magnetic field are related by the permeability μ of the material, which is the slope of the induction plotted against the field. In non magnetic materials such as air, the magnetic field and induction are linearly proportional to each other. In free space this relation is

$$B = \mu_0 H \tag{1.1}$$

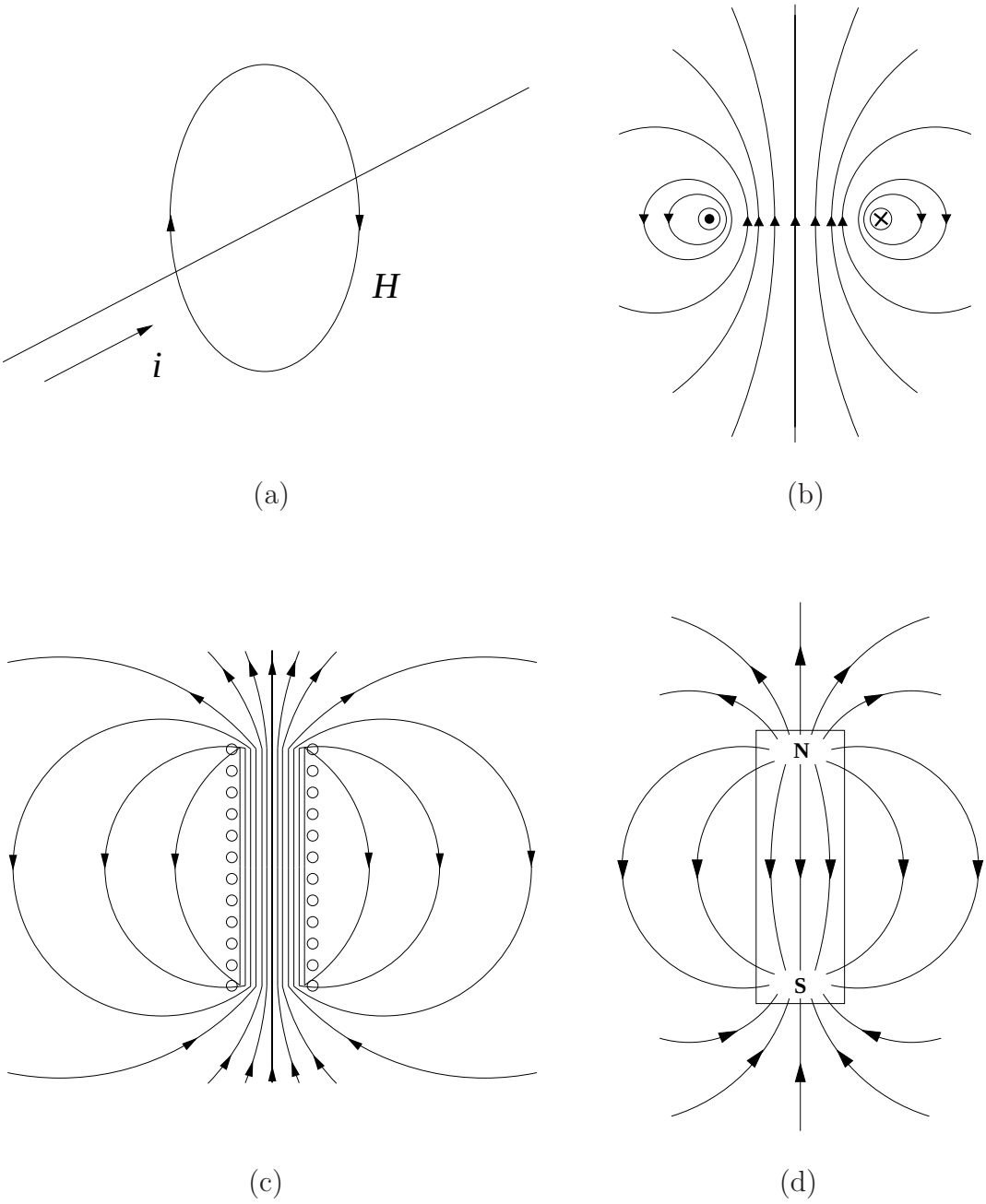

Figure 1.1: Magnetic field lines induced by: (a) single straight line conductor, (b) single wire loop, (c) a solenoid composed of many loops, and (d) a permanent bar magnet. [12]

where μ_0 is a universal constant of the permeability of free space. The units of H will be A/m in this paper and induction will be in Tesla (Vs/m^2). From these, the units for μ are volt second/amp meter or henries/meter with a value of 4πx10^{-7} H/m for μ_0 [19]. In ferromagnetic material, μ is not a constant and varies greatly depending on the field intensity.

A change in flux induces an e.m.f. in a circuit by electromagnetic induction, described by Faraday and Lenz laws. Faraday's law states that the voltage induced in an electrical circuit is proportional to the rate of change of magnetic flux linking the circuit. Lenz's law states that the induced voltage is in a direction which opposes the flux change producing it. This enables an electric circuit to measure the magnetic flux ϕ of a system. The voltage induced is given by

$$V = \frac{-Nd\phi}{dt} \tag{1.2}$$

where N is the number of turns of the coil and $d\phi/dt$ is the rate of change of flux flowing through the coil. Magnetic induction is defined as the flux density

$$B = \frac{\phi}{A} \tag{1.3}$$

so the induced voltage can now be written as

$$V = \frac{-NAdB}{dt} \tag{1.4}$$

This is the principle that generators use to create electricity. A conducting coil placed around ferromagnetic material allow the measurement of induction by integrating the induced voltage.

1.1.2 Magnetization

The magnetization of a material contributes to the total induction, from the existence of magnetic moments m generated by electron motion at the atomic level [19]. A torque τ is created as the magnetic moment tries to align with an external magnetic induction, allowing the moment to be calculated as

$$m = \frac{\tau_{max}}{B}. \tag{1.5}$$

This torque creates the force that causes opposite poles of a magnet or magnetic field to attract and aligns a compass needles with the earth's magnetic field. The magnetization of a material is defined as the magnetic moment per unit volume

$$M = \frac{m}{V}. \tag{1.6}$$

The magnetic induction arises from a magnetic field, and the magnetization as represented by the vector sum of the two

$$B = \mu_0(H + M) \tag{1.7}$$

where B is in Tesla, with H and M in amperes per meter. The field is generated by an external source such as a permanent magnet or a wound coil, while the magnetization is generated by the spin and orbital angular momenta of electrons within the material. Technical saturation M_s is achieved when all dipoles within a medium are aligned with the magnetic field. Higher magnetic fields will slowly increase the magnetization by increasing the alignment within the dipoles, which are not perfectly aligned due to thermal activation.

Magnetic materials are usually classified by the values of their permeability and susceptibility of which are often not linear for magnetic materials. The permeability is defined

as

$$\mu = \frac{B}{H} \tag{1.8}$$

and the susceptibility is defined as

$$\chi = \frac{M}{H}. \tag{1.9}$$

Another useful property that is often used to describe magnetic materials is the relative permeability

$$\mu_r = \frac{\mu}{\mu_0}. \tag{1.10}$$

The relative permeability of free space is always 1 and related to the susceptibility by

$$\mu_r = \chi + 1. \tag{1.11}$$

1.1.3 Magnetization Curve

Measuring the induction while cycling a magnetic field from positive to negative saturation of a material will record what is referred to as a hysteresis loop or BH curve, as shown in Fig. 1.2. Most technical properties can be obtained from this graph. The curve demonstrates hysteresis or energy loss, which means that B is not a single valued function of H. Reducing the field to zero after the material is saturated will reach the point of remanence induction B_r. The field is decreased from zero until the induction reaches coercive field $-H_c$. Cycling the material to negative saturation and increasing the field will cross a corresponding point for $-B_r$ and H_c after the induction has returned to zero.

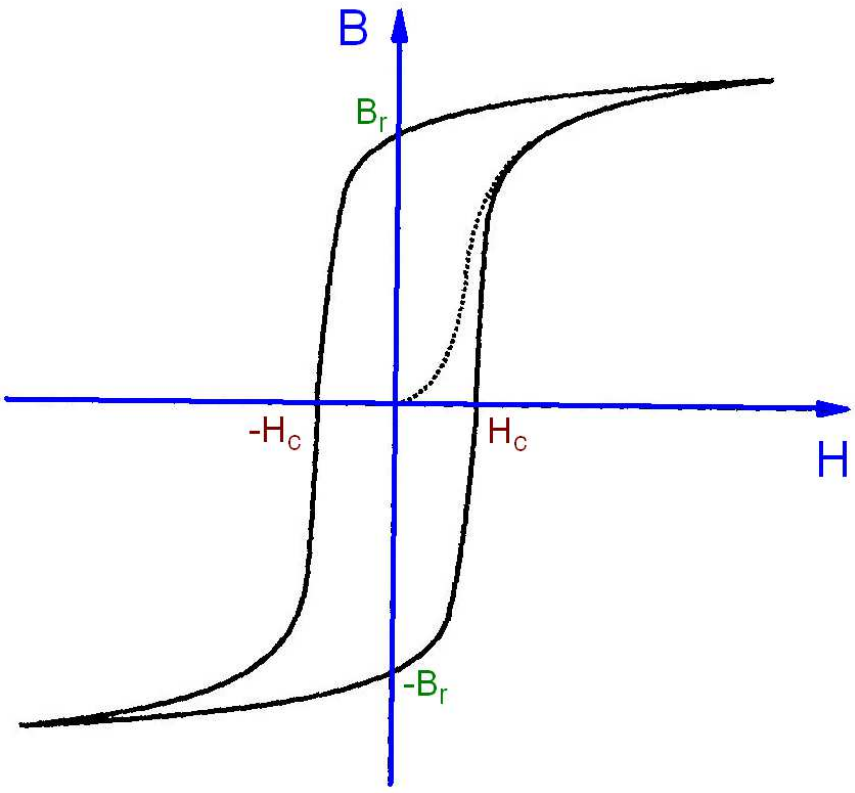

Figure 1.2: A typical BH curve for a magnetic material showing the coercive points and the remanence points. The dotted line is the approximate path for a material starting at zero induction and field [20].

1.1.4 Magnetic Materials

The class of magnetic materials of most interest in this study is ferromagnetics [19]. Paramagnetic and diamagnetic materials are two other types, but due to their limited applications are of little interest. Diamagnets such as copper and gold have relative permeabilites of slightly less than unity, while paramagnets such as aluminum and manganese have permeabilites of slightly more than unity. These materials can be effectively treated as air or free space for most calculations. Ferromagnetic materials have μ_r values ranging from as low as 4-5 for monolithic Terfenol-D to as high as 200,000 for iron. Properties for paramagnetic, diamagnetic, and ferromagnetic material are presented in Table 1.1, to

demonstrate the vast difference between what is normally referred to as magnetic and non magnetic materials. Note the permeability of Terfenol-D, introduced in Sec. 1.2.3, is low compared to other ferroelectric material but several times that of non ferromagnetic materials. Ferromagnetic materials retain magnetization after a magnetic field is removed while paramagnetic materials do not. Ferromagnetic materials experience hysteresis when cycled through a magnetic field, characterized by a lag in material response, as shown in Fig. 1.2. The unusual shape of the response can be explained by looking at the domains of the material at the crystal level.

Class	Material	χ	μ_r
Diamagnets	Cu	$-0.77x10^{-6}$	0.99999
	Ag	$-2.02x10^{-6}$	0.99997
Paramagnets	Al	$1.65x10^{-6}$	1.00002
	β-Sn	$0.19x10^{-6}$	1.00000
	Mn	$66.1x10^{-6}$	1.00083
Ferromagnets	Fe	-	10,000-200,000
	Ni	-	50-150
	Co	-	400-1200
	Terfenol-D	-	4-5

Table 1.1: Susceptibility and relative permeability of different types of magnetic materials [20, 19].

In magnetic materials, the magnetic moments group together to form domains where all the moments are in the same direction, thus minimizing the potential energy. The domains can complete a flux path within a material at the surfaces which creates a lower energy state. The application of a magnetic field causes the domains to rotate and preferentially oriented domains to grow [19]. The domain processes describe the unique response of magnetic materials to both applied fields and stress.

Consider a material that has not been cycled through a magnetic field as shown in Fig. 1.3. The domains are randomly oriented without an applied field and have no net induction. Application of a low field causes domains to grow that are oriented in the direction of the field. Increasing the field causes all of the domains to align along a preferred orientation within the material that is in the orientation nearest to the field direction. A large field rotates the domains until they are in the same direction as the field. A material will reach technical saturation when all of the domains are oriented parallel to the magnetic field essentially producing one domain. Further magnetization is possible to a small extent at higher fields. This is due to the individual magnetic moments within a domain continuing to align with the field, which are not perfectly oriented due to thermal energy.

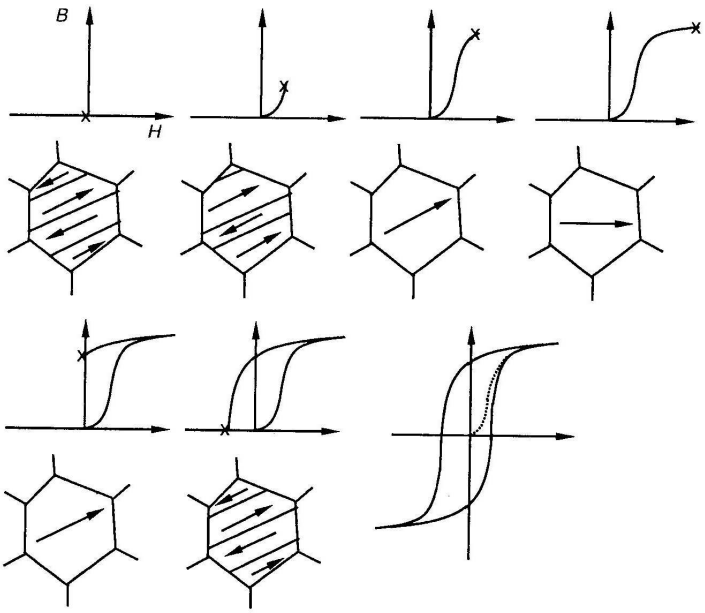

Figure 1.3: Domain growth and motion induced by an applied magnetic field [20].

The boundary between two domains can be thought of as a continually variable wall of finite thickness that gradually transitions between directions of the domains, as shown

in Fig. 1.4. The application of a small field will cause a wall to move increasing the size of the domain in the direction of the field. In a perfect specimen free of irregularities and impurities the domain wall would move in a continual wave, but in real materials the walls move until they reach a pinning site caused by an impurity or void in the material. The domain wall will begin to bend around the pinning site until there is enough energy to cause it to jump to the next pinning site, causing domain wall motion to be a series of small jumps within a material and creating an irreversible energy loss.

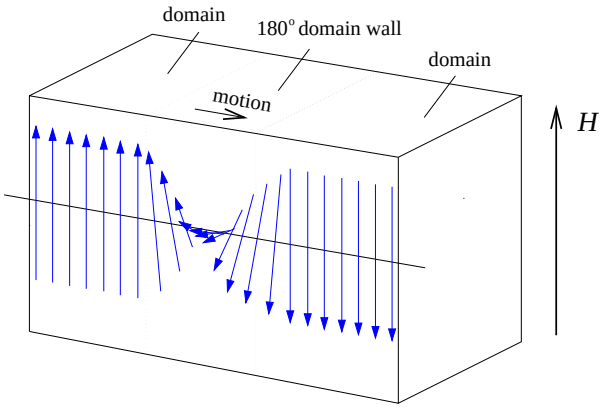

Figure 1.4: A domain wall can be considered as a wave of finite thickness that separates domains [19].

1.2 Magnetostriction

1.2.1 History

Magnetostriction was first studied by James Prescott Joule in the 1840s [8] when he measured the strain in iron resulting from the application of a magnetic field, and the volume change associated with the deformations, concluding that magnetostriction is a constant volume process. In the 1860s Villari experimented with iron wires placed in tension and discovered permeability is strongly effected by stress along the axis of applied

field. Villari discovered iron increases permeability with the application of tension until reaching a certain point at which further tension causes the permeability to decrease. Magnetostriction without significant volume change is named Joule magnetostriction and the effect of permeability reversal is named the Villari effect, in honor of these men. Nagaoka and Honda were able to measure a change in volume during magnetization using a highly refined fluid bath and graduated capillary tube in 1898. They noticed that a change in elasticity occurs upon application of a magnetic field in ferromagnetic material. Honda published the first thorough study of this phenomenon in 1902 for iron, steel, nickel and cobalt.

1.2.2 Magnetostrictive Process

Most magnetic materials undergo a strain when a magnetic field is applied, which is referred to as magnetostriction and denoted as λ. Spontaneous magnetostriction is caused by the ordering of the material into domains as the temperature is decreased below the curie temperature, but this effect is of little use in applications [8]. In this study we are interested in the field induced magnetostriction, which arises from the application of a magnetic field to a magnetostrictive material at temperatures below the curie temperature. A generalized way of thinking of this process can be understood by considering the material as spheres while above the curie temperature. The spheres transform into randomly oriented domains in the shape of ellipsoids below the curie temperature. This is where the spontaneous magnetostrictions occurs as illustrated in Fig. 1.5. When a field is applied, the domains align themselves in the direction of the field, creating the field induced magnetostriction. A material will achieve technical saturation when all of the domains are aligned in the same direction forming a single domain oriented sample. Forced magnetostriction is the slow increase in strain occurring from application of magnetic fields above the saturating field. This is a highly temperature dependent phenomenon caused by the increased ordering of

magnetic moments within the domain. This magnetostriction occurs at a high field and is of little use in practical applications.

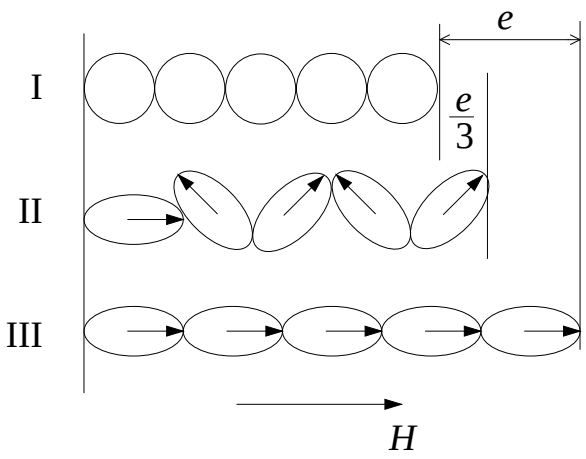

Figure 1.5: Visualization of magnetostriction (a) above the curie temperature, (b) below the curie temperature with no field, and (c) application of a magnetic field. [8].

1.2.3 Terfenol-D

Pure metals achieve low magnetostriction, but it was discovered that combinations of rare earth metals could achieve high magnetostriction at certain temperatures. In the 1970's, a material combination was discovered that could provide high magnetostriction at room temperatures. This material is named Terfenol-D ($Tb_xDy_{1-x}Fe_y$ after the materials and founding laboratory (Terbium **Ter**, Iron **Fe**, Naval Ordnance Laboratory **NOL**, Dysprosium **D**) [8]. Terfenol-D is currently available in thin films, monolithic material, and powder. The manufacturing of Terfenol-D requires high quality materials, carefully controlled crystal growth, heat treating and magnetic annealing, its price in some cases higher than other active materials.

Terfenol-D exhibits a cubic crystal structure, as seen in Fig. 1.6. Current manufacturing methods produce monolithic Terfenol-D rods, such that the rod axis corresponds to the

[112] direction which can achieve λ_{112}=1200 ppm. The [111] direction provides the highest magnetostriction λ_{111}=1640 ppm while only λ_{100}=90 ppm [26].

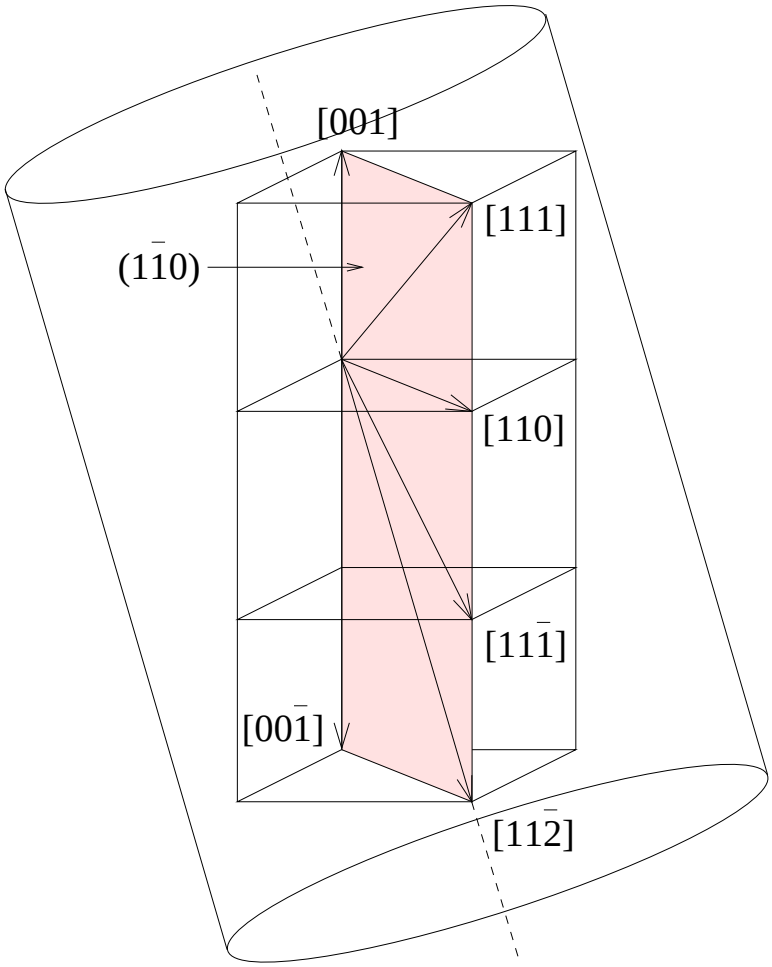

Figure 1.6: Crystal structure of monolithic Terfenol-D.

Terfenol-D requires a prestress for maximum performance. The application of a prestress causes a jump in magnetostriction at low fields, and can be explained by looking at the magnetic domains within the material. The domains can be oriented in 8 possible directions within the crystal. Applying a field will cause the more energetically favorable domains to grow at the expense of the less favorable directions. In Terfenol-D the easy axis

family is [111], which means the magnetization causes rotations of 71, 109, and 180 degrees. The domains oriented along the direction of applied field are considered 180 degree domains, and the rotation will cause a change in magnetization but not magnetostriction. The other domains are non 180 degree domains, causing a change in magnetostriction and magnetization. Application of a stress in compression increases the number of non 180 degree domains, which make it possible for a higher maximum magnetostriction. A comparison of magnetostriction for of Terfenol-D to other ferromagnetic material is presented in Table 1.2.

Material	$\lambda_{100}(10^{-6})$	$\lambda_{111}(10^{-6})$
Iron	21	-21
Nickel	-46	-24
Terfenol-D	90	1600

Table 1.2: Magnetostriction for common cubic materials [19].

There are three characteristic regions of magnetostriction in Terfenol-D, as demonstrated in Fig. 1.7. At low magnetic fields, there is little deformation due to the rotation of mostly 180 degree domains, which require the least amount of energy to rotate. Magnetostriction at this region is mostly domain wall motion or the growth of favorably aligned domains. The second region is characterized by a rapid increase in magnetostriction caused by the non 180 degree domains rotating to more energetically favorable directions. The third region shows a slow increase in magnetostriction from the forced rotation of less energetically favorable 180 degree domains and an increase in distance between atoms [9].

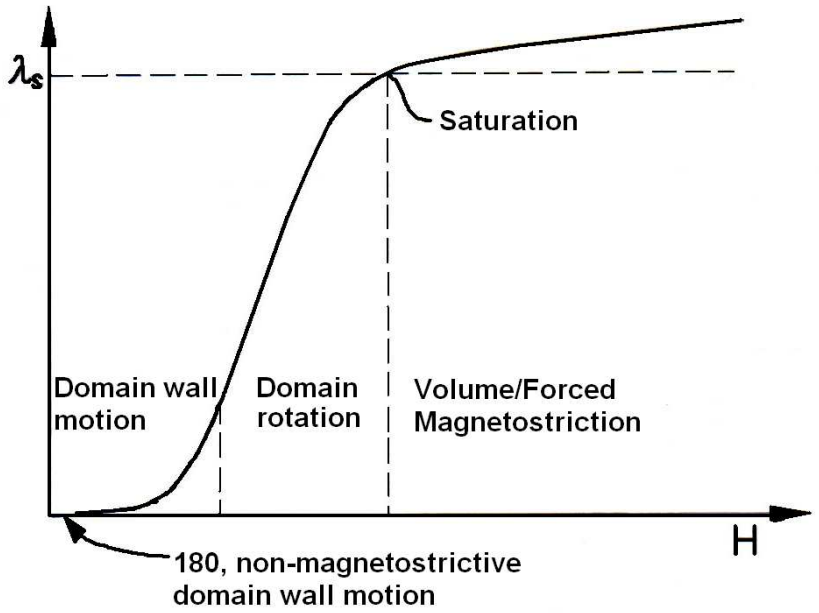

Figure 1.7: Magnetostriction as a function of magnetic field with the mechanisms dominating the response in the particular region [9].

1.3 Magnetostrictive Composites

It is generally believed that composites with high volume fractions of Terfenol-D powder were explored as early as the 1980's, but Sandlund [22] was the first to publish results in 1994, investigating (0-3) and (1-3) architecture. Testing included the measurement of the modulus of elasticity for constant magnetic field and constant flux conditions with the corresponding coupling coefficients calculated. This was the first published measurement of giant magnetostrictive composite properties and inspired further studies of similar materials. The (0-3) condition is equivalent to randomly oriented and distributed particles which approaches a constant stress condition. The (1-3) configuration is achieved by aligning the particles in a magnetic field, that creates chains of Terfenol-D within the composite matrix and is similar to a constant strain condition. Sandlund tested high volume fraction composites and reported results for magnetostriction, magnetization, and elastic modulus.

It proved that high magnetostriction could be achieved while greatly reducing the conductivity, while the aligned specimens achieved improved magnetostriction and coupling. The improvement in the aligned specimens is attributed to the preferred crystal orientation of the particles along the easy axis. Low volume fraction (1-3) composites were explored by Duenas and Carman [30, 13, 14], who observed that by curing composites at an elevated temperature a prestress will develop from the difference in thermal expansions of the materials after cooling. They concluded that a volume fraction of 20% yields the highest magnetostriction without a preload, measuring 900 ppm with no load and 1000 ppm with a compressive stress of 4-8 MPa.

Ruiz de Angulo performed dynamic measurements to calculate the coupling coefficient and discovered a large reduction from the coupling of monolithic material that was later confirmed by Hudson [21, 17]. Ruiz noticed the coupling is independent of bias field by performing tests from 18-120 kA/m while measuring the resonance and antiresonance, which both decrease with increasing magnetic bias. The low coupling coefficient of magnetostrictive composites is undesirable for actuators but is beneficial for damping applications, as explored by McKnight and Carman [25]. McKnight cycled composite specimens through tension and compression to measure the tan delta of the material. He discovering that high stress amplitudes reduced the energy absorption and the volume fraction have little effect on the damping, which may be attributed to the pre-stress mechanism from the curing process.

Armstrong developed a model for composites that successfully models some of the nonlinear properties of the materials [1]. The model successful predicts the nonlinear effects of an applied stress to the magnetostrictive behavior, the different effects of unaligned and aligned particles, and even variations between spherical and elongated particles. The model also captures the highly nonlinear behavior of monolithic Terfenol-D, including the interactions of stress, crystal structure, and magnetic field.

Composites have been extensively investigated in terms of binder materials, manufacturing methods, composite geometry, and modeling due to the various benefits and wide range of achievable properties. Design and testing of laminates has been investigated, but the process greatly increases the cost and complexity of a system. Recently composite research has been extended to ferromagnetic shape memory alloys for a new potential level of actuators and damping applications.

Terfenol-D produces large magnetostriction at room temperature with moderate fields but it has some limiting features such as brittleness and hysteresis loss at high frequencies. The material is solid and conductive in monolithic form allowing eddy currents to develop within the rod. The eddy currents represent energy loss, as shown in Fig 1.2, that becomes more noticeable at higher frequency operation. Combining Terfenol-D particles or powder with a binder can overcome the brittleness and eddy current loss, but at the cost of maximum magnetostriction and a reduction of the coupling coefficient. The composites can be machined, cast and molded to almost any form, for a wide range of applications.

Experiments have been done with hard and soft binders indicating the elastic modulus of the binder restricts the strain, causing the maximum magnetostriction to be inversely proportional to the binder modulus [10]. A practical limit on the lower bound of elasticity is realized by the necessary mechanical properties of the desired application of the composite. Soft binders such as epoxies are often used since they allow relatively high strain and insulate the particles to remove energy loss from eddy currents in high frequency applications. However, Busbridge indicated that a stiffer matrix may achieve higher coupling coefficients [2]. He prepared samples with a lead-glass matrix processed under high temperature and stress, a phenol matrix of thermoset polymer molded at elevated temperature and stress, and a conventional epoxy matrix, measuring their corresponding coupling coefficients. The research concluded that the maximum coupling coefficient should be achieved when the matrix modulus is slightly less than the particulate modulus.

1.4 Hybrid Transducers

Conventional smart material transducers utilize a single active element for actuation or sensing, but a hybrid transducer using multiple active elements may extend operating performance when utilized in the right applications. An example of one hybrid design is displayed in Fig. 1.8. The transducer consists of three masses compressing an electrostrictive PMN-PT stack and magnetostrictive Terfenol-D rod, with a center bolt to provide compression. Performance is improved if the two smart materials are complimentary, such as ferroelectric and ferromagnetic materials that demonstrate capacitive and inductive behavior respectively. Several performance metrics have been pursued for hybrid designs, including energy efficiency, coupling coefficient, projection directionality and frequency bandwidth.

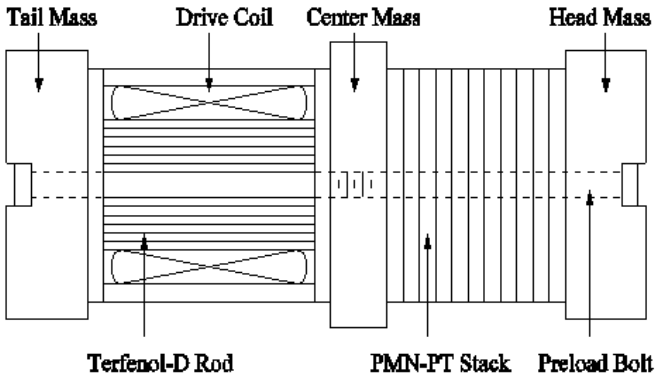

Figure 1.8: A hybrid transducer utilizing a magnetostrictive and electrostrictive element.

An increase in efficiency may be realized for a hybrid system from the increased mechanical work produced from less electrical energy assuming the two devices are inductive and capacitive. It has long been known that inductance and capacitance create complex

resistances that generate reactive power loss in an electrical system. If the complex resistance is canceled, the power dissipated is decreased. The same principle works for two smart materials in an electrical circuit. The greatest efficiency occurs when the materials are operated at their resonant frequencies,which often varies with load in smart materials, making proper tuning difficult for these systems.

A similar metric of performance is the coupling coefficient, defined as the square root of the mechanical energy stored divide by total energy stored. Previous research has calculated the theoretical improvement for a hybrid piezoelectric/magnetostrictive transducer to be 0.52 to 0.60 (18%) and 0.42 to 0.60 (43%) for the sections respectively [5]. A coupling coefficient improvement of 25% over a conventional Tonpilz type transducer was achieved in practice for a Terfenol-D/PZT-4 hybrid transducer by Butler [6]. Composites are not well suited for improvements in efficiency due to their decrease in coupling coefficient.

A large deflection at one end of the transducer with a reduced motion at the other end, enhances the directionality and performance of a sonar transducer. A quarter wave length design of a hybrid system combined with a 90 degree phase shift between materials velocities can achieve this directionality. The wave propagation through one material is canceled at one end as the material contracts and enhanced at the opposite end as the other material expands, as described by Butler [4, 3]. The key factors in this design is the speed of sound of the material which is dependent on the elasticity and density, and the phase shift between the two materials that varies with damping. Composites may be formed with a wide range of properties making them attractive to this application.

An increase in frequency bandwidth is of the most interest to this project. Previous experiments have proven the use of a hybrid actuator can expand the velocity bandwidth to lower frequencies as compared to conventional single element transducers. A series arrangement of a magnetostrictive and piezoelectric hybrid transducer, optimized for broadband performance was originally present by Butler and Tito [7] for a three mass

system similar to Fig. 1.8. One goal of this paper is to obtain an increase in bandwidth through a mechanical series arrangement of ferroelectric and ferromagnetic sections, which are electrically connected in parallel. The ferroelectric material is lead magnesium niobate ($Pb(Mg_{1/3}Nb_{2/3})O_3$) doped with lead titanate ($PbTiO_3$) for enhanced linearity and high electrostriction. The ferromagnetic section was originally tested with a cylindrical Terfenol-D rod but is now replaced with a Terfenol-D composite rod. The monolithic rod successfully increased bandwidth compared to the PMN-PT powered alone. PMN-PT has a high stiffness giving a high resonance, while Terfenol-D has a lower stiffness and dominates the lower frequency range of the transducer. Terfenol-D epoxy composites have very low stiffness that should lower the bandwidth for a hybrid system. The PMN-PT and monolithic Terfenol-D have an internal 90 degree phase shift causing the forces to be out of phase and extending the bandwidth of the transducer. This phase shift will be discussed in more detail later in Chapter 3 after discussing the fabrication of the Terfenol-D composites in Chapter 2.

CHAPTER 2

COMPOSITE FABRICATION

In this section the design and manufacture of Terfenol-D particle composites will be examined. All of the composite samples tested were manufactured in the Smart Materials and Structures Laboratory. A mold was designed and constructed for the desired testing geometry, incorporating a magnetic circuit to improve the alignment of the active phase and therefore, sample performance. Base materials were mixed and cast with minimal machining after curing to produce samples of different volume fraction of powder.

Magnetostrictive composites were fabricated to characterize the static and dynamic properties for the material and to obtain a better understanding of possible applications. One particular application includes the utilization of the composite in a magnetostrictive/electrostrictive broadband hybrid transducer as described in Sec1.4.

The two most common types of particulate composites include aligned and randomly oriented particles. The main challenge with randomly oriented particles is to ensure they are homogenously mixed throughout the specimen and do not settle before the binder hardens. If the binder is a solid, settling of the particles is not a problem. The common convention used for randomly aligned particles is known as (0-3) composites as illustrated in Fig. 2.1(a), resembling a constant stress condition. Aligned particles form chains in the epoxy, but do not occur without some external influence to provide the alignment. If the particles are ferromagnetic they are aligned by using a magnetic field. Aligned particles

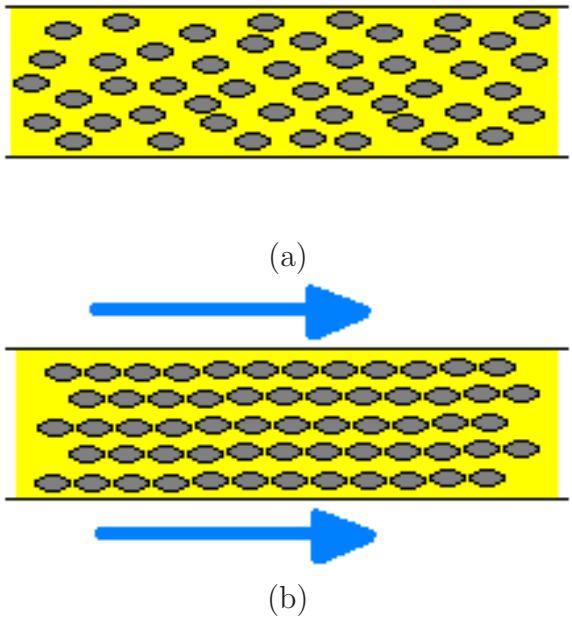

Figure 2.1: (a) Without any aligning force particles remain randomly distributed forming a (0-3) configuration. (b) In the (1-3) configuration particle align resembling oriented fibers.

are known as (1-3) composites as depicted in Fig. 2.1(b), resembling a constant strain condition.

A (1-3) configuration is necessary to achieve high magnetostriction in Terfenol-D composites. This requires the particles to be aligned with a magnetic field during the casting process, creating chains of Terfenol-D particles which act like columns when the particles strain.

2.1 Mold Development

The fabrication of composites usually involves a casting process for a mixture of binder material and particulate or fibers. This section examines the development of a mold to satisfy specific geometry and magnetic circuit requirements of obtaining a homogenous field.

2.1.1 Design Goals

The desired geometry of the composite samples is a long rod with a diameter of a 0.25 in and a length of approximately 2 in. A water cooled testing transducer can accept rods of a wide range of lengths; however, a hybrid transducer that will be discussed in Chapter 4 is designed to work with only a two inch rod. While the mold geometry for the specimen is known, a magnetic circuit around the mold is required to achieve (1-3) configuration. A magnetic circuit often incorporates a high permeability material as a return path for the magnetic flux. This creates a continuous circuit for the flux, allowing the generation of a more homogenous magnetic field.

The mold requires application of a strong magnetic field for approximately an hour to allow the composite to harden. This requires high currents generating excess heat that needs to be removed with a cooling system, thus permanent magnets are more appropriate for extended application of fields. The challenge does not come from the source of the magnetic field but creating a nearly homogenous magnetic field across a specimen. The difficulty arises from a high length to diameter ratio and a specimen permeability much lower than that of steel. A strong imbalance in the magnetic field may separate the particles during casting and create a nonhomogeneous sample, while a weak field at the middle of the mold may not be strong enough to properly align the particles at the center of the sample. The mold material needs to be non ferrous to avoid magnetic flux from flowing around the specimen. Finite element software was necessary to develop a magnetic circuit with these properties.

2.1.2 Finite Element Analysis

Finite element software for magnetics was utilized to design the magnetic circuit for a mold to meet the criteria outlined in Sec. 2.1.1. The most common and simple construction for a magnetic circuit is the use of strong magnets located at either end of the mold to create the field, which will be referred to as an end magnet design. End magnets has been successfully implemented [25, 30, 22], but this is often used to create small samples with low length to diameter ratios that are machined on all sides to remove variations in particle distribution and orientation throughout the specimen. An axisymetric, two dimensional model of the mold using an end magnet design was simulated with Finite Element Method for Magnetics (femm v3.2), a freeware available at (http://femm.foster - miller.net) The program allows geometry construction, material property definitions and boundary conditions for a magnetic system, while capable of calculating the magnetic field, flux, induction and several other properties. An end magnet design creates a strong magnetic field concentrated at the ends with a low field in the middle as shown in Appendix B. The use of steel end caps does not increase the homogeneity of the design.

A permanent magnet in the shape of a hollow cylinder, sized to slip over the mold has been developed. The magnetic field is aligned along the cylindrical axis creating a similar field to a long solenoid as depicted earlier in Fig. 1.1. There are three possible variables for the magnet, which are the length, inside and outside diameters. The outside diameter is the least constrained parameter, while the length has the largest effect on the magnetic field distribution along the rod. The inside diameter is restricted by the need of a mold between the sample and magnet. A cylindrical magnet creates a large improvement over the end magnet design in terms of field homogeneity, but the field strength is much lower with a non continuous magnetic circuit. Placing steel caps over the magnet and mold creates strong field concentrations similar to an end magnet design. A smaller steel cap with square edges

does not create a smooth flow in the magnetic circuit, however an angled end cap is utilized with an angle of 45 degrees which acts like a funnel for the flux to follow. This effectively reduces high concentrations of magnetic field at the ends of the mold as seen in Fig. 2.3. The length of the magnet is optimized for the end cap design when it is the same length as the mold. The outside diameter is selected to create the most homogenous magnetic induction through the sample of the rod as seen in Fig. 2.2. A field of approximately 140 kA/m is desired, corresponding to previous research for similar materials [24]. The alnico and Samarium Cobalt permanent magnets do not generate enough magnetic field, so a Neodymium Iron Boron (NdFeB) magnet is utilized for the final design. This creates an almost continuous magnet circuit that uses a gap of low permeability material between the steel end caps and the magnet to balance out the field intensity as demonstrated in Fig 2.2. Several design iterations for the mold are contained in Appendix B.

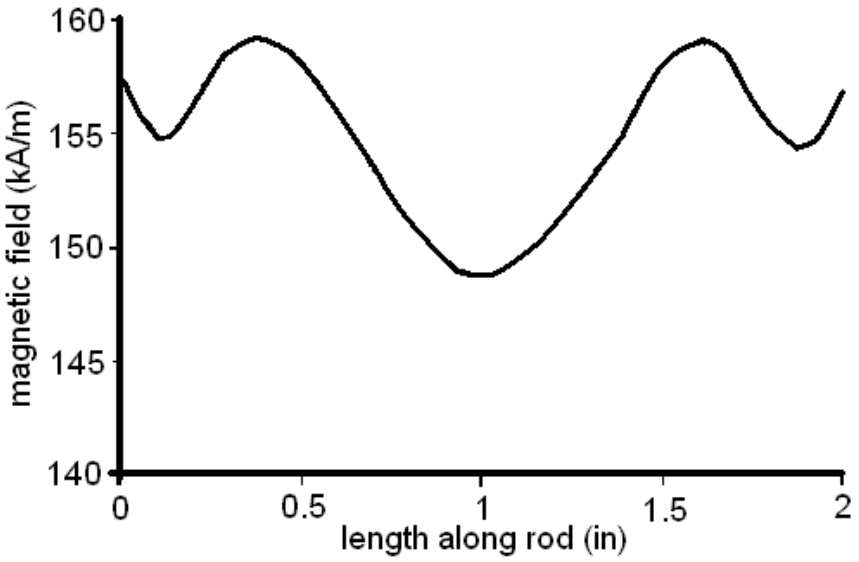

Figure 2.2: Field intensity along the center of the composite rod obtained from the induction plot of Fig 2.3. The field varies between 150-160 kA/m, less than a 5% deviation from the average value.

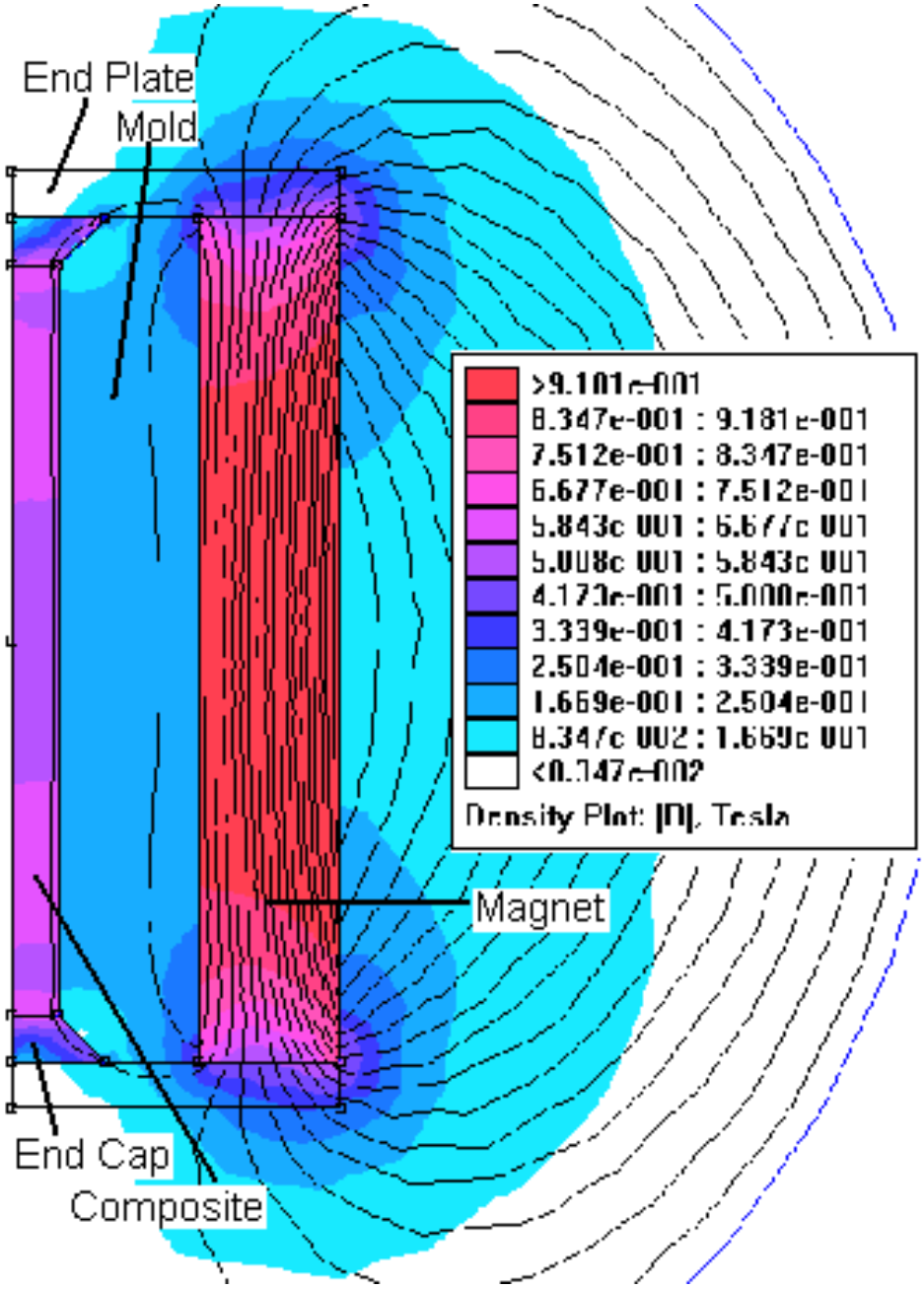

Figure 2.3: Finite element calculations of magnetic induction in the mold and magnet of the final design.

2.1.3 Mold Design

The core of the mold is composed of two blocks of 6061 aluminum utilizing aluminum pins to align both parts. The aluminum blocks are pinned together and machined on the lathe to achieve concentricity of the mold cavity and outside surface. The mold cavity is 2 in long while the entire mold is 2.5 in long to allow the quarter inch thick steel end caps to fit flush along the ends of the mold. The inside diameter of the mold is drilled to 0.25 in and the outside has a diameter of 1.00 in. The end caps are machined from rolled mild steel plates with a diameter of 0.25 in on the specimen side and 0.50 in at the outside surface, thus giving the caps a 45 degree tapper as shown in Fig. 2.4. The top and bottom surfaces of the mold are drilled and tapped for bolts with the holes offset 45 degree from the mold part line.

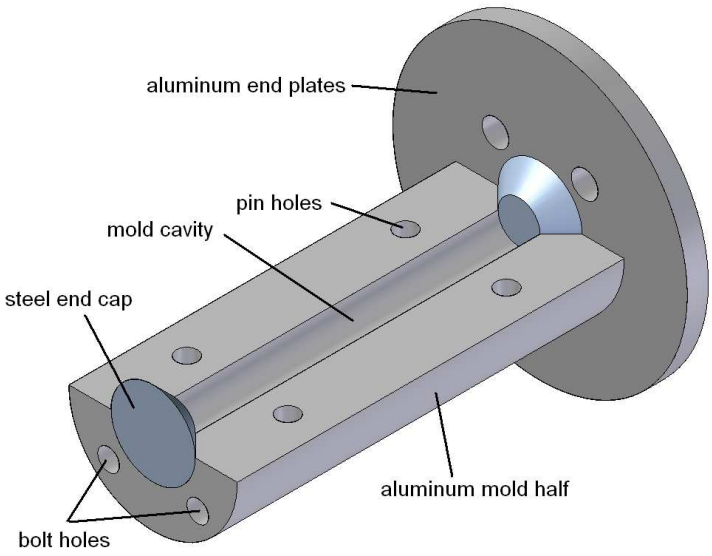

Figure 2.4: Mold cavity displaying placement of steel end caps and aluminum end plate.

Thin aluminum end plates hold the caps and magnet in place during the casting process. The nickel plated NdFeB 35 magnet is custom made by Magnetic Materials and Components Enterprises Corp. of Hauppauge, NY. The magnet has an inside diameter of 1.01 in, an outside diameter of 2.00 in, and the same length as the mold of 2.5 in. When fully assembled the magnet and end plates are held securely in place as shown in Fig. 2.5. Steel bolts have a high permeability and would alter the homogeneity of the magnetic circuit, therefore the mold is assembled by size 8 titanium bolts which are not ferromagnetic.

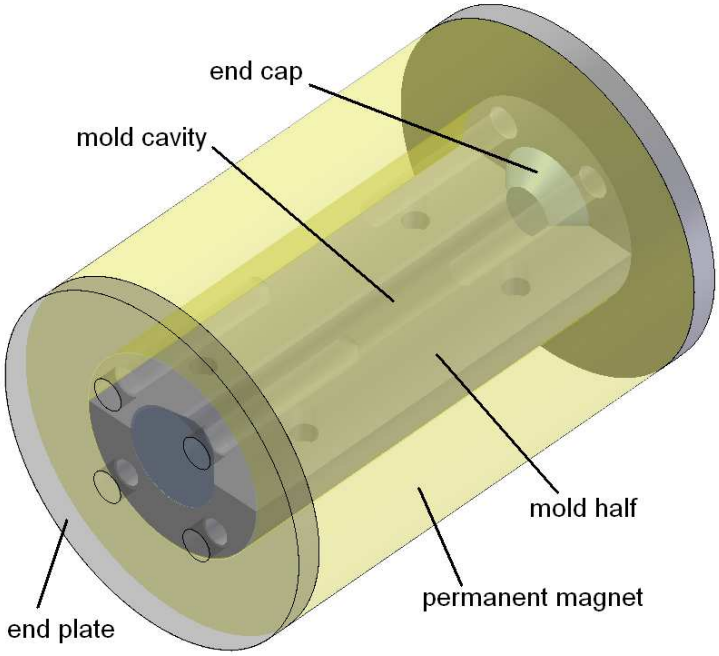

Figure 2.5: A phantom view of the entire assembly shows the permanent magnet in yellow.

2.2 Material Selection

Magnetostriction of the Terfenol-D is resisted by the modulus of elasticity of the binder material, thus a soft binder was selected for high levels of magnetostriction [10]. Derakane 411-C-50 epoxy vinyl ester resin from Dow Chemical Company of Channahon, IL, was utilized as the binder, and the material properties can be found in Table 2.1. Derakane 411-C-50 is a soft low viscosity resin that hardens at room temperature when combined with a catalyst and promoter.

411-C-50	Viscosity	112	cSt
	Density	1.028	g/mL
411	Tensile Strength	11-12	ksi
Family	Tensile Modulus	0.49	Mpsi
	Elongation	5-6	%
	Compressive Strength	16-17	ksi
	Compressive Modulus	0.35	Mpsi
	Barcol Hardness	35	-

Table 2.1: Viscosity and density of Derakane 411-C-50 and typical mechanical properties of the 411 family of epoxy vinyl ester resins.

Low viscosity resins permit more effective wetting of the particles, which decreases the void content of the material caused by small gas pockets clinging to the particles [24]. The catalyst used in this study is Methyl Ethyl Ketone Peroxide (MEKP), a thin clear liquid, while the promoter is Cobalt Naphthenate (CoNap), a thick purple fluid. The amount of catalyst and promoter may be varied for temperature, humidity and cure time. A ratio of 2% MEKP and 0.2% by mass CoNap is used for the lab temperature and humidity, allowing the epoxy to set up in less than an hour. The resin becomes a yellow color after hardening for a pure epoxy sample, but the Terfenol-D samples take a dark green tint when cured. The epoxy has a recommended shelf life of 6 months and turns into a thick gel if

stored for a long time. To prolong the self life, the epoxy is stored in glass jars and sealed, significantly extending the material life cycle.

Terfenol-D ball-milled powder is created from breaking brittle material in an inert gas atmosphere to prevent oxidation and was obtained from ETREMA Products, Inc of Ames, Iowa. The particles are randomly sized, having a low length to diameter ratio and characterized by irregular surfaces as shown in Fig. 2.6. The particle size selected ranges from 106-300 microns, which is one of the larger size ranges available. This was selected since previous research demonstrated that very small particles below 50 microns exhibit less strain when compared to particles of other dimensions [30], and diversity in size of particles can improve the packing density within the specimen [15]. An increase in composite properties was achieved by cutting high aspect ratio, needle shaped particles from a monolithic block along the crystal [112] axis, but machining the particles is very labor intensive and tends to wasted large amounts of Terfenol-D in the production of the particles [24]. The improved performance was attributed to the increase in non-180 degree domain wall motion in the larger particles compared to ball-milled powder.

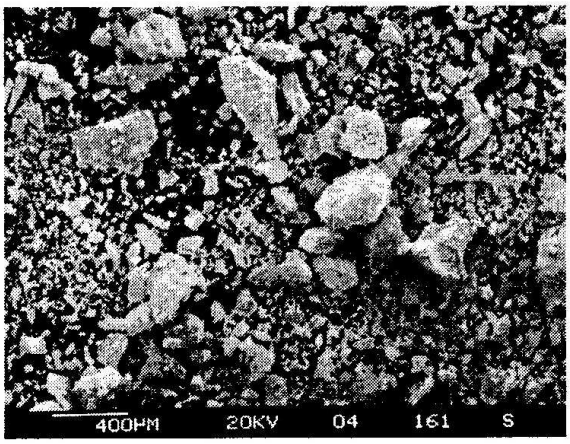

Figure 2.6: Magnification of ball-milled Terfenol-D powder [30].

2.3 Casting Process

The epoxy is very reactive with polymers, dissolving plastics and styrofoam, requiring the epoxy to be mixed in a glass or metal container. A small metal container was used for mixing of the materials while the fabrication was performed in an open air environment with no degassing. This is unusual for magnetostrictive composites, but it has been demonstrated that preparing samples in an argon environment and repeated degassing carries little or no benefit on the composite performance [15] compared to the manufacturing of composites in an open air environment. This greatly simplifies the manufacturing process and makes mass production more economical. The epoxy, catalyst, and promoter were mixed first and the desired amount of Terfenol-d powder was added to the mixture.

The mold was sealed with silicone to prevent the epoxy from leaking through the part line of the mold halves. The magnet was assembled over the mold when the epoxy was poured and the steel cap was in place. A guide was used to slide the magnet over the mold quickly to prevent particle separation and to hold the steel cap in place. Placing the magnet on slowly pulls all of the particles to the poles. The steel end cap must be held securely in place or the magnet attracts the cap and removes all of the Terfenol-D particles from the mold. The samples were cured in a forced air convection oven at 70 degrees Celsius for 6 hours to ensure complete reaction of the epoxy, and the samples were machined on a lathe to obtain flat ends after removal from the mold. A few of the low volume fraction samples prepared are displayed in Fig 2.7

The epoxy shrinks as it dries creating a stress on the particles, aiding in the activation of magnetostriction as discussed in Sec. 1.2.2. The Terfenol-D powder has a lower thermal coefficient of expansion than the epoxy, so curing in an oven causes the epoxy to expand more than the particles creating a stress on the sample at room temperature. This stress is built into the specimen and reduces the preload necessary to achieve optimal performance

Figure 2.7: Samples prepared in the Smart Materials and Structures Laboratory with 5.0%, 2.1%, 3.6%, and 7.3% volume fraction of Terfenol-D powder from top to bottom respectively.

from the specimen. The mold is cleaned after every sample is removed and the surfaces are waxed to prevent the epoxy from sticking to the aluminum mold. Proper maintenance ensures many samples may be made from the same mold.

CHAPTER 3

LINEAR MODEL

The behavior of a Terfenol-D/PMN-PT hybrid transducer such as the one described in Sec. 1.4 can be modeled by considering four linear models. A linear model may be justified for these highly nonlinear materials by operating at a biased, low signal regime where the materials exhibit quasilinear behavior. The PMN-PT stack has been doped to improved linear response, the Terfenol-D rod is being operated in a biased linear region, well below saturation. The first model describes mechanical motion through classical vibrations theory by modeling the hybrid transducer as a mass-spring-damper system with corresponding boundary and initial conditions. In the second model component, electroacoustics theory is used to couple the mechanical motion and electrical power delivered to the system. The third model employs impedance and transduction terms which are derived from piezomagnetic and piezoelectric constitutive relations for smart materials. The final step is combining these three models into a system capable of describing the electrical and mechanical response of the transducer to an applied voltage.

3.1 Mechanical Vibrations Model

The Terfenol-D/PMN-PT hybrid transducer constructed in the Smart Materials and Structures Laboratory can be simplified to two active elements in mechanical series with three lumped masses, creating a three-degree-of-freedom system, as shown in Fig. 3.1. Each active element may be treated as a tunable massless compliance arranged in parallel with

a damper. The system thus has three degrees of freedom and three natural frequencies but one is zero, thus creating a double resonant system.

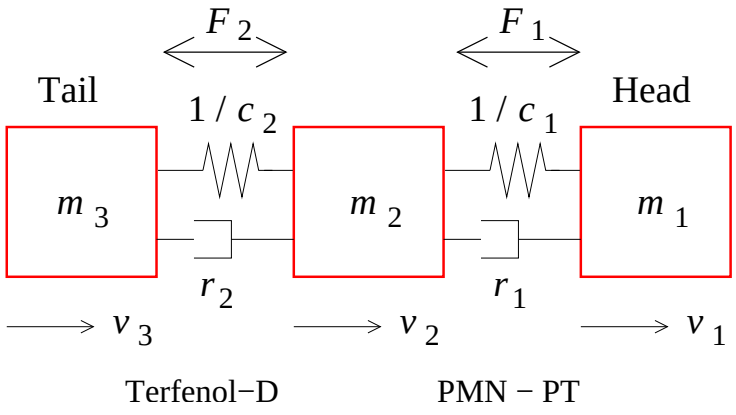

Figure 3.1: Representation of the hybrid transducer. Mechanical three-degree-of-freedom. [12]

Here, m represents a lumped mass, r the damping coefficient of an active element, c the mechanical compliance of an element, v the velocity of a mass, F the force produced by an active elements in response to magnetic or electric fields, and s the Laplace derivative operator, s=$j\omega$. The subscripts 1 and 2 on the applied forces, damping elements and compliances respectively denote the PMN-PT and Terfenol-D sections. The subscripts 1, 2, and 3 on the velocity vector respectively denote the head, center, and tail mass motions.

One goal of this project is to achieve an improvement in bandwidth over the 1-6 kHz frequency range, which is of primary interest to the US Navy for sound navigation ranging (SONAR). The ideal mass and stiffness ratios need to be determined from the mechanical model and classical vibrations theory to achieve this.

The equations of motion are written for each mass and arranged in matrix form, so the system can be expressed in the frequency domain in terms of the element force and mass

velocity,

$$\left([M]\, s + [C] + [K]\, \frac{1}{s} \right) \vec{v} = \vec{F}, \tag{3.1}$$

where the structural matrices and vectors are defined by

$$\begin{aligned}
[M] &= \begin{bmatrix} m_1 & 0 & 0 \\ 0 & m_2 & 0 \\ 0 & 0 & m_3 \end{bmatrix} \\
[C] &= \begin{bmatrix} r_1 & -r_1 & 0 \\ -r_1 & r_1 + r_2 & -r_2 \\ 0 & -r_2 & r_2 \end{bmatrix} \\
[K] &= \begin{bmatrix} 1/c_1 & -1/c_1 & 0 \\ -1/c_1 & 1/c_1 + 1/c_2 & -1/c_2 \\ 0 & -1/c_2 & 1/c_2 \end{bmatrix} \\
\vec{v} &= \begin{bmatrix} v_1 \\ v_2 \\ v_3 \end{bmatrix} \\
\vec{F} &= \begin{bmatrix} F_1 \\ F_2 - F_1 \\ -F_2 \end{bmatrix}.
\end{aligned}$$

Prior work by Butler [7], and Downey and Dapino [11] established that for broad band actuation, the ideal ratio for the head : center : tail mass must be approximately 1 : 2 : 2.5, and the piezoceramic stack must be much stiffer than the magnetostrictive section. The system's resonant frequencies were calculated using eigenvector modal analysis with monolithic Terfenol-D properties. The first, second and third natural frequencies of are 0 Hz, 1250 Hz, and 4000 Hz.

The phase between the forces generated by the active elements has an important effect on the response of the system as depicted in Fig. 3.2, for a system with head : center : tail masses in a ratio of 1 : 2 : 2.5. If two forces are in phase, the response will have a large antiresonance around 3 kHz, while a phase of 180 degrees will give a flat response without covering the lower frequency range. On the other hand, a 90 degree phase between the forces provides a relatively flat response over a broad frequency bandwidth. This is because

magnetostrictive materials and ferroelectric compounds naturally exhibit a 90 degree phase shift in their force response when driven in electrical parallel.

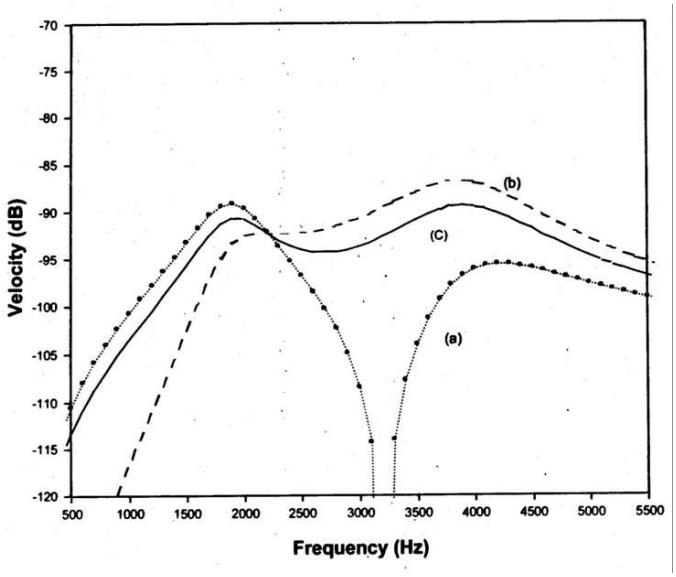

Figure 3.2: Head velocity response when the forces of F_1 and F_2 are (a) in phase (b) 180 degrees out of phase, (c) 90 degrees out of phase.

The upper resonance is controlled by the PMN-PT stack where the tail mass essentially decouples from the system, with the head and center masses vibrating out of phase from each other. The lower resonance is controlled by the Terfenol-D section and is characterized by the head and center masses lumped together, vibrating out of phase with the tail mass, as depicted in Fig. 3.3.

The mechanical impedance is defined as the transfer function force per velocity, a useful measure of broadband motion of the head mass. To analyze the PMN-PT section, the force F_2 produced by the Terfenol-D composite rod is set equal to zero. The resulting mechanical impedance F_1/v_1 then takes the form [11]

$$Z_{mech,E} = \frac{F_1}{v_1} = \frac{As^4 + Bs^2 + C}{sc_1(m_2 m_3 c_2 s^2 + (m_2 + m_3)(r_2 c_2 s + 1)}. \tag{3.2}$$

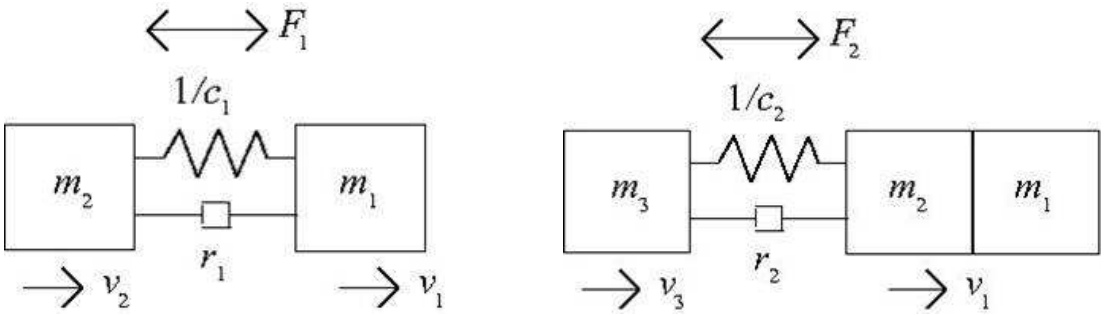

Figure 3.3: Simplified mechanical model for the (a) high frequency mode (PMN-PT) and (b) low frequency mode (Terfenol-D) [11].

Likewise, the mechanical impedance for the Terfenol-D rod can be obtained from setting the force of the PMN-PT section equal to zero

$$Z_{mech,M} = \frac{F_2}{v_1} = \frac{As^4 + Bs^2 + C}{sc_2m_3(r_1c_1s + 1)}. \tag{3.3}$$

The subscripts E and M respectively denote "electric" and "magnetic" for the PMN-PT and Terfenol-D elements. In equations (3.2)-(3.3), the terms A, B, and C have the form

$$\begin{aligned} A &= (m_1m_2m_3c_1c_2) \\ B &= m_3(m_1 + m_2)c_2(r_1c_1s + 1) + m_1(m_2 + m_3)c_1(r_2c_2s + 1) \\ C &= (r_1c_1s + 1)(r_2c_2s + 1)(m_1 + m_2 + m_3). \end{aligned}$$

Relations (3.2)-(3.3) are sufficiently general to characterize the transducer's output response due to activation of either smart material given suitable values for the material properties.

3.2 Electroacoustics Model

The vibratory mechanical model can be coupled to the electrical regime using classical electroacoustic transduction theory [18]. Electroacoustics theory is constructed from a "black box" transducer system which couples two different energy regimes. Each regime

has a potential, flow, resistance, and coupling term, as depicted in Fig. 3.4. The general electromechanical system consists of a velocity and force on the mechanical side, a voltage and current on the electrical side, and two transduction terms coupling the mechanical and electrical regimes. Assuming linearity, the expressions relating these two regimes are

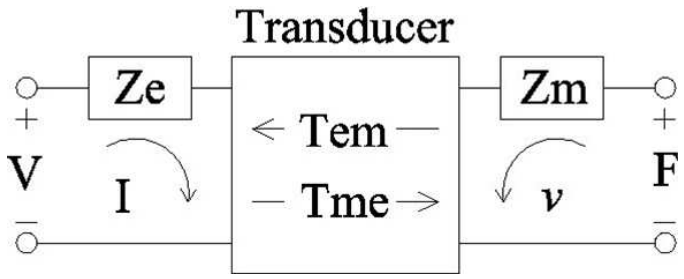

Figure 3.4: Four-pole electroacoustics model for electromechanical systems [12].

$$V = Z_e I + T_{em} v \tag{3.4}$$

$$F = T_{me} I + Z_m v, \tag{3.5}$$

where V is the voltage across the transducer terminals, I is the current flow through the transducer, v is the velocity, F is the force, Z_e and Z_m respectively denote the blocked electrical and mechanical impedances, and T_{em} and T_{me} are coefficients that describe the electromechanical transduction. The subscripts *em* and *me* respectively denote "electrical due to mechanical" and "mechanical due to electrical" energy transduction processes.

The electrical impedance at the terminals is the complex ratio of voltage to current, which is useful for studying material properties. For a general electromechanical system that can be described by the electroacoustics equations (3.4)-(3.5), it is assumed that the force F acts on a load of impedance Z_L, which allows (3.5) to be written in the form

$$v = \frac{-T_{me} I}{Z_m + Z_L}. \tag{3.6}$$

Substitution of this equation in (3.4) gives the total electrical impedance transfer function

$$Z_{ee} = \frac{V}{I} = Z_e + \frac{-T_{em}T_{me}}{Z_m + Z_L} = Z_e + Z_{mot}. \tag{3.7}$$

The total electrical impedance Z_{ee} consists of a combination of a blocked component Z_e, equal to the ratio between voltage and current when the transducer is prevented from moving, and a motional component Z_{mot} that is associated with the mechanical motion of the transducer and effect of load as shown in Fig. 3.5. The motional component provides a measure of the amount of electromechanical coupling between the regimes within the transducer.

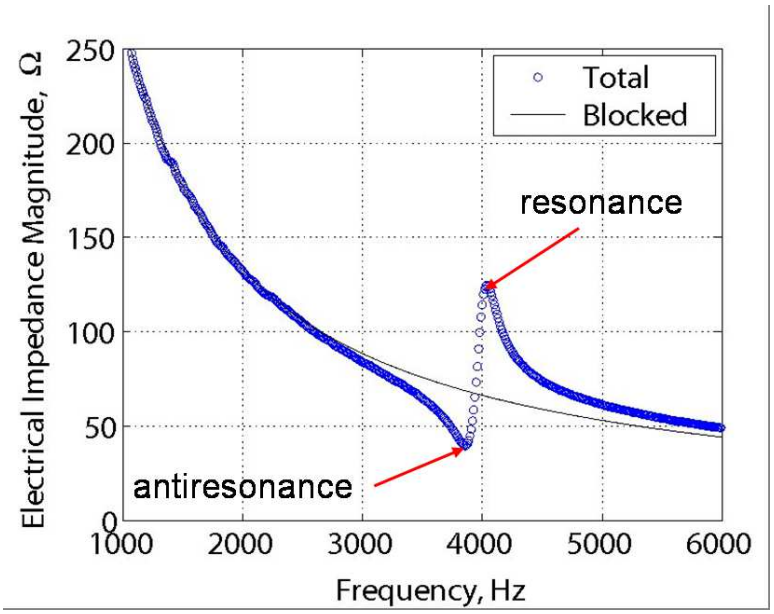

Figure 3.5: Electrical impedance demonstrating the motional and blocked components [11].

A Nyquist plot can be obtained from the the complex electrical impedance transfer function by plotting the data on real and imaginary axes, Fig. 3.6, of which the electrical resonance frequency f_r is determined from the principal diameter of this Nyquist [11]. The electrical impedance function and its inverse, the admittance function $Y_{ee} = 1/Z_{ee}$, provide

measures of performance and properties of the transducer such as coupling coefficients, quality factors, elastic moduli, and speeds of sound [28, 18, 27]. The total impedance and admittance functions are the inverse of one another, while the coupled motional effects are not; $Y_{mot} \neq 1/Z_{mot}$. One difference between these functions is that in the admittance loop the frequency opposite the crossover point is the antiresonance frequency f_{ar} rather than f_r for the same point on the impedance plot. As detailed for Terfenol-D by Dapino et al. [27], the resonant and antiresonant frequencies quantify the effective coupling coefficient through the relations

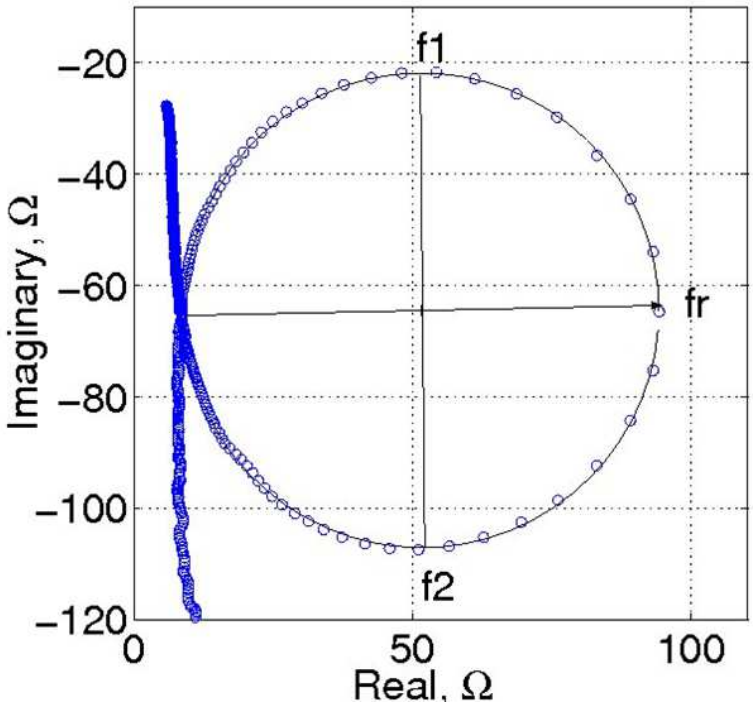

Figure 3.6: Nyquist plot of electrical impedance indicating the resonant frequency and half power points [11].

$$k_{eff}^2 = \begin{cases} 1 - \left(\frac{f_{ar}}{f_r}\right)^2, & \text{if } f_{ar} < f_r \\ 1 - \left(\frac{f_r}{f_{ar}}\right)^2, & \text{if } f_{ar} > f_r \end{cases} \tag{3.8}$$

which both apply to the PMN-PT and Terfenol-D elements. The system masses and the resonance and antiresonance frequencies allow the calculation of the stiffness of each drive element. The stiffness is determined by setting the imaginary component equal to zero in expressions (3.2) and (3.3) and rearranging

$$k_m^E = \frac{1}{c_1} = \frac{(2\pi f_r)^2 m_1 m_2}{m_1 + m_2},$$
$$k_m^M = \frac{1}{c_2} = \frac{(2\pi f_r)^2 (m_1 + m_2) m_3}{m_1 + m_2 + m_3}.$$

Here, the superscripts E and M respectively denote the PMN-PT (electric field) and Terfenol-D (magnetic field) sections. The assumption of linearly elastic behavior entails the Young's moduli of the PMN-PT and Terfenol-D drivers as given by

$$E_y^E = \frac{k_m^E L_{e,1}}{A_1} \tag{3.9}$$
$$E_y^M = \frac{k_m^M L_{e,2}}{A_2}, \tag{3.10}$$

where L_e and A (with appropriate subindices) denote length and cross sectional area of each active element.

The intrinsic sound speeds are subsequently calculated as

$$c_E = \sqrt{\frac{E_y^E}{\rho_E}}$$
$$c_M = \sqrt{\frac{E_y^M}{\rho_M}}$$

where ρ_E and ρ_M denote the material mass densities.

The electrical impedance and admittance measurements allow the direct determination of two quality factors for each section by indicating the resonant, antiresonant frequencies and half power points as displayed in Fig 3.6 and Fig. 3.7

$$Q_r = \frac{f_r}{f_2 - f_1} \tag{3.11}$$
$$Q_{ar} = \frac{f_{ar}}{f_{a2} - f_{a1}}. \tag{3.12}$$

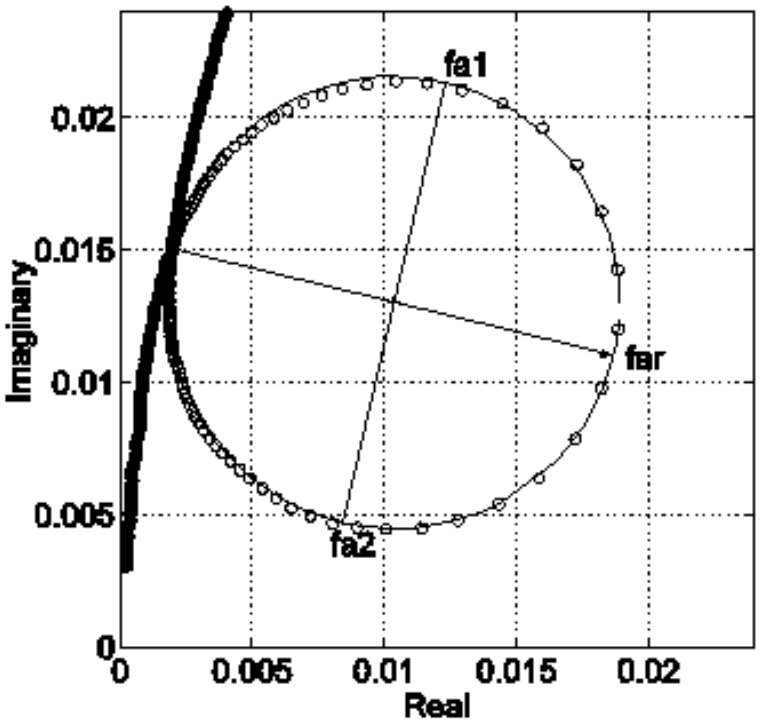

Figure 3.7: Nyquist plot of electrical admittance corresponding to the impedance shown in Fig 3.6, indicating the antiresonance frequency and half power points. [11].

Since each section has two values for Q (one from impedance and one from admittance), the average value is used for transducer design and analysis. By inspection of the mechanical equations of motion, the internal damping is estimated by

$$r_1 = \frac{2\pi f_r m_1 m_2}{Q(m_1 + m_2)} \tag{3.13}$$

$$r_2 = \frac{2\pi f_r (m_1 + m_2) m_3}{Q(m_1 + m_2 + m_3)} \quad , \tag{3.14}$$

respectively for the PMN-PT and Terfenol-D sections. The above equations relating experimental measurements to transducer figures of merit were utilized in this study to determine the model parameters where available.

3.3 Constitutive Piezomagnetic and Piezoelectric Relations

The equations of Sec. 3.2 are general in that they permit analyzing a variety of electromechanical systems without regard to phase interaction between the applied voltage and ensuing force. In order to account for the ferroelectric and ferromagnetic properties of the transducer, especially in regard to the phase between the velocity responses. Electroacoustics relations (3.4)-(3.5) are combined with linear constitutive equations describing the strain, magnetization and polarization of the active materials. The blocked impedances and transduction coefficients may now be expressed in terms of material properties and design parameters.

3.3.1 Terfenol-D Section

Operating over a small field with a bias field validates use of the linear piezomagnetic constitutive relations for a Terfenol-D rod driven along the longitudinal "33" direction,

$$\varepsilon = \frac{\sigma}{E_y^M} + qH \tag{3.15}$$

$$B = q^*\sigma + \mu^\sigma H, \tag{3.16}$$

where ε is strain, σ is axial stress, H is applied magnetic field, B is magnetic flux density in the material, μ^σ is permeability at constant stress, and $q = q^*$ is a symmetric magnetoelastic coupling coefficient relating mechanical and magnetic terms. The equations can be converted to the desired form for relations (3.4) - (3.5) from the following fundamental relations

$$H = nI$$

$$\varepsilon = \frac{v}{j\omega L_{e,2}}$$

$$\sigma = \frac{F}{A_2}$$

$$V = RI + j\omega NBA_2,$$

where n is the turns ratio of the magnetic coil ($n = N/L_{e,2}$), $L_{e,2}$ is the length of the coil and composite rod, A_2 is the rod cross sectional area and internal area of the coil, and R is the wire resistance of the coil. The total voltage drop is that of a DC resistance R in series with an electrical inductance. Substitution of these expressions into (3.15) and (3.16), and subsequent rearrangement yields [16]

$$V = [R + j\omega\mu^{\sigma}(1 - k_{eff}^2)n^2 A_2 L_{e,2}]\, I + Nqk_m^M\, v, \tag{3.17}$$

$$F = -Nqk_m^M\, I + \frac{k_m^M}{j\omega}\, v. \tag{3.18}$$

Comparison of these equations with the general electroacoustic relations (3.4)-(3.5) gives

$$Z_{e,M} = R + j\omega\mu^{\sigma}(1 - k_{eff}^2)n^2 A_2 L_{e,2} = R + j\omega L_{block}, \tag{3.19}$$

where L_{block} is defined as $\mu^{\sigma}(1 - k_{eff}^2)n^2 A_2 L_{e,2}$. This indicates that the blocked electrical impedance $Z_{e,M}$ for the Terfenol-D section can be represented by an ideal resistor in series with an inductor L_{block} which can be directly determined from measured material properties.

Equations (3.17) and (3.18) also determine the transduction coefficients T_{em} and T_{me}. These terms describe the coupling between the electrical and mechanical regimes and can be related to material properties by

$$T_{em,M} = Nqk_m^M \tag{3.20}$$

$$T_{me,M} = -Nqk_m^M = -T_{em,M}. \tag{3.21}$$

It is observed that $T_{em,M}$ and $T_{me,M}$ are equal in magnitude while opposite in sign, as is expected of all magnetostrictive transducers because of the spatial orthogonality of current and magnetic field. [18]

3.3.2 PMN-PT Section

Operating at a low voltage with a bias, places the operation within a linear range when operated at room temperature. The behavior of the individual layers may be approximated by the linear piezoelectric constitutive relations as given by

$$\varepsilon = \frac{\sigma}{E_y^E} + dE \tag{3.22}$$

$$D = d^*\sigma + \epsilon^\sigma E, \tag{3.23}$$

where E is electric field, D is electric charge density, E_y^E is Young's modulus at constant field, ϵ^σ is electric permittivity at constant stress, and $d = d^*$ is a symmetric electroelastic coupling coefficient relating mechanical and electrical terms. To link the constitutive relations to the electroacoustics model we use some fundamental electromechanical equations as in Sec 3.3.1

$$E = \frac{V}{t}$$
$$\varepsilon = \frac{v}{j\omega L_{e,1}}$$
$$\sigma = \frac{F}{A_1}$$
$$D = \frac{I}{j\omega A_1},$$

in which it is assumed that each layer has thickness t and cross-sectional area A_1. Substitution of these expressions into (3.22) and (3.23), and rearranging yields

$$V = \frac{t}{A_1 j\omega N(\epsilon^\sigma - E_y^E d^2)}\, I + \frac{-dE_y^E}{j\omega N(\epsilon^\sigma - E_y^E d^2)}\, v \tag{3.24}$$

$$F = \frac{-dE_y^E}{j\omega N(\epsilon^\sigma - E_y^E d^2)}\, I + \frac{\epsilon^\sigma E_y^E A_1}{j\omega N(\epsilon^\sigma - E_y^E d^2)}\, v. \tag{3.25}$$

Comparison of these relations with the general electroacoustic relations (3.4)-(3.5) indicates that the blocked electrical impedance of the PMN-PT stack is purely capacitive in

nature,

$$Z_{e,E} = \frac{t}{j\omega A_1 N(\epsilon^\sigma - E_y^E d^2)} = \frac{1}{j\omega C_{block}}, \tag{3.26}$$

where $C_{block} \equiv A_1 N(\epsilon^\sigma - E_y^E d^2)/t$. The two coefficients that characterize the electromechanical transduction can be written from equations (3.24) and (3.25) as

$$T_{em,E} = \frac{-dE_y^E}{j\omega N(\epsilon^\sigma - E_y^E d^2)} \tag{3.27}$$

$$T_{me,E} = \frac{-dE_y^E}{j\omega N(\epsilon^\sigma - E_y^E d^2)}. \tag{3.28}$$

The coefficients are symmetric in magnitude and sign as predicted by ferroelectric transduction while the Terfenol-D section has coefficients of opposite sign as expected. The two active elements are 90 degrees out of phase as mentioned earlier which effectively extends the bandwidth of the material [7]. This inherent phase shift can be proven by comparing the transduction coefficients T_{em} of each section as shown by Downey and Dapino. [28]

3.4 Combined Linear Transducer Model

The electroacoustics coefficients are defined entirely in terms of physical parameters such that the relations (3.17)-(3.18) and (3.24)-(3.25) may be used to calculate the velocity response for a given applied voltage. The relationship between applied voltage and velocity is determined by the transduction coefficients $T_{em,M}$ and $T_{em,E}$.

The PMN-PT and Terfenol-D sections are wired in electrical parallel, summing the total electrical impedances including motional contributions as in a simple circuit. This leaves the transducer's total electrical impedance, incorporating electrical and mechanical effects in both active sections as

$$Z_{ee,total} = \frac{Z_{ee,E} Z_{ee,M}}{Z_{ee,E} + Z_{ee,M}}, \tag{3.29}$$

in which $Z_{ee,M}$ is quantified by (3.7), (3.19), (3.20) and (3.21), and $Z_{ee,E}$ by (3.7), (3.26), (3.27) and (3.28).

The current applied to each active element is calculated from the definition of electrical impedance before determining the head mass velocity

$$I_E = \frac{V}{Z_{ee,E}}$$
$$I_M = \frac{V}{Z_{ee,M}},$$

where the applied voltage is V for both sections. The velocity from each section is now given by (3.6),

$$v_E = \frac{-T_{me,E}\, I_E}{Z_{m,E}+Z_L}$$
$$v_M = \frac{-T_{me,M}\, I_M}{Z_{m,M}+Z_L}.$$

The system is a mechanical series arrangement of active elements, which enables the superposition of the head mass velocities from each section

$$v = v_E + v_M. \tag{3.30}$$

Separate equations for section velocities allow comparison of the individual response for only the piezoelectric or piezomagnetic element powered. Each equation assumes excitation from the other section but does not account for the coupling of the attached mechanical components of the transducer.

CHAPTER 4

TRANSDUCER DESIGN AND TESTING

Design and testing of a hybrid PMN-PT/Terfenol-D transducer is presented in this chapter where mechanical components, magnetic return circuit, and the electrical system are of primary interest. Sensors and data acquisition equipment were utilized for quasistatic characterization of the composite samples, as well as dynamic testing of a hybrid transducer up to a frequency of 6 kHz. The quasistatic information was used for identification of suitable operating ranges for the composite, while the dynamic measurements were utilized for analysis of transducer bandwidth and validation of the linear model developed in Chapter 3.

4.1 Hybrid Transducer Design

A broadband Tonpilz hybrid transducer based around the mechanical and magnetic properties of a monolithic Terfenol-D rod and a PMN-PT electrostrictive element was designed by Downey in the Smart Materials and Structures Laboratory [12]. The monolithic rod is now replaced with a Terfenol-D particle composite rod with a goal of improving bandwidth at the lower frequency range, compared to a single, active element. Initial experiments indicate a stronger magnetic field is needed for a composite sample, which motivated a revision to the magnetic circuit design of the hybrid transducer. The original design of the hybrid transducer intended the use of a monolithic rod and is discussed in this section along with the revised magnetic coil design.

4.1.1 Original Design

The hybrid transducer was designed and constructed to use an ETREMA Terfenol-D rod ($Tb_{0.73}$, $Dy_{0.27}$, $Fe_{1.95}$) with a length of 2 in (50.8 mm), a diameter of 0.25 in (6.35 mm) and a stiffness of 28 MN/m [12]. The electrostrictive component of the transducer consists of an EDO Ceramic model EP200-62 EC-98 stack. The material is lead magnesium niobate - lead titanate in a 65-35 ratio which enables the use of linear piezoelectric equations with accuracy. The ceramic is selected for its stiffness of approximately 120 MN/m to create two mechanical resonances when placed in series with the magnetostrictive section. The stack is composed of 62 individual layers and has a total length of 1.385 in (35.2 mm) and a diameter of 0.63 in (16 mm).

The three masses are selected to be in a ratio of 1 : 2 : 2.5 respectively for the head, center and tail masses, in agreement with previous work for broadband transducers operating in the 1-6 kHz frequency range [4, 7]. To achieve target resonances of 1300 and 3900 Hz, masses of 0.33 kg, 0.67 kg, and 0.83 kg are required, according to the stiffnesses of the active elements. A diameter of 3 in is used for all three masses with their thicknesses selected to match the target mass. The center and tail masses are made of non-magnetic steel, while the head mass is made of aluminum. While the final masses after manufacturing and assembly are actually 0.308 kg for the head, 0.670 kg for the center, and 0.777 kg for the tail mass, the deviation from ideal values has a negligible effect on the system bandwidth. The PMN-PT stack is compressed between the head and center masses to control the high frequency range, and the Terfenol-D rod is compressed between the center and tail masses to control the low frequency range. A three-bolt design is used to hold either end masses to the center, with Belleville washers under the bolt heads providing a preload to the active elements. Each washer has a stiffness of approximately 0.684 MN/m which is reduced by respectively placing three and five in series on each bolt that holds the PMN-PT and

Terfenol-D rod. The finished transducer has a length of 6 in (152.4 mm) as shown in Fig. 4.1.

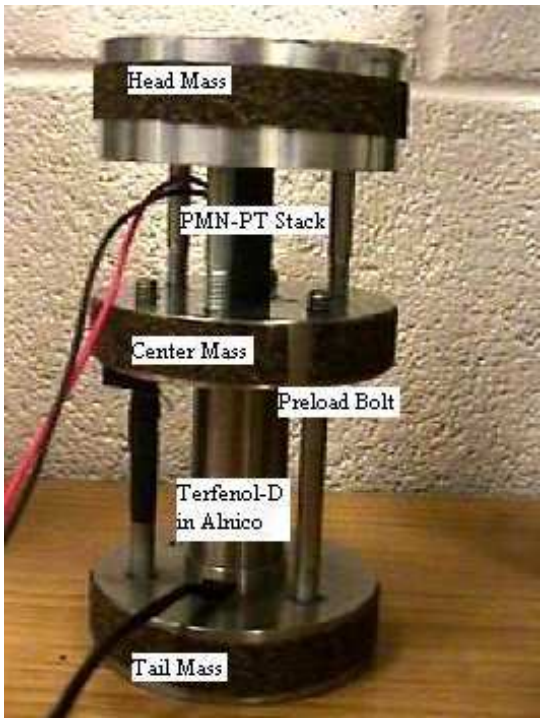

Figure 4.1: Fully assembled hybrid transducer indicating the individual masses and active element. Each element is compressed by three bolts. [12]

Terfenol-D achieves optimal performance in a homogenous field, thus requiring a magnetic return path for the drive coil. The key components of the flux return path consist of the Terfenol-D sample, cylindrical permanent magnet and steel connecting pieces. An Alnico V permanent magnet surrounds the drive coil and sample producing a constant magnetic field of approximately 125 Oe (10 kA/m). The magnet is 2 in long, has an inside diameter of 0.75 in and an outside diameter of 1.0 in with an axial slit to reduce eddy

current losses. The Terfenol-D rod and magnet are magnetically connected by high permeability 1018 steel pieces at either end. A small gap exists between the steel end plate and steel end cap that is against the rod as illustrated in Fig 4.2.

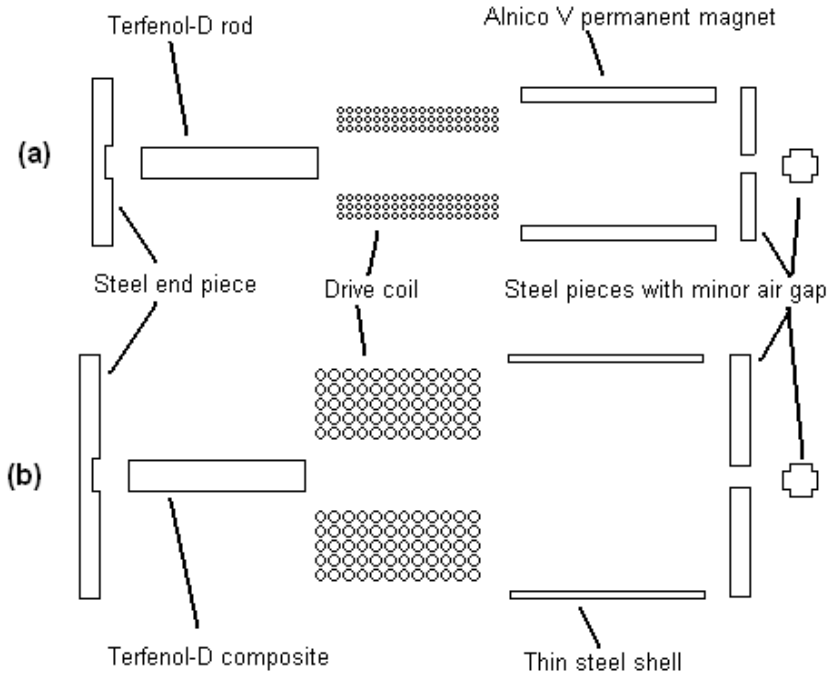

Figure 4.2: Magnetic circuit of (a) the original design incorporating a permanent magnet around the drive coil and (b) the new design with a larger drive coil and a steel housing.

The drive solenoid for the magnetostrictive section of the transducer is powered by a 1232 turn coil of 26 AWG enameled wire producing a field of 300 Oe/A (23.9 kA/m), a resistance of 6.73 Ω and an approximate inductance of 6 mH with the Terfenol-D rod in place [12]. The inner diameter of the coil is 0.28 in and the length is 2.0 in, approximately the same length as the Terfenol-D rod. A 112 turn pick up coil of the same wire is wound on the inside of the drive coil for sensing the change in flux within the rod. The magnetic circuit was designed using the same software as the composite mold.

4.1.2 Modified Design

The broadband hybrid transducer was modified to work with a 50% volume fraction composite rod of the same size as the monolithic rod it replaces (2 in long by 0.25 in diameter). Because composites require a higher field for similar magnetostriction as a monolithic rod, a larger coil was wound and placed in a new magnetic circuit. The spacing of the three bolts holding the tail mass to the center mass is the limiting factor for the coil size as seen in Fig. 4.3. The main drive coil is composed of an 850 turn coil of 20 AWG magnet wire with a single-layer, 52-turn sensing/drive coil on the inside diameter. The main coil has a resistance of 2.3 Ω and has a field rating of 242 Oe/A (19.2 kA/m), while the inner coil has a resistance of 0.78 Ω and a field rating of 28 Oe/A (2.2 kA/m). The need for a larger drive coil does not allow any room for a permanent magnet due to limited space. The original coil creates a higher field per current, but the new coil has a lower resistance creating a stronger field per voltage (110 Oe/V as compared to 44.6 Oe/V). The coil is contained within a steel cylinder with steel plates at either end to create a complete magnetic circuit with a minimal air gap between the end cap and drive coil casing. The housing is split down the side to reduce generation of eddy currents. A diagram of the basic parts is shown in Fig. 4.2 and a finite element model of the magnetic circuit showing the distribution of flux throughout the system is displayed in Fig. 4.4. The composite sample has a lower stiffness than the monolithic rod, so another Belleville washer is added on each bolt in series to lower the stiffness of the loading springs.

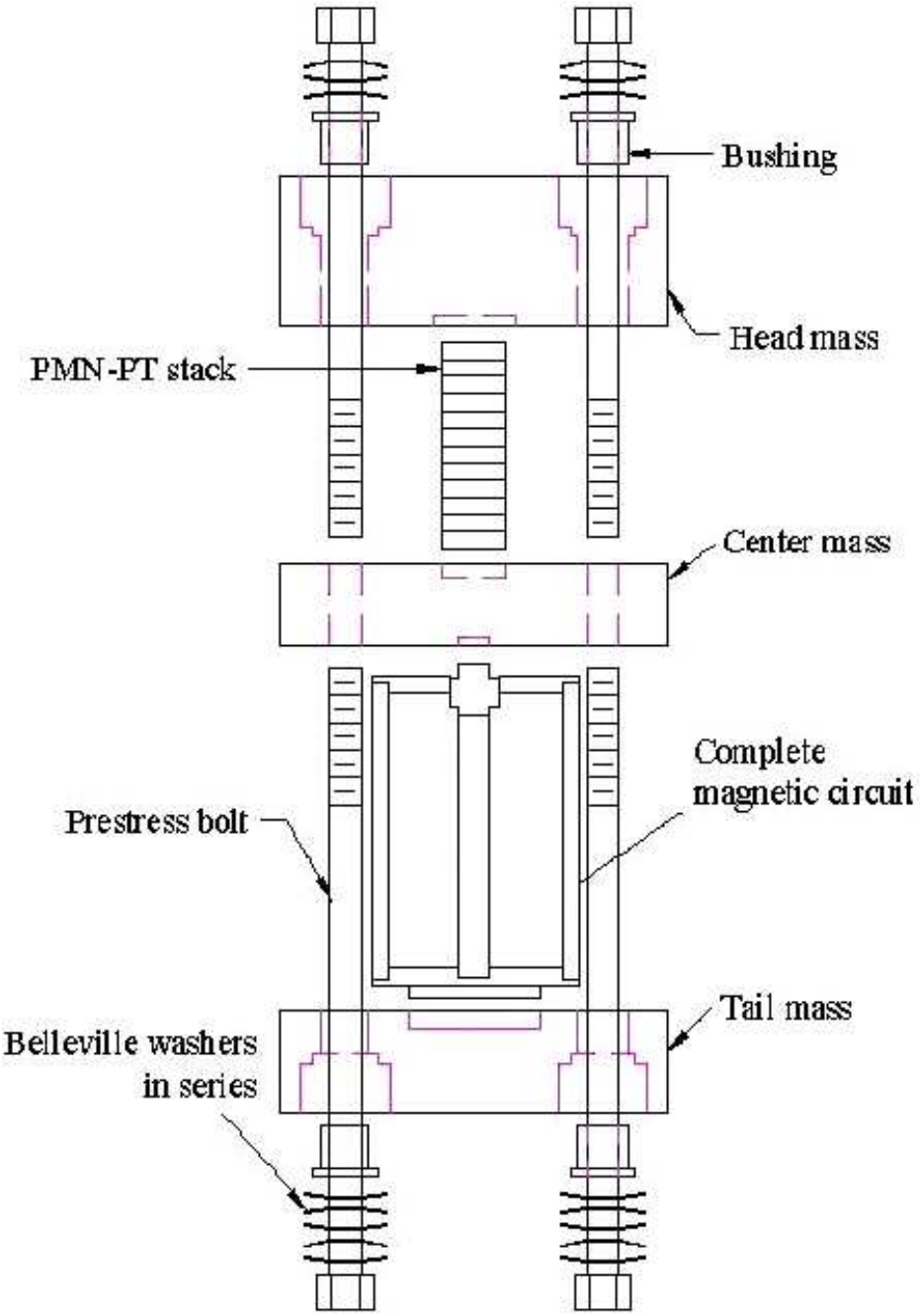

Figure 4.3: Construction diagram for the modified broadband hybrid transducer design. [12]

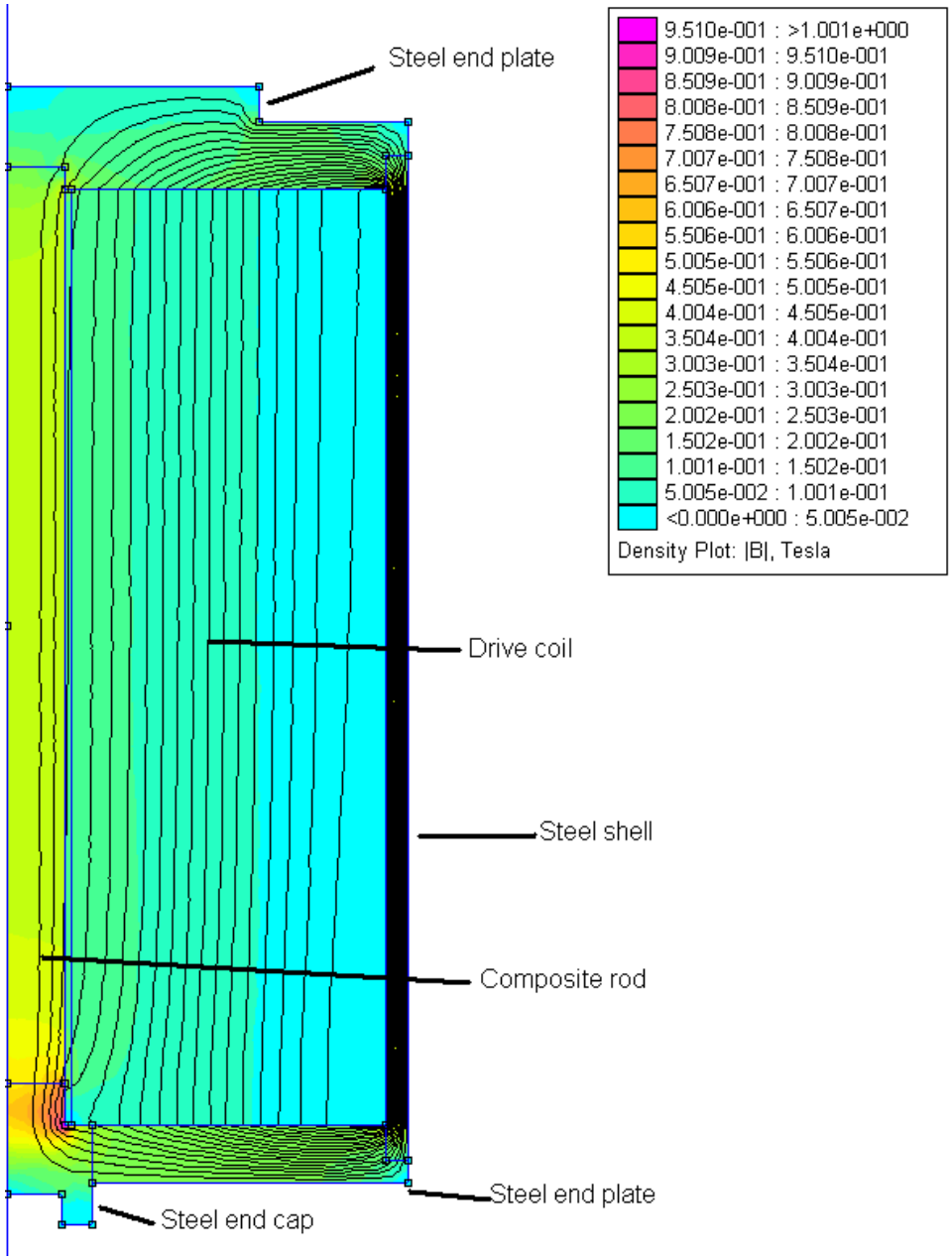

Figure 4.4: Finite element analysis for the modified drive coil showing homogeneity of the magnetic induction throughout the composite rod. [12]

4.2 Static Testing

Quasistatic measurements on the composite samples were conducted in a water-cooled solenoid transducer created in the Smart Materials and Structures Laboratory, as shown in Fig. 4.5. The transducer accepts a specimen of dimensions up to 0.5 in diameter and 4.5 in length for d_{33} mode of magnetization along the longitudinal axis. The top plate, bottom plate, and cylindrical housing were machined from 1018 mild steel due to its high permeability [23]. The specimen holder consists of a 1018 steel bottom cap holding a stress proof 1144 steel base with a stainless steel sample housing screwed to the base. The sample holder is a nonmagnetic tube with a magnetic linear bearing pressed into the top to support a sliding push rod. The housing, pushrod and linear bearing form a closed magnetic circuit for effective routing of magnetic flux through the composite sample. Loading of the composite sample is produced by a cantilevered beam with weights suspended approximately in the middle, as pictured in Fig. 4.6. The system was calibrated by measuring the force applied to the push rod for various suspended weights.

The drive fields are induced by a water-cooled solenoid consisting of 15 AWG magnet wire wound in two groups of 14 layers with approximately 48 turns per layer. The solenoid has a resistance of 3.7 Ω, a gain of 167 Oe/A (13.3 kA/m), and a maximum field of 8.1 kOe at a maximum voltage of 210 V. The magnetic gain was determined from an average of three values from theoretical calculations, finite element modeling, and testing. The input voltage is provided to the coil by two Techron 7780 amplifiers connected in series and producing a voltage gain of 60. Temperature control is provided by a cooling circuit consisting of 0.25 in diameter flexible copper tubing that completely surrounds the entire coil, as depicted in Fig. 4.5. Water is circulated through the cooling coil while monitoring the temperature of the water into and out of the transducer. The surface within the testing chamber is measured with Omega thermocouples connected to a 10-channel Omega signal

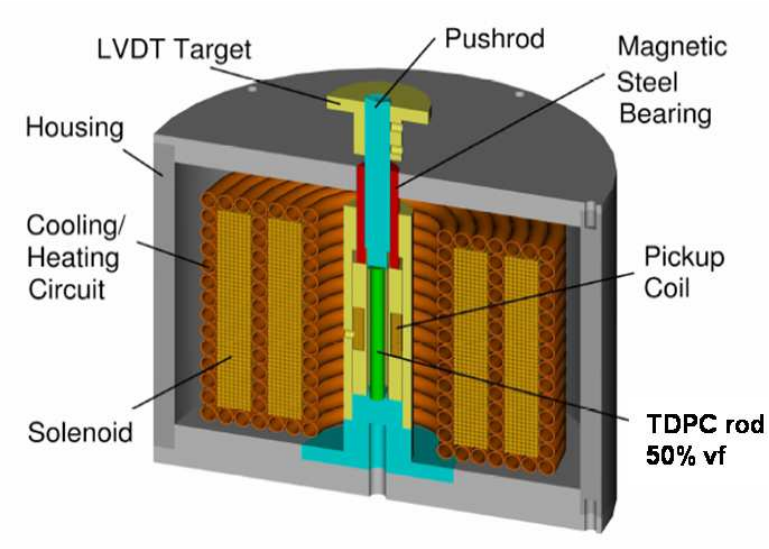

Figure 4.5: Cross sectional view of the water cooled transducer used for quasistatic testing [23].

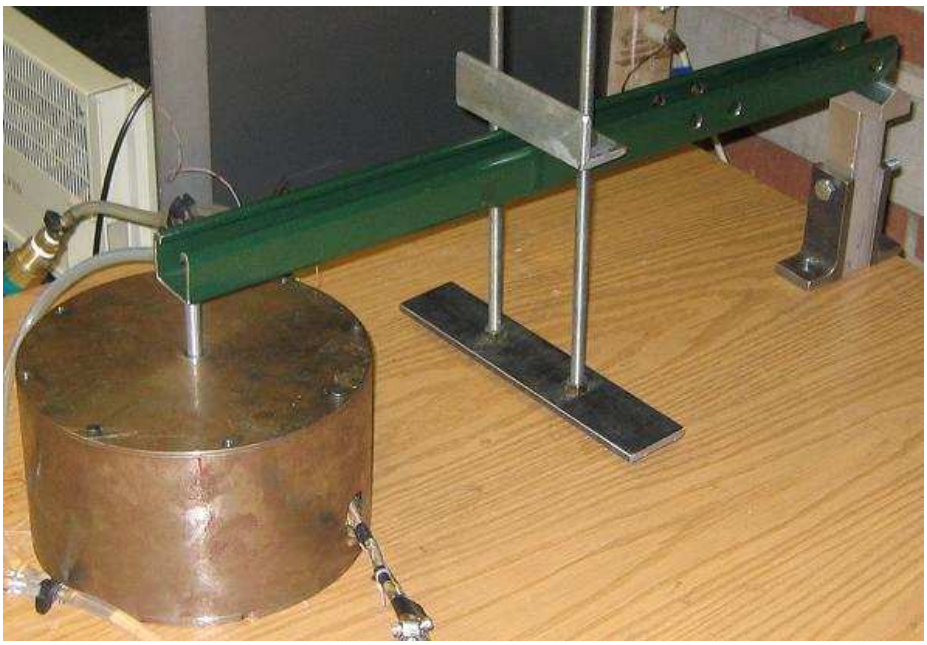

Figure 4.6: The water cooled transducer with loading arm setup.

conditioner. The magnetic flux is measured with a small sensing coil of 104 turns made from 33 AWG enameled wire with a length of 0.6 in and a diameter slightly greater than 0.25 in to clear the composite rods. The sensing coil is connected to a Walker Scientific Incorporated, integrating flux meter with the area per turns ratio set to 33.7 to measure inductance. The strain is calculated from the displacement measured at the push rod by a Lucas Schaevitz MHR-025 linear variable differential transducer (LVDT). The magnetic field is calculated from the current monitor from the Techron amplifiers and the calibrated gain of the transducer, while the magnetization is calculated from the magnetic field and induction.

Due to the low stiffness of the rods, an aluminum push rod is used to test the Terfenol-D particulate composites. A strong magnetic field pulls on a steel push rod with enough force to compress the samples and significantly alter the measurement. Compressive stresses are provided by the loading arm with a steel bearing between the arm and push rod to reduce moments from forming on the sample. The weights are calibrated for loading in increment of 2 MPa of stress on a 0.25 in diameter rod.

The data is recorded using a 5 channel input, 1 channel output SignalStar Vector data acquisition system from Data Physics Corporartion and SignalCalc Mobilyzer Dynamic Signal Analyzer software. The minimum input voltage range was selected for all tests to maximize resolution of the data. The specimens were tested for various loading conditions, measuring the displacement, induction, and current from the amplifiers. Tests were run with a sine wave of 0.16 Hz and an output voltage of 3 V from the software corresponding to a 180 V signal to the transducer. The frequency allows two full cycles for a test time of 12.6 seconds, while the tests were performed with a chamber temperature of 62-65 degrees F. Low frequency tests were conducted independently for the Terfenol-D composite and the PMN-PT stack to determine quasistatic linear coupling coefficients, constant stress permeability μ^{σ} and magnetoelastic coupling coefficient q.

4.3 Dynamic Testing

Dynamic experiments were conducted with the transducer suspended by string,as shown in Fig. 4.7, to isolate the system and prevent exogenous dynamics from affecting the transducer. The magnetic bias and AC drive level were selected to limit motion to the steepest and most linear region on the magnetostrictive curve. Broadband tests were conducted using a sine sweep function from 100-6000 Hz, measuring acceleration of the head mass, applied voltage, and applied current. The dynamic tests were conducted with each section driven independently and with both sections wired in parallel. The transducer was tested with a constant preload applied to the composite and varying AC field or DC bias to characterize the material dynamically. Acceleration tests were also performed for varying preload on the composite with constant static bias and dynamic field.

The Techron 7780 amplifiers provide a voltage and current monitor to record the output signal and calculate the impedance of the system. A PCB U353B16 accelerometer with a PCB 482 signal conditioner box measures the acceleration of the head mass of the transducer. A dsp SigLab 20-22A data acquisition system provides the sine sweeps and DC bias for the dynamic tests performed while recording two channels. Additional dynamic tests were performed with the Data Physics system and SignalCalc software, including sine sweeps and spectrum analysis from band limited noise. The software does not provide a bias signal, so an operational amplifier circuit was used to add a DC voltage bias to the AC signals. Dynamic testing also include a series of tests with the main drive coil powered by an Agilent E3831 DC power supply to provide the bias field and the inner sensing/drive coil to produce the dynamic magnetic field.

The transducer is powered by two Techron 7780 amplifiers connected in electrical series, operating in constant voltage mode, capable of producing up to 240 V_{rms} from a voltage gain of 60. The transducer is operated at low voltages requiring the amplifiers to be

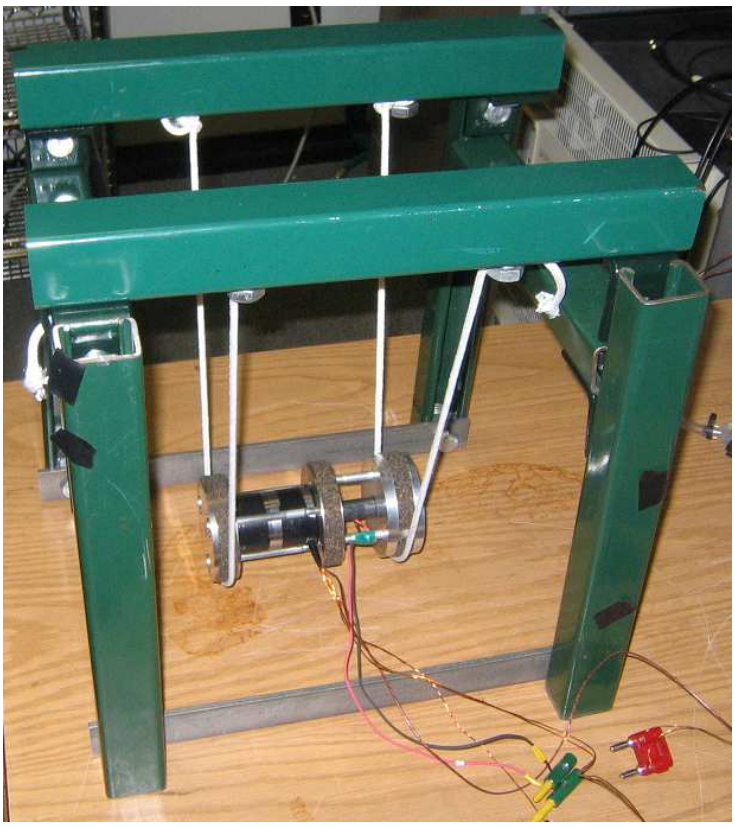

Figure 4.7: The hybrid transducer is suspended to isolate the system.

characterized for low voltages and high frequencies to quantify magnitude and phase shifts. Previous test were conducted using three separate loads to test a resistor, capacitor, and inductor for amplifier response [12]. Tests were conducted up to 20 kHz with an input of 100 mV of band limited noise. The tests concluded the amplifiers have a steady voltage gain of approximately 60 for the full frequency range up to 20 kHz and a consistent phase shift of -1 degree/kHz.

CHAPTER 5

RESULTS AND ANALYSIS

Experiments were performed at quasistatic frequencies to verify operation of Terfenol-D composite rods and to quantify coefficients necessary for the model presented in Chapter 3 to describe the dynamic hybrid transducer. Testing the broadband hybrid transducer was focused on the implementation of the increased bandwidth concept over a single element transducer and validation of the model for a composite rod. The tests show that this Terfenol-D composite sample does not have a clear resonance in the impedance and does not generate a usable Nyquist plot to obtain dynamic material properties. For this reason, quasistatic properties of the composite were measured and applied to the model with some modifications necessary for correlation with the data.

5.1 Quasistatic Testing

The Terfenol-D composite samples were tested at quasistatic frequencies in the water cooled transducer described in Sec. 4.2 for verification of magnetostriction and characterization of its magnetoelastic properties. Low volume fraction samples ranging from 2-7% were tested at high magnetic fields with various loadings but were not tested in the hybrid transducer due to their poor dynamic response. Quasistatic strain comparisons, for varying load and composition is covered in Appendix B for volume fraction samples below 8%.

Previous studies indicate promising dynamic results for epoxy composites of approximately 50% volume fraction inspiring further investigation in the Smart Materials and

Structures Laboratory [29, 24]. A composite rod was fabricated with a volume fraction of 50%, near the upper limit of composition for the current manufacturing method. A composite rod and monolithic Terfenol-D rod were tested at a frequency of 0.16 Hz to approximate a static response. The butterfly curves, for magnetostriction of monolithic and composite Terfenol-D specimens are compared in Fig. 5.1. The slope for the composite is much less than that of the monolithic material, indicating a large decrease in response for a given magnetic field excitation. The strain curves have similar widths,suggesting little hysteresis at low frequencies.

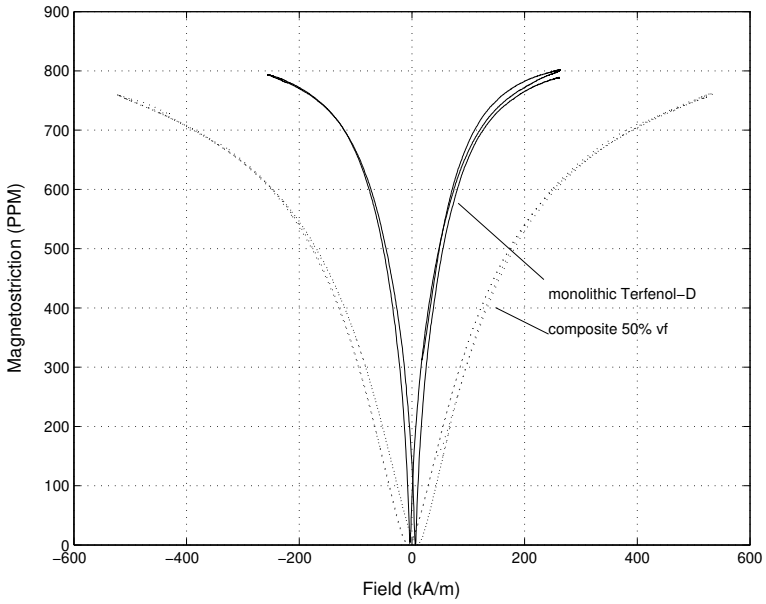

Figure 5.1: Strain versus magnetic field for a Terfenol-D monolithic and 50% volume fraction particle composite rod tested at 0.16 Hz.

The steepest and most linear range of the magnetostriction curve for the Terfenol-D composite is displayed in Fig. 5.2 and concentrated between 30 and 60 kA/m with only a slight decrease in slope immediately above these values. This is a desirable operating range due to the steep strain per magnetic field slope, while being a linear region validates use

of linear piezomagnetic constitutive relations. At low fields the composite displays lower permeability and susceptibly values than the monolithic rod while exhibiting a smooth transition to saturation as displayed in Fig. 5.3.

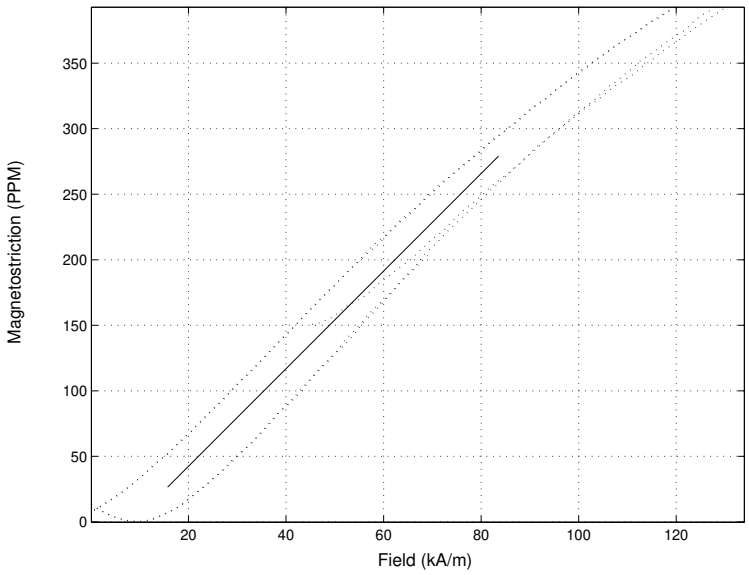

Figure 5.2: A closer look at the most linear region of the strain-magnetic field plot with a line added for comparison.

Two properties needed for model implementation include the magnetoelastic coupling coefficient q (strain per field) and constant stress permeability μ^{σ} (induction per field) for the composite rod. These properties are calculated from a biased minor loop test from 27-40 kA/m with a 4 MPa load on the composite rod corresponding to the load found in dynamic conditions. Measurements were taken for frequencies between 1-5 Hz which yield similar values as shown in Table 5.1.

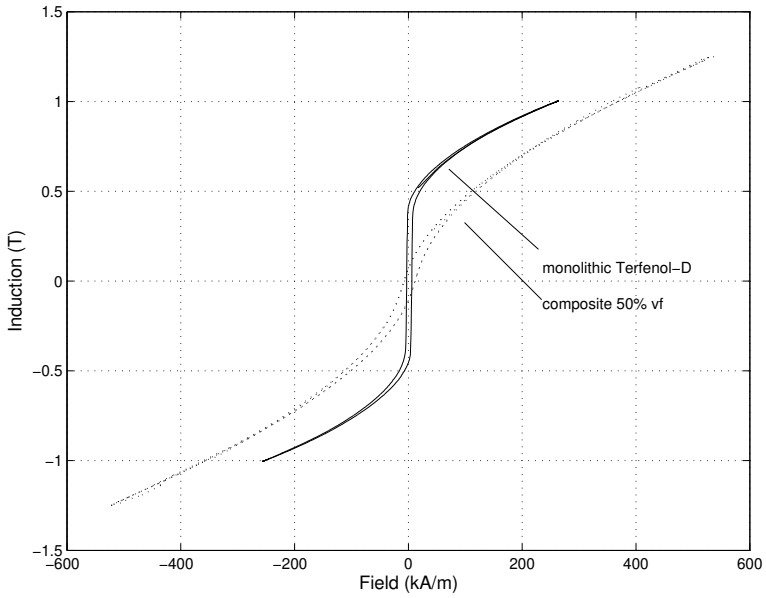

(a)

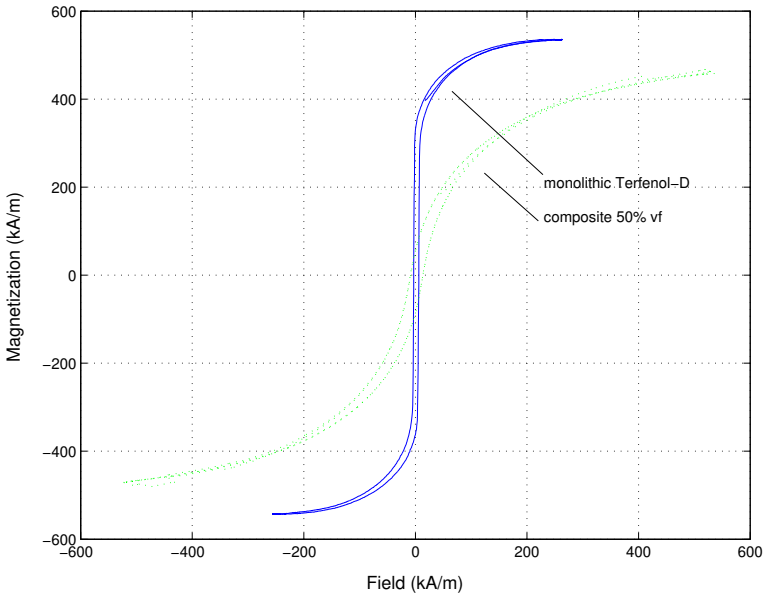

(b)

Figure 5.3: (a) Strain versus magnetic field and (b) magnetization versus magnetic field for a Terfenol-D monolithic and 50% volume fraction particle composite rod tested at 0.16 Hz.

	Monolithic	50% Composite	
q	$4.96\text{x}10^{-9}$	$2.71\text{x}10^{-9}$	m/A
μ^{σ}	$6.28\text{x}10^{-6}$	$3.36\text{x}10^{-6}$	H/m

Table 5.1: Coefficients calculated from recorded data for Terfenol-D [12].

5.2 Dynamic Testing

Initial dynamic measurements were conducted in an existing hybrid transducer which had been optimized by Downey and Dapino for a monolithic Terfenol-D rod [12]. All dynamic testing was performed with the full transducer assembled and suspended by the testing rig as shown previously unless specified. The magnetic circuit has been modified with a different magnetic circuit and further testing was performed with a different data acquisition system. All dynamic tests reported were performed with a 50% Terfenol-D particle composite fabricated with epoxy vinyl ester resin. The transducer was operated in three modes: the magnetic coil for the composite powered with the PMN-PT stack as an open circuit, the PMN-PT stack powered with the coil open, or with both parts powered in electrical parallel.

5.2.1 Original Hybrid Testing

SigLab provides the signal and data acquisition for the original transducer configuration with software capable of providing a DC offset to generate a bias magnetic field and a swept sinusoidal excitation to generate a dynamic magnetic field. Electrical impedance measurements represented as Nyquist plots, are necessary for determining the coupling coefficient, mechanical stiffness, modulus of elasticity, quality factor, and internal damping for the composite rod at given operating conditions. The measurements suggest a clear

acceleration response from the composite but of a lower magnitude than that of the monolithic Terfenol-D rod. The resonant frequency response in the electrical impedance plot was recorded as a small peak only noticeable upon close inspection and too small to generate a usable Nyquist plot.

Fields higher than optimal as determined by quasistatic tests were employed to quantify the dynamic performance of the composite rod over a wide operating range. The preload remained constant while varying the magnetic field and magnetic bias with only the magnetic coil powered. The electrical impedance was measured as the complex transfer function of applied voltage divided by current. Bias tests were run from 1250-1400 Hz with a sinusoidal magnetic field of 12.5 kA/m and static bias fields from 20-250 kA/m as shown in Fig.5.4(a). A narrow frequency range was used to compensate for the small response of the composite which is not clearly displayed with a larger magnitude plot. Testing indicates that increasing the magnetic bias field increases the change in magnitude between the peak and valley of the impedance and shifts these occurrences to a lower frequency. A series of tests were performed for the same frequency range, a magnetic bias of 60 kA/m and dynamic field from 3-37 kA/m in small increments as shown in Fig.5.4(b). Increasing the dynamic field decreases the impedance response for the composite and decreases the resonant frequency.

Acceleration tests were performed recording the transfer function acceleration of the head mass per current while varying the load on the composite sample to determine the optimal preload. The bolts holding the tail mass to the center mass, compressing the composite rod were tightened until the rod has a small stress of which is considered a base setting. The load was increased by turning all three bolts in increments of a half turn up to 2 turns with the Belleville washers increasing the preload. A test was run from 600-1800 Hz on the hybrid transducer with only the composite powered using a bias field of 60 kA/m and drive field of 12.5 kA/m to determine the performance of the composite

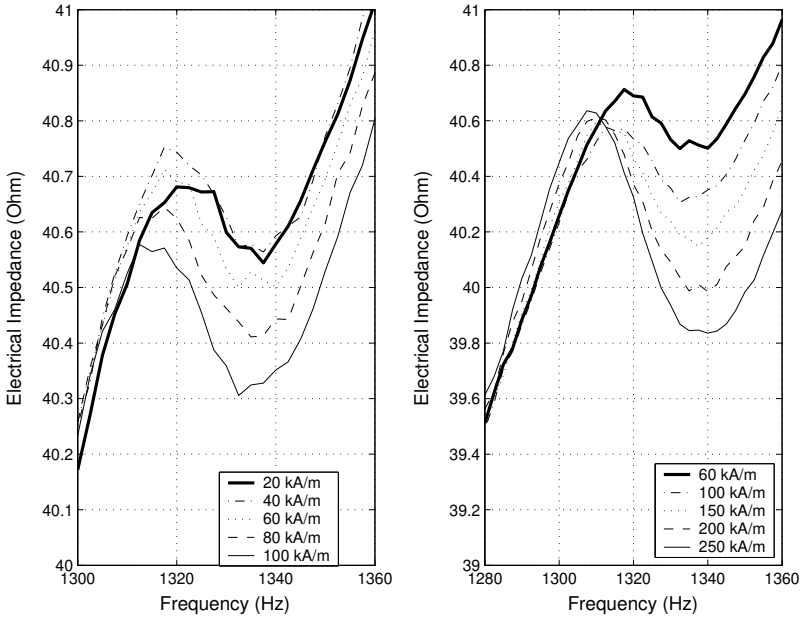

(a)

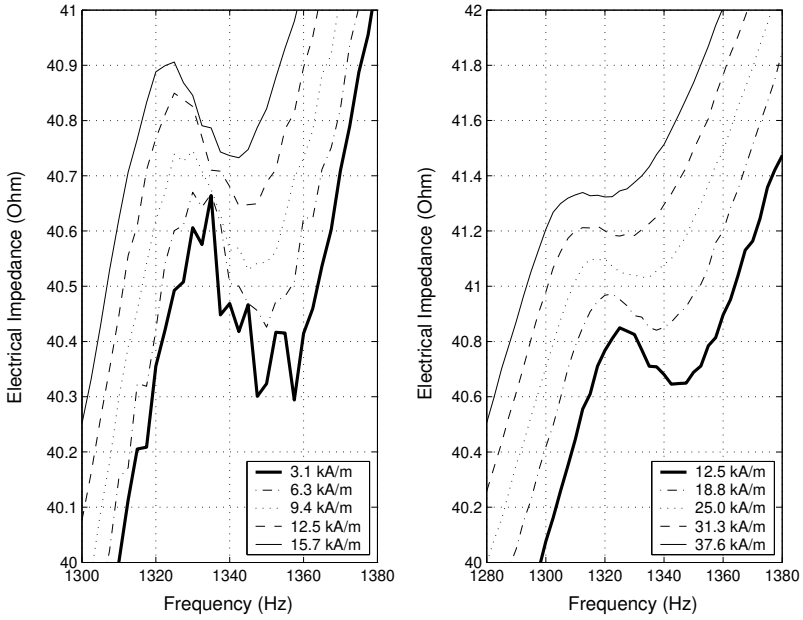

(b)

Figure 5.4: (a) Electrical impedance with varying bias and (b) electrical impedance with varying field for the composite rod at constant stress and only the magnetostrictive section powered.

rod alone while operating in its linear range. Increasing the preload on the composite rod, increases the resonant frequency of the system by increasing the stiffness of the rod as displayed in Fig. 5.5, where a maximum performance was achieved with one half turn from the base setting. A similar test was performed with both elements powered in parallel, a bias field of 150 kA/m and a dynamic field of 100 kA/m while varying loads. The head velocity was calculated from the integral of the acceleration as shown in Fig/ 5.6. The same trend is observed for the low frequency resonance, but there is no change in the high frequency resonance, indicating a lack of coupling between the preload and PMN-PT stack. A significant antiresonance occurs at 2000 Hz in all tests with this experimental setup. This may be attributed to a deviation from the ideal 90 degree phase shift between the forces generated as discussed in Chapter 3, due to increased damping of the epoxy binder over the monolithic material.

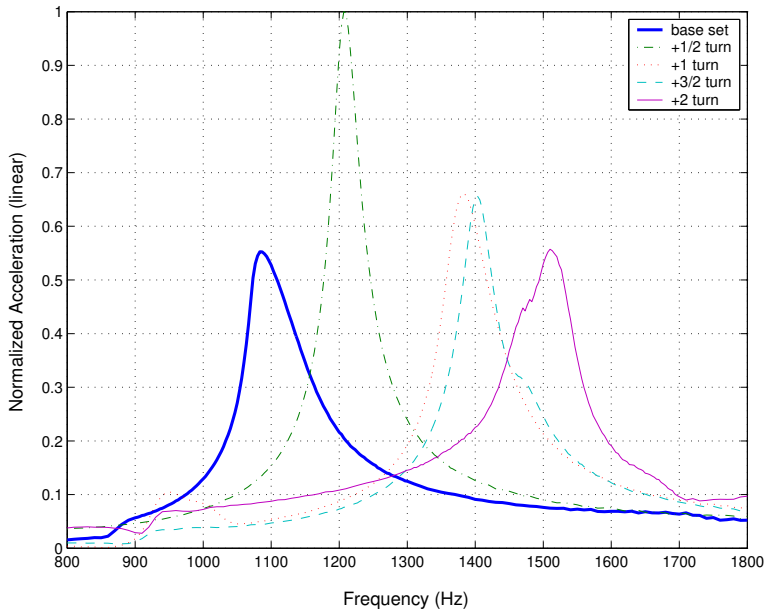

Figure 5.5: Normalized transfer function head acceleration response per current with only composite powered.

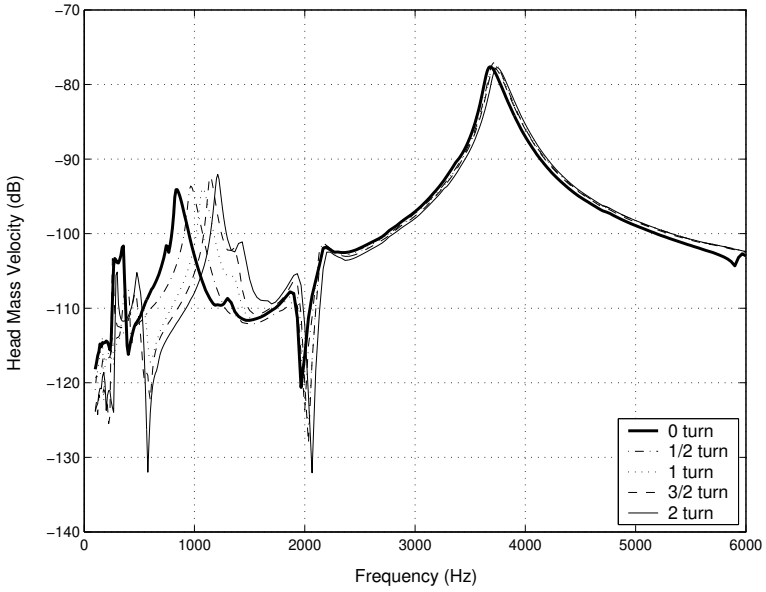

Figure 5.6: Head mass velocity velocity response with full transducer powered for constant static and dynamic magnetic fields and varying preload.

A series of tests were conducted powering the Terfenol-D composite section, the PMN-PT electrostrictive stack, and both sections wired in parallel to quantify the change in bandwidth while keeping all other variables constant. Typical results for head velocity are shown in Fig. 5.7 for a 150 kA/m bias and 100 kA/m dynamic field with a constant preload. The composite extends the bandwidth from 100 to 1500 Hz, but the response is of low magnitude compared to the performance of a PMN-PT stack or monolithic Terfenol-D rod as tested previously [12].

The electrical impedance was measured for each section and the full transducer, excited by a sinusoidal voltage sweep of 100-6000 Hz, a bias field of 150 kA/m and a dynamic field of 100 kA/m. The impedance and Nyquist plot with the PMN-PT section powered are shown in Fig. 5.8. The response is characterized by a decreasing impedance with increasing frequencies and a clear resonance displayed as expected for a capacitive element. The electrical impedance of the composite rod consists of a straight line with a slight deviation

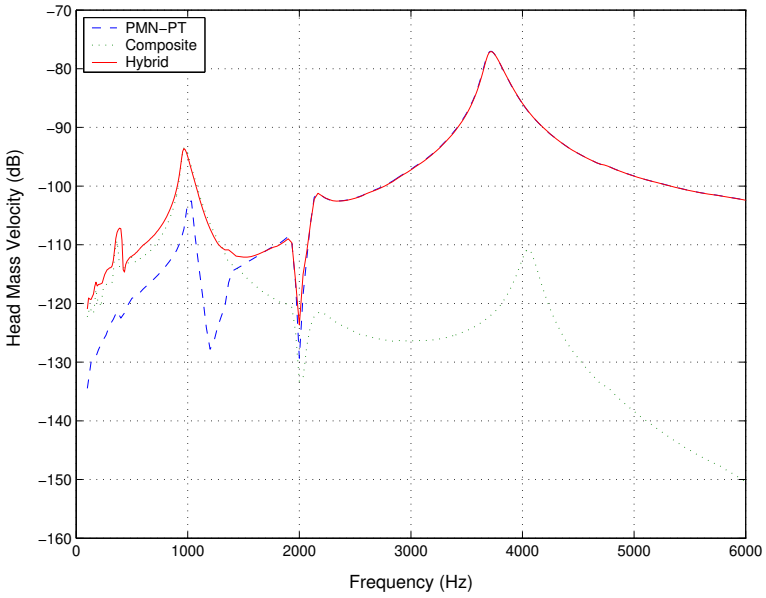

Figure 5.7: Transfer function of head velocity response per current for each section powered individually and for the full hybrid transducer powered in parallel.

of phase for this drive level and frequency range and is not displayed in the results. The full system has an impedance as shown in Fig. 5.9 displaying two resonances and clear Nyquist loops. The large loop is for the electrical system, the smaller loop is for the PMN-PT section, but a third smaller loop should be apparent for the composite that was evident when the system used a monolithic rod [11]. The weak composite response from the hybrid transducer motivated further testing with a new drive coil.

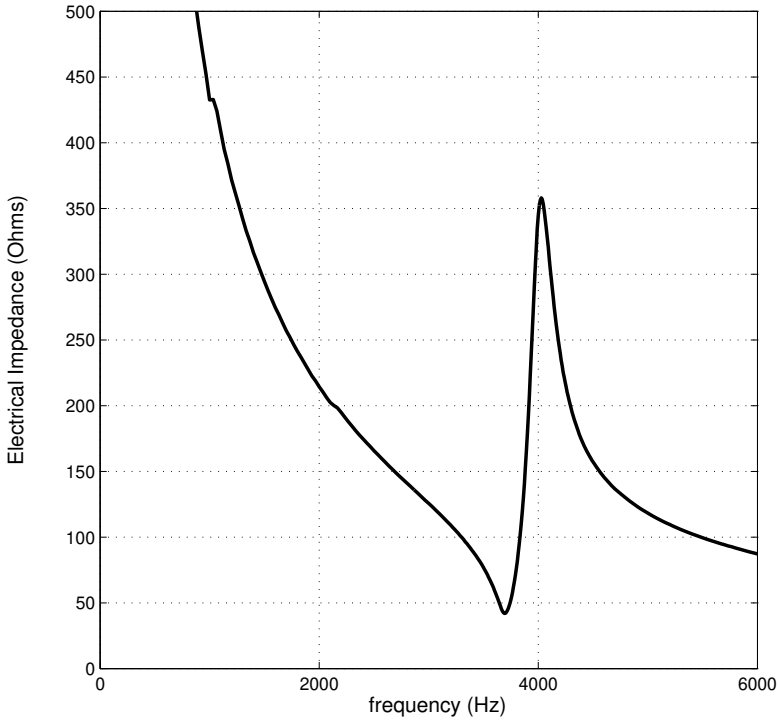

(a)

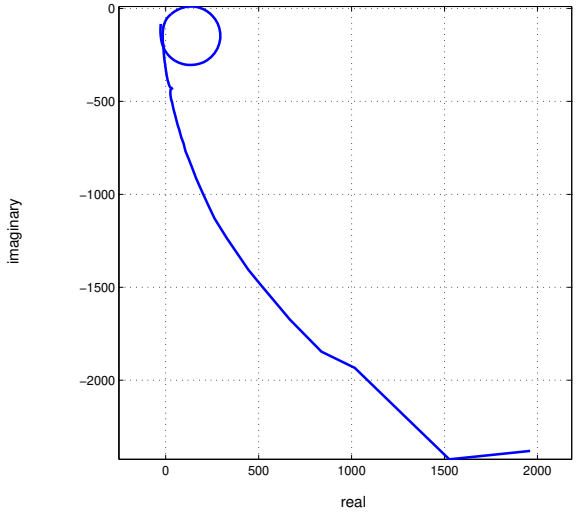

(b)

Figure 5.8: (a) Transducer electrical impedance function with only PMN-PT section powered and (b) corresponding Nyquist plot of the data.

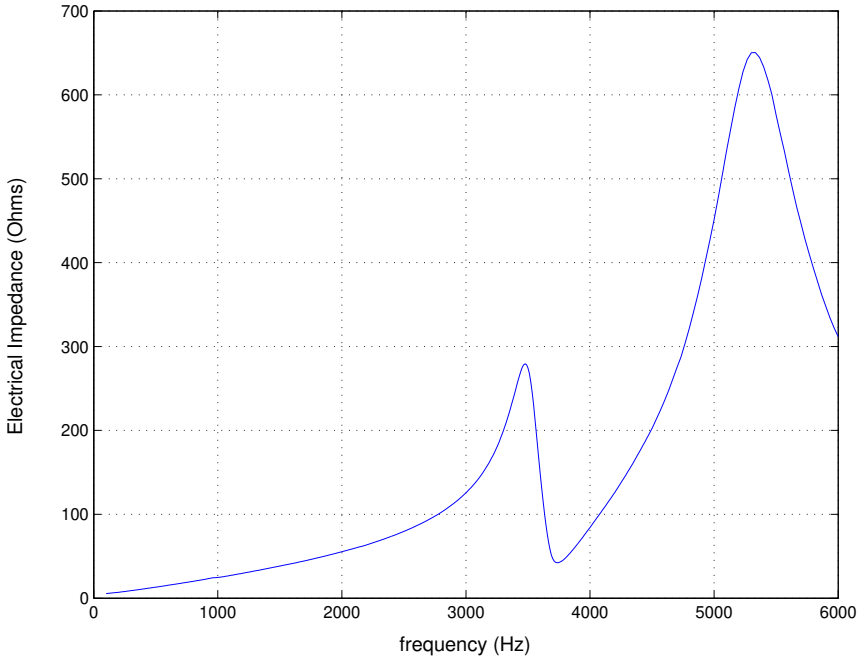

(a)

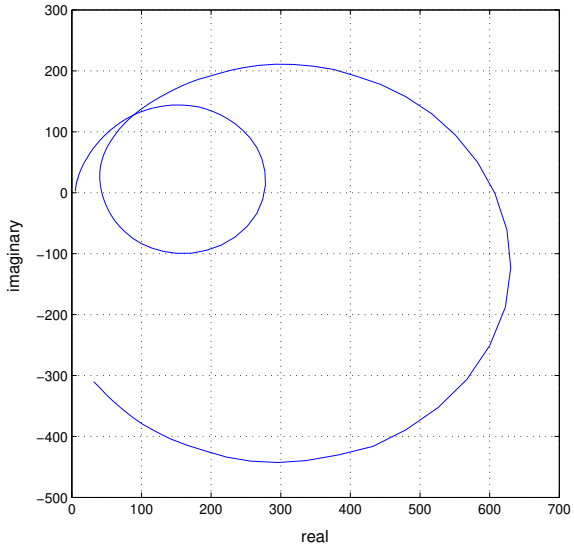

(b)

Figure 5.9: (a) Transducer electrical impedance function with both sections powered in parallel and (b) corresponding Nyquist plot of the data.

5.2.2 Modified Hybrid Testing

A more powerful coil was wound to decrease the resistance of the coil and increase the drive field for a given voltage. The coil consists of 850 turns of 20 AWG wire, with a resistance of 2.3 Ω, and an output of 242 Oe/A. A single row of 26 AWG wire, 0.8 Ω resistance, and 28 Oe/A output was wound at the center for a pickup/drive coil. The Data Physics system was used in this series of tests with a bias circuit providing the static offset for the magnetic field. The software allows for sinusoidal frequency sweep testing with recording of two transfer functions and average power spectrum allowing direct measurement of the acceleration as opposed to the transfer function acceleration per current as in the previous dynamic tests. Testing with a swept sinusoidal field with a static bias for the main drive coil indicated similar response from the composite as with the first coil. A new set of test were performed with the main drive coil powered by a DC power supply to create a static bias field and a separate pickup/drive coil utilized to create the dynamic magnetic field. All tests presented in this section correspond to the latter set up with the dynamic and static magnetic fields decoupled in separate circuits.

The head mass velocity was recorded with the composite powered, varying bias from 8-48 kA/m and a 5 kA/m dynamic field over the full operating frequency as shown in Fig. 5.10(a). A significant increase in response is observed up to 32 kA/m as the increase in bias increases the resonant frequency. Dynamic field testing was performed with the full transducer powered to characterized velocity response as shown in Fig. 5.10(b). The velocity continues to increase with increasing magnetic field while the resonant frequency decreases. The large antiresonance apparent in the original design is reduced with the new magnetic circuit, likely from the large difference between resistance and inductance of the different coils shifting the phase of the generated forces.

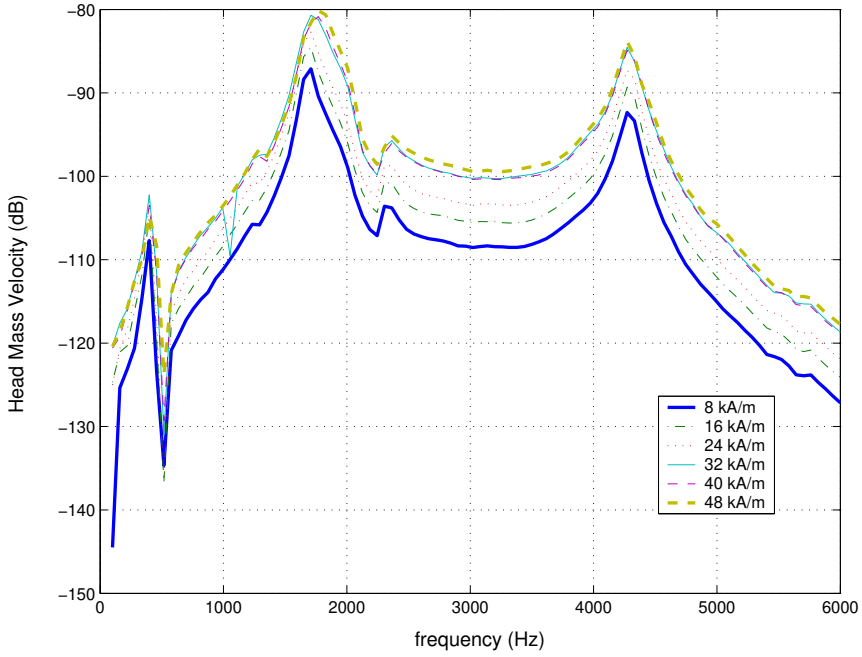

(a)

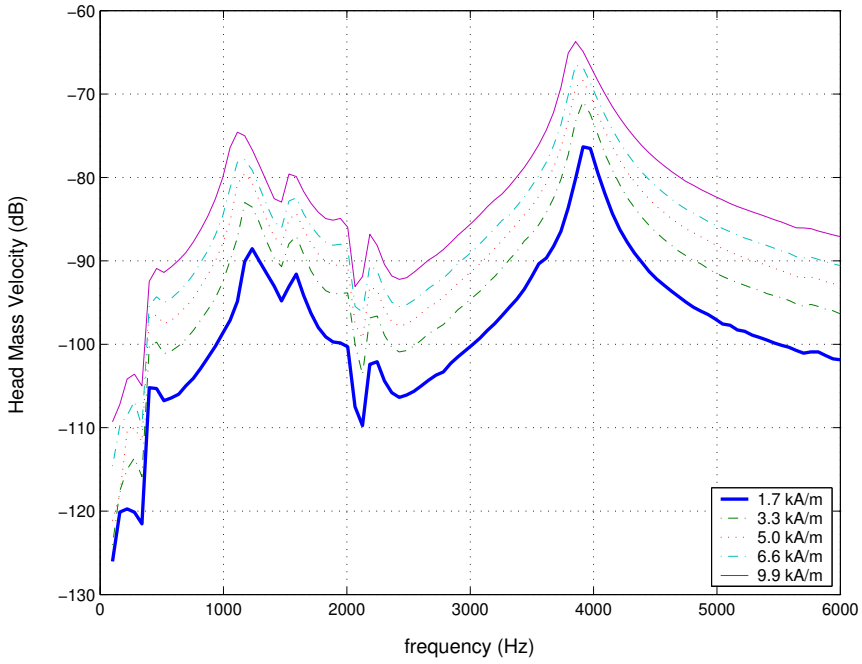

(b)

Figure 5.10: (b) Head velocity response with varying field powered by magnetostrictive section and (a) varying bias with full transducer powered.

The head mass velocity was measured for varying preload as discussed in Sec. 5.2.1, for only the magnetostrictive section powered at a bias of 24 kA/m and dynamic field of 6.6 kA/m, as shown in Fig. 5.11. A similar trend to that in Fig 5.6 was observed, and an optimal setting of 1 turn for maximum response was established. Each active section of the transducer was tested individually and with the whole transducer powered with the optimal preload, a bias of 24 kA/m and field of 6.6 kA/m, as shown in Fig. 5.12, to compare frequency responses. The bandwidth is effectively increased for lower frequencies but to a much smaller magnitude than the monolithic rod. The new design has an irregular response between 1200-2500 Hz that may be caused by vibrations in the individual components comprising the magnetic circuit.

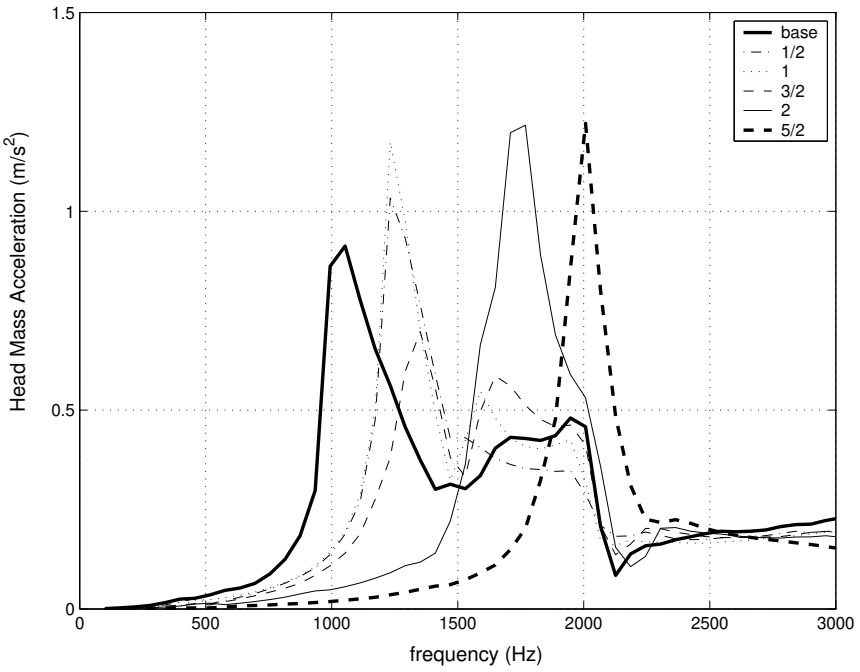

Figure 5.11: Head velocity response with only the coil powered, constant magnetic field and varying preload.

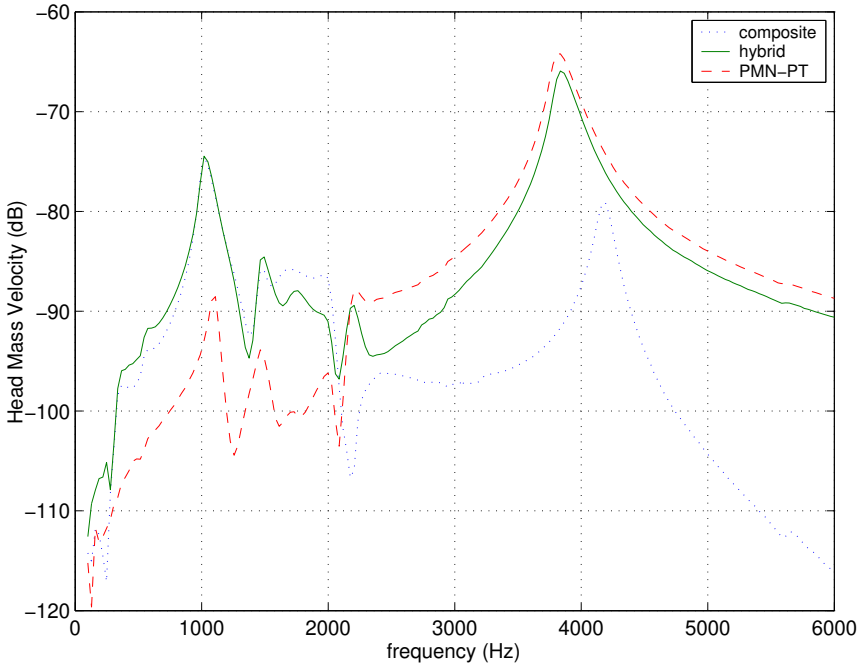

Figure 5.12: Head velocity response for each section powered individually and for the full hybrid transducer powered in parallel

A clear resonance is not evident in the electrical impedance from the swept sinusoidal testing of the composite motivating another set of tests using band limited noise of 2.4 V (6.6 kA/m) and a bias field of 0.13 V (32 kA/m) averaging over 100 runs. The composite rod is placed inside the coil laying on its side with both ends unrestrained to test up to 20 kHz, the maximum bandwidth of the data acquisition system. With no load a resonance is apparent at 16.2 kHz and an antiresonance at 16.85 kHz as shown in Fig. 5.13(a). The rod will not do any work without a load, but the test validates the existence of a measurable resonance within the material. With the transducer vertical and a mass sitting on the rod, the electrical impedance resonance decreases in frequency, as expected, and in magnitude. The composite rod does not appear to generate enough force to measure an electrical impedance loop under the full loading conditions of the hybrid transducer. The electrical impedance of the full system powered by the random noise excitation is displayed

in Fig. 5.13(b), where it is evident that the flat response of the composite dominates the overall response of the system with only a small effect from the PMN-PT stack. This is likely from the low resistance and inductance of the small drive coil.

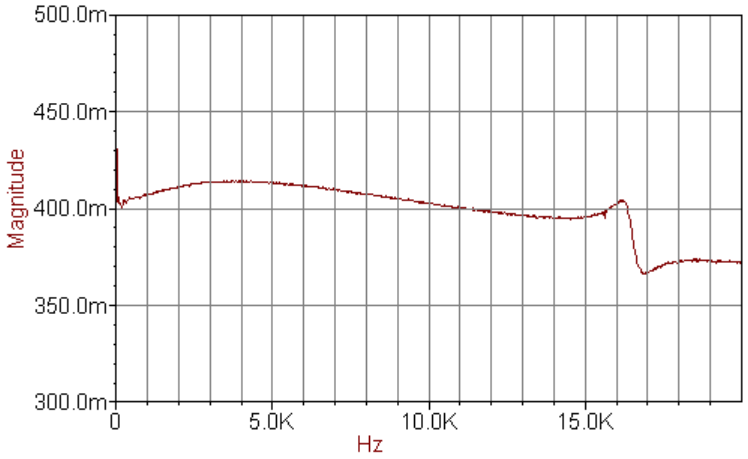

(a)

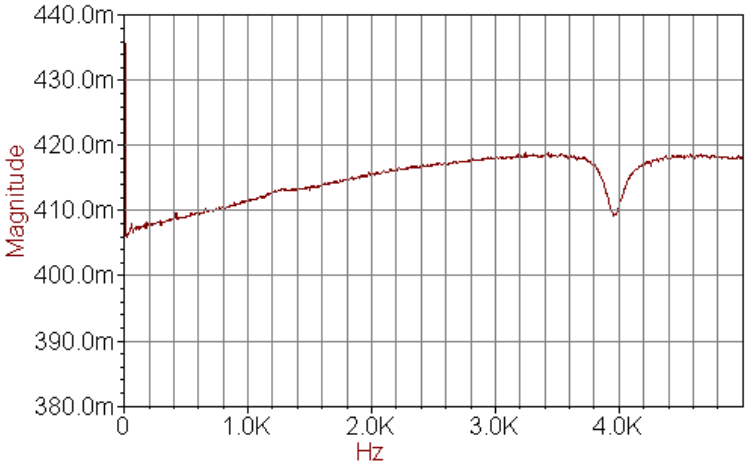

(b)

Figure 5.13: (a) Electrical Impedance of unrestrained Terfenol-D composite rod and (b) full transducer powered in parallel excited by band limited noise.

5.3 Model Correlation

The linear model of Chapter 3 is compared to the measurements shown in Fig. 5.12. Entering the quasistatic properties into the model yields a poor fit, but the properties can be justifiably modified for correlation to the model. If dynamic properties are capable of being obtained, this would not be necessary since the model has already been verified for a hybrid system utilizing a monolithic Terfenol-D rod and PMN-PT stack with varying loads and impedances [12, 28, 11]. The values utilized in the model are shown in Table 5.2.

	Terfenol-D			PMN-PT	
c_2	$5.11\text{x}10^{-8}$	m/N	c_1	$7.78\text{x}10^{-9}$	m/N
r_2	250	Ns/m	r_1	200	Ns/m
k_2	0.08		k_1	0.279	
q	$2.71\text{x}10^{-9}$	m/A	d_{33}	$3.08\text{x}10^{-10}$	m/V
μ^σ	$8.36\text{x}10^{-6}$	H/m	ϵ^σ	$3.25\text{x}10^{-8}$	F/m
n	2090	turns/m	N	62	layers

Table 5.2: Material properties used for model.

The electrostrictive section was dismantled and reassembled to approximately the same preload as originally tested. The properties utilized in the model were recorded from previous work, indicating the chance of a slight variation in preload that would effect the stiffness. An increase of only 6% in the PMN-PT stack compliance is necessary for the high frequency resonance to match the data as displayed in Fig. 5.14 for the PMN-PT section powered. The lower frequency fits well with only slight deviation, but the 1200-2500 Hz range will be ignored due to the irregularities in the data. The model predicts a lower first resonance for the composite without power due to the increased stiffness of the open circuit of the drive coil.

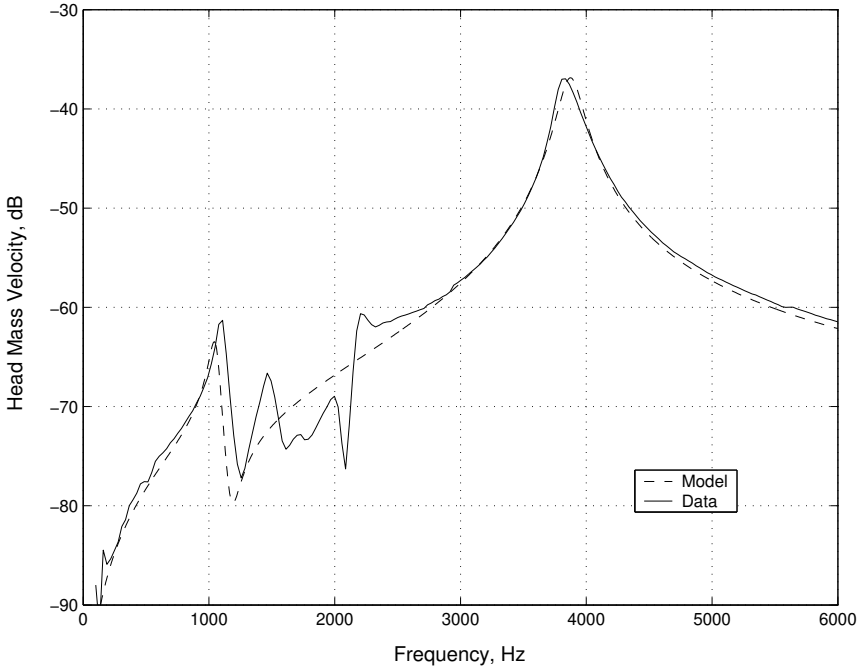

Figure 5.14: Linear model correlation to collected data for the hybrid transducer with only the PMN-PT section powered.

The modulus of elasticity for the composite was measured by MTS testing in the load range of 2-10 MPa yielding a value of 6.7 GPa for the elasticity and 4.3 MN/m stiffness with no applied magnetic field. While These values predict a resonant frequency of half the measured value, a large increase in stiffness (reduction in compliance) shifts the model resonance to the measured data as shown in Fig. 5.15 with only the composite powered. This can be justified since the elasticity was measured without an applied magnetic field, which would increase the stiffness due to activation of the Terfenol-D in a soft matrix. The permeability was also increased to adjust the magnitude of the second resonant frequency. The loading procedure for the composite makes it difficult to determine the exact preload which may be less than the static load of 4 MPa the permeability was calculated from. A lower stress level would increase the slope of the permeability as seen in the low volume fraction samples in Appendix B. The shift of the high frequency resonance with only the

composite section powered is caused by the increase in stiffness from the open circuit condition of the PMN-PT.

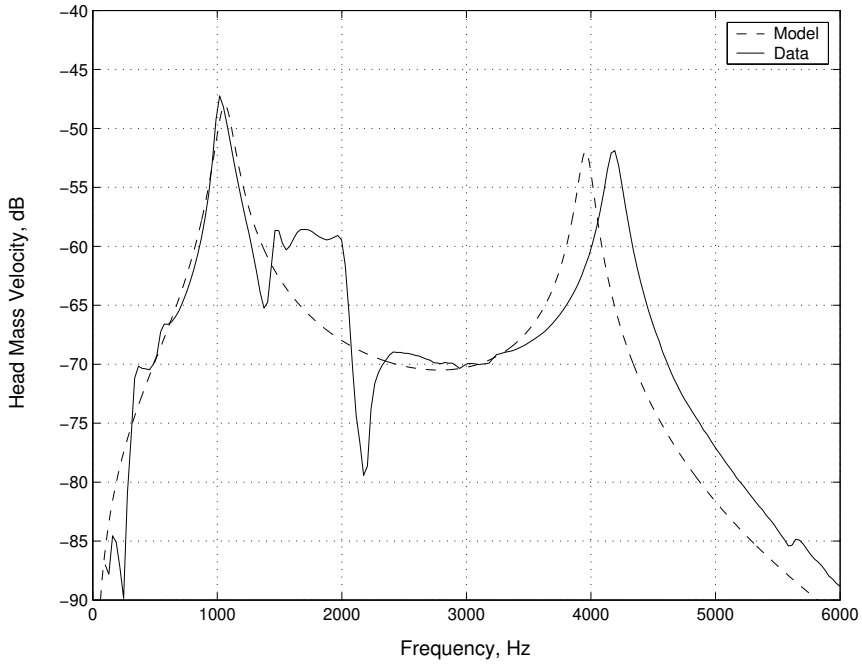

Figure 5.15: Linear model correlation to collected data for the hybrid transducer with only the Terfenol-D section powered.

The head mass velocity with the full transducer powered was tested and modeled as shown in Fig. 5.16. The bandwidth is extended below 1000 Hz with the hybrid design, and refinement of the transducer assembly should reduce the distortion of the 1200-2500 Hz range of response to enable accurate modeling. This model could be used for design or control applications with little error due to the close correlation of the model with proper material properties.

The variation in head mass velocity response is too great to be useful for a sonar device application as tested. Downey demonstrated large improvement for response variation by testing a loaded condition to simulate water [12], thus greatly reducing the sharp peaks

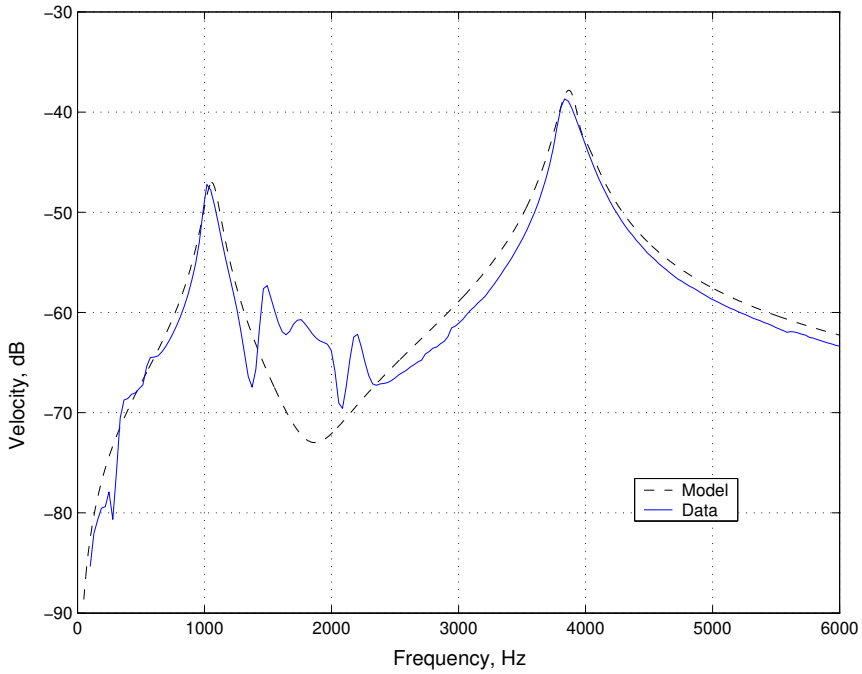

Figure 5.16: Linear model correlation to collected data for the hybrid transducer with the full system powered.

created by the active elements. In U.S. Navy applications, Tonpilz sonar transducers are often placed in arrays with multiple units that decrease the variation which means the design may be applicable [7] if a greater response can be realized.

CHAPTER 6

CONCLUDING REMARKS

The goal of this project evolved from characterizing quasistatic performance of Terfenol-D composite material to application of composites to a hybrid transducer design and validation of an existing linear model for describing smart material hybrid systems.

This thesis was presented as follows. The first chapter presents background information on magnetics, concepts of magnetostriction, previous studies on Terfenol-D composites and applications of hybrid smart material transducers. The magnetic circuit mold design and fabrication of the aligned Terfenol-D particle composites is examined in Chapter 2. A linear model is presented in Chapter 3 comprising a mechanical system to characterize the physical geometry, an electroacoustics section to couple the mechanical and electrical regimes and quantify material properties, and piezoelectric and piezomagnetic constitutive relations to characterize the response and phase of the active elements. Chapter 4 examines the design of a hybrid Terfenol-D/PMN-PT broadband transducer, a set of modifications made to the design, and the testing methods and equipment utilized for the experimentation. The results of the quasistatic testing, broadband dynamic testing, and model correlation are discussed in Chapter 5.

6.1 Conclusions

Fabrication and testing of Terfenol-D aligned particle epoxy composites was completed to obtain a better understanding of their performance and behavior. The magnetostrictive

composites were studied at quasistatic conditions to quantify material properties yielding a high level of strain, but a noticeable decrease in performance occurred, relative to monolithic Terfenol-D, in regards to total strain and coupling coefficient.

The analysis of a hybrid smart material broadband transducer was evaluated for two different configurations. An increase in bandwidth over a single element was realized, but the response was comparably weak compared to that of a monolithic rod. The size of the transducer appears to be beyond the ideal performance range of the composite in terms of mass and stiffness. The PMN-PT overpowers the composite sample indicating that for the geometries considered, they are not adequate as complementary materials due to their force generation imbalance.

A linear model is generally inadequate to describe highly nonlinear materials, but its use is justified in this study due to the biased, low signal operating range of the materials. The model can be derived from classical mechanical vibrations principles, electroacoustics theory and smart material constitutive relations readily available in the literature. The model also allows for dynamic characterization of material properties which are more accurate than static properties for use in the dynamic model, although the properties were quantified from a combination of quasistatic measurements and fit to experimental data.

6.2 Future Work

Numerous studies have been published for soft aligned Terfenol-D composite properties, but few transducer applications have been realized. The low elasticity in not ideal for large actuators but may be suitable as a sensor material. Adding various particles to the epoxy to customize properties is worth further investigation, such as adding electrostrictive and magnetostrictive materials to balance out the inductance and capacitance. Recent studies have explored the fabrication and material properties of ferromagnetic shape memory alloy particle composites which may hold more potential than Terfenol-D composites.

A small mass transducer may be capable of utilizing a composite rod of a lower volume fraction to provide a more economical solution for an existing design or using a high volume fraction for high performance applications. A hybrid transducer with magnetostrictive and electrostrictive composites could warrant further investigation by optimizing the response, phase shift and balancing the magnitude response of the two materials. A hybrid composite design would require small masses and a low preload to achieve significant response as concluded from the composite testing.

APPENDIX A

ELECTROMAGNETISM UNITS AND CONVERSIONS

Quantity	Symbol	CGS	SI	Conversion/Value
Electric charge	q	-	coulomb (C)	C=A*cdot*s
Current	I	-	ampere (A)	-
Electrical potential	V	-	volt (V)	-
Resistance	R	-	ohm (Ω)	Ω=V/A
Inductance	L	-	henry (H)	H=V·s/A
Capacitance	C	-	farad (F)	F=A·s/V
Electric Field	E	-	V/m	-
Electric Displacement	D	-	C/m^2	-
Permittivity	ϵ_0	-	$C^2/N{\cdot}m^2$	$8.85x10^{-12}$
Magnetic Field	M	oersted (Oe)	A/m	Oe=79.58 A/m
Magnetic Induction	B	gauss	Tesla (T)	gauss=10^{-4} T
Magnetization	M	emu/cc	$A{\cdot}m^2$	-
Magnetic Flux	Φ	maxwell	weber (Wb)	maswell=$10^{-}8$
Permeability	μ_0	-	H/m	-
magnetic moment	m	emu	$A{\cdot}m^2$	-

Table A.1: Variables, units and conversions of electricity and magnetism.

APPENDIX B

LOW VOLUME FRACTION ANALYSIS

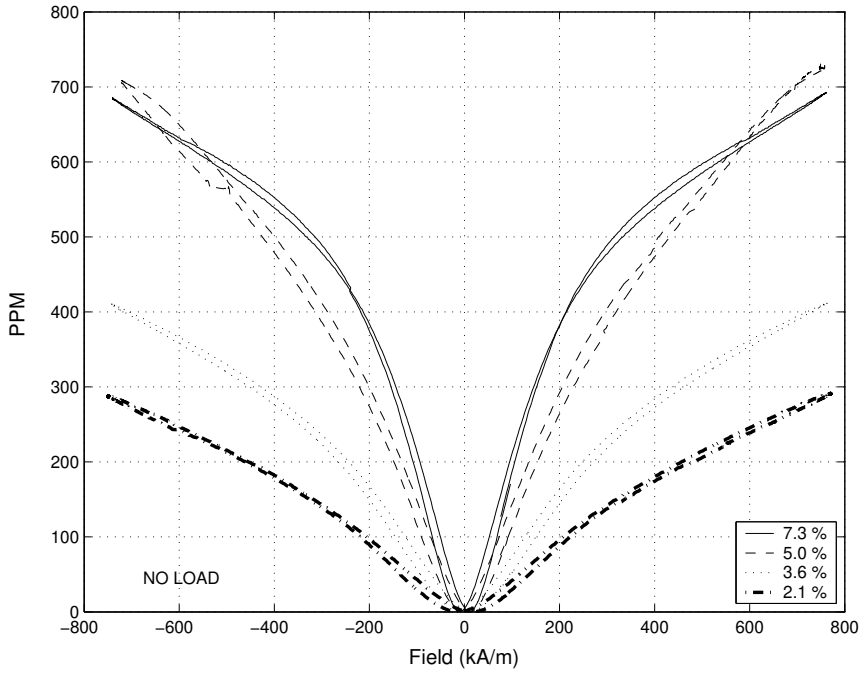

(a)

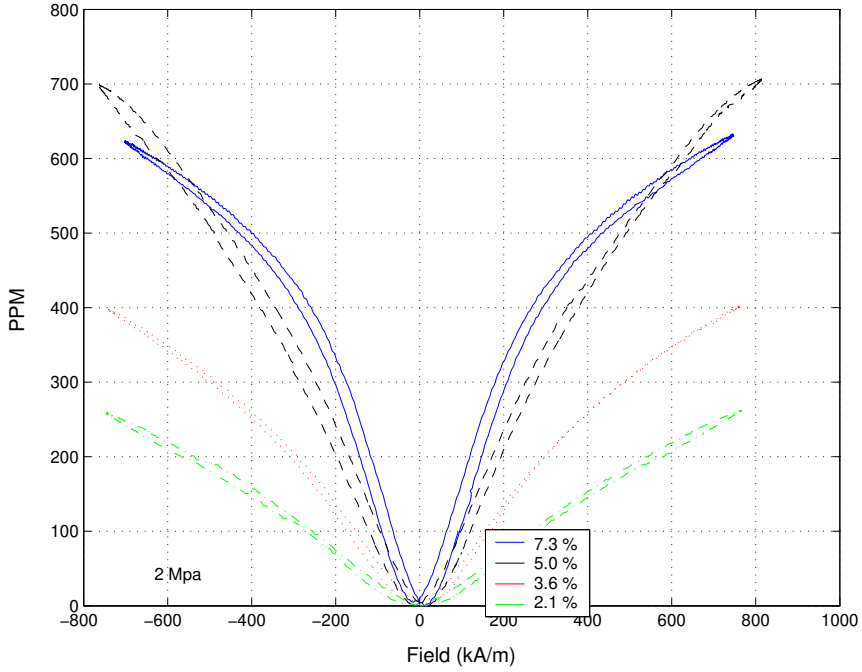

(b)

Figure B.1: Strain versus field for varying volume fraction Terfenol-D epoxy composites magnetically aligned with (a) no load (b) 2 MPa compression.

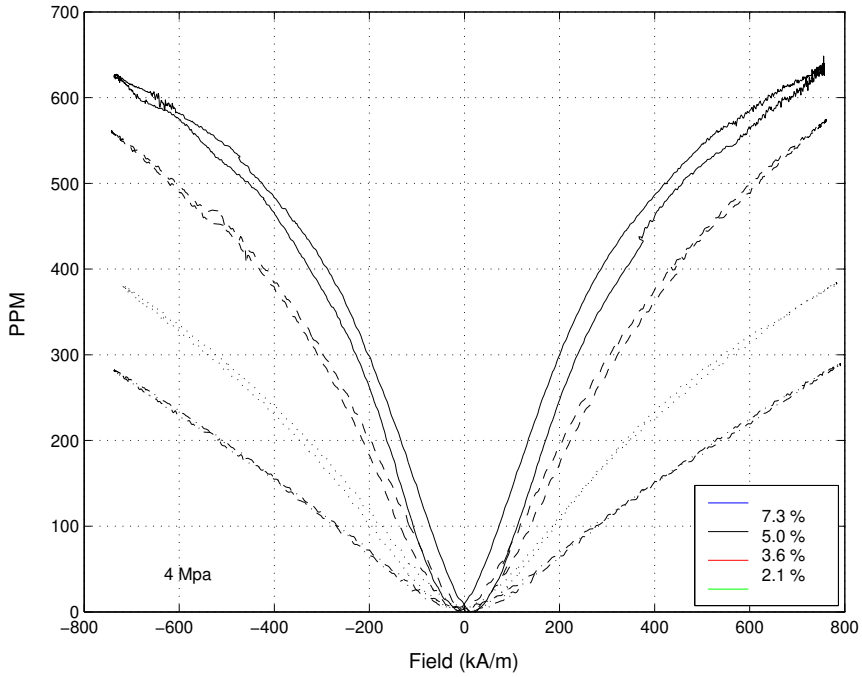

(a)

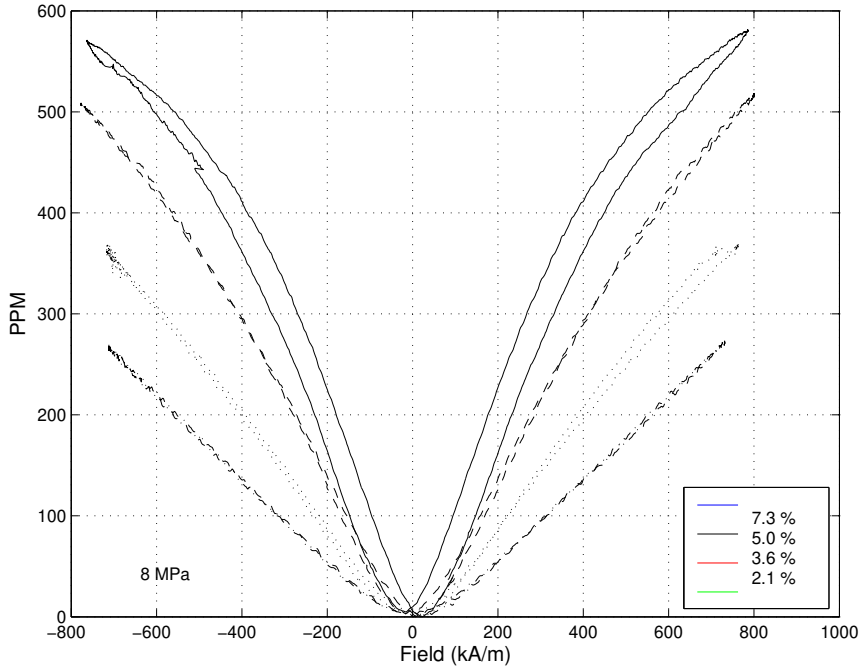

(b)

Figure B.2: Strain versus field for varying volume fraction Terfenol-D epoxy composites magnetically aligned with (a) 4 MPa (b) 8 MPa compression.

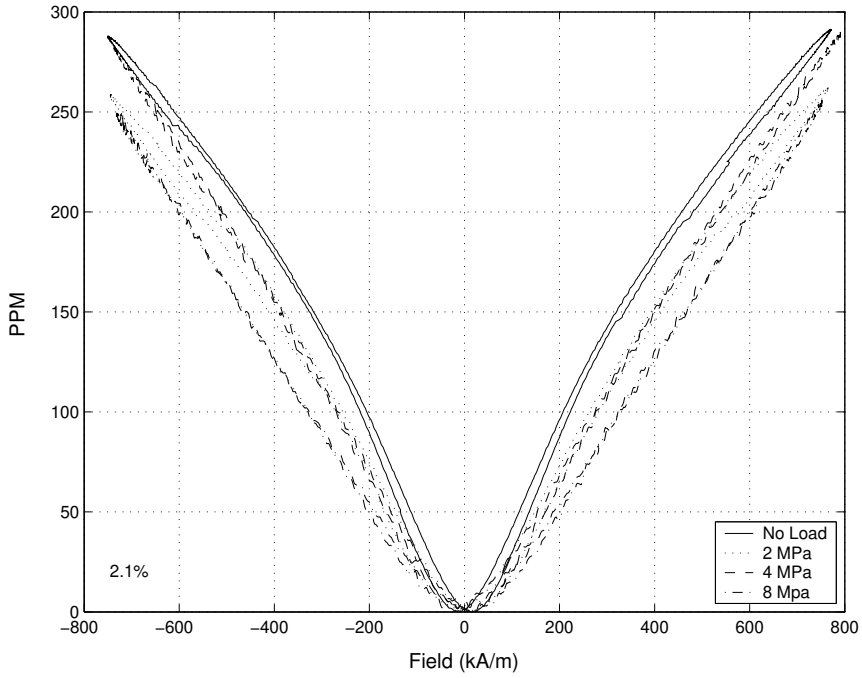

(a)

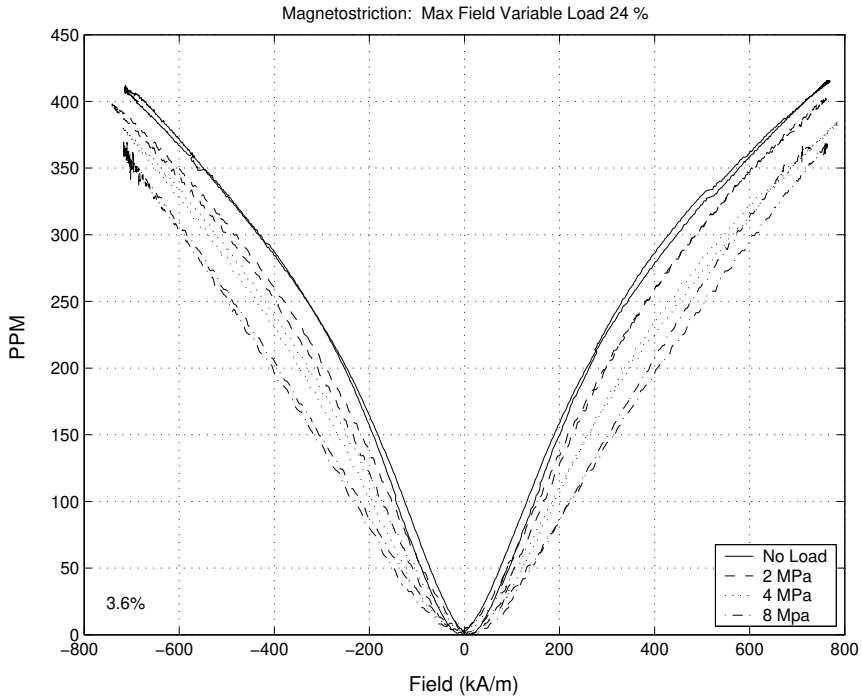

(b)

Figure B.3: Varying load for Terfenol-D epoxy composites of (a) 2.1% and (b) 3.6% volume fraction.

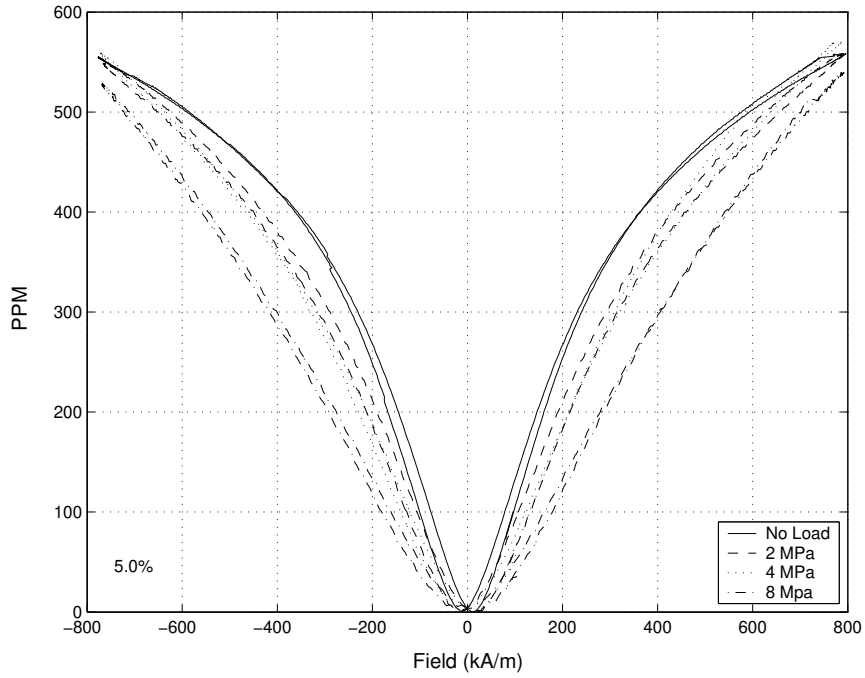

(a)

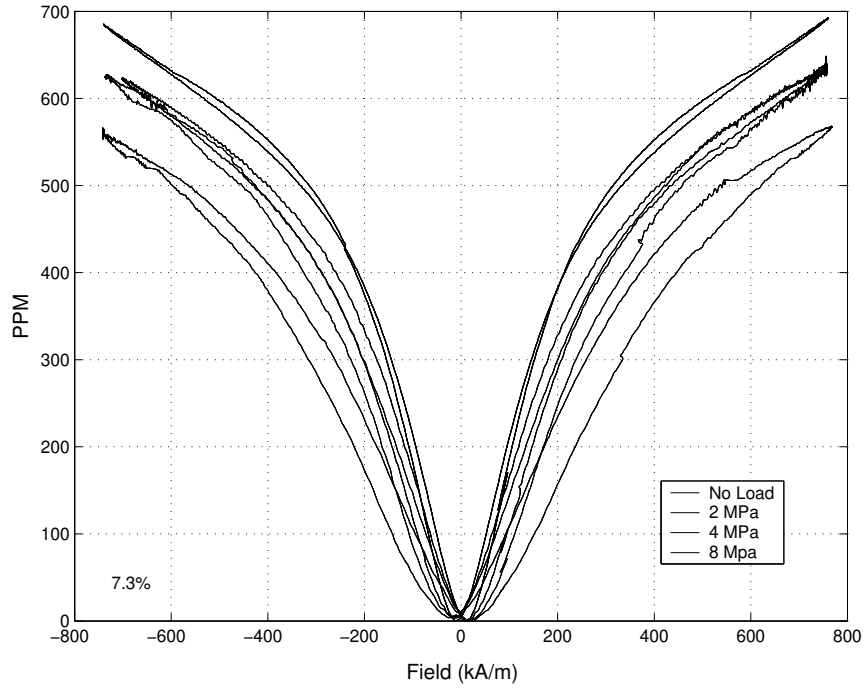

(b)

Figure B.4: Varying load for Terfenol-D epoxy composites of (a) 5.0% and (b) 7.3% volume fraction.

APPENDIX C

PART DRAWINGS

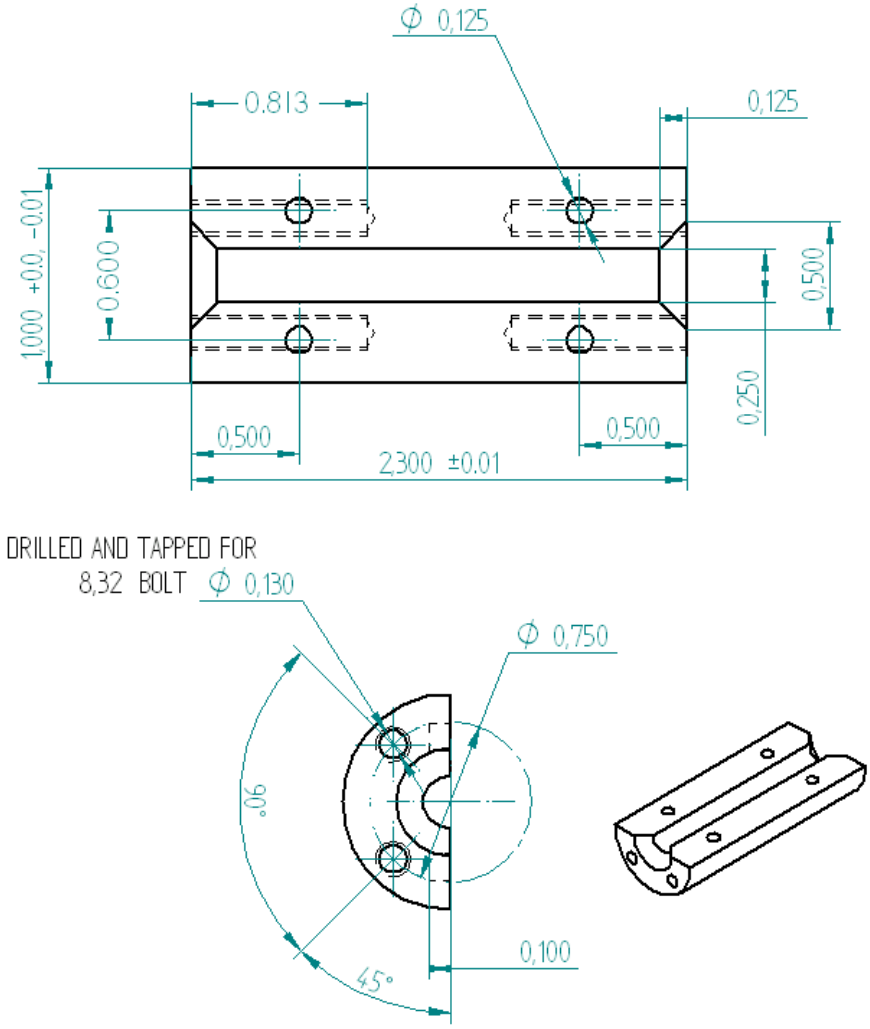

Figure C.1: Aluminum mold half

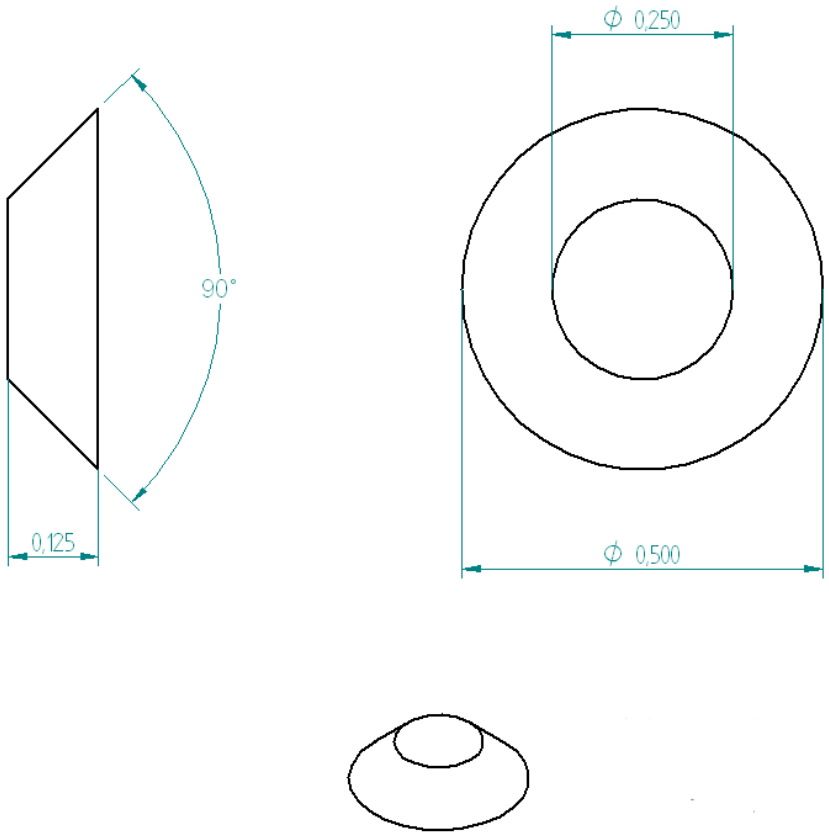

Figure C.2: Steel angled end cap

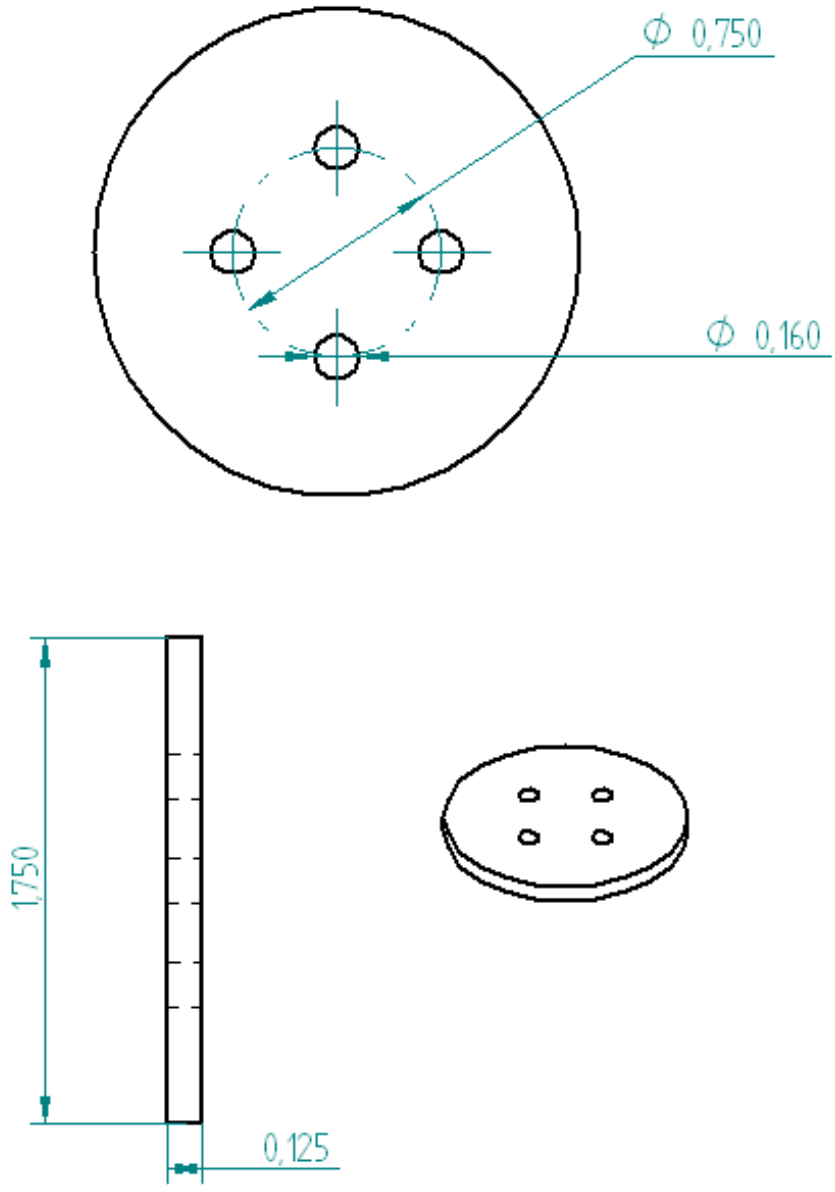

Figure C.3: Aluminum end plate

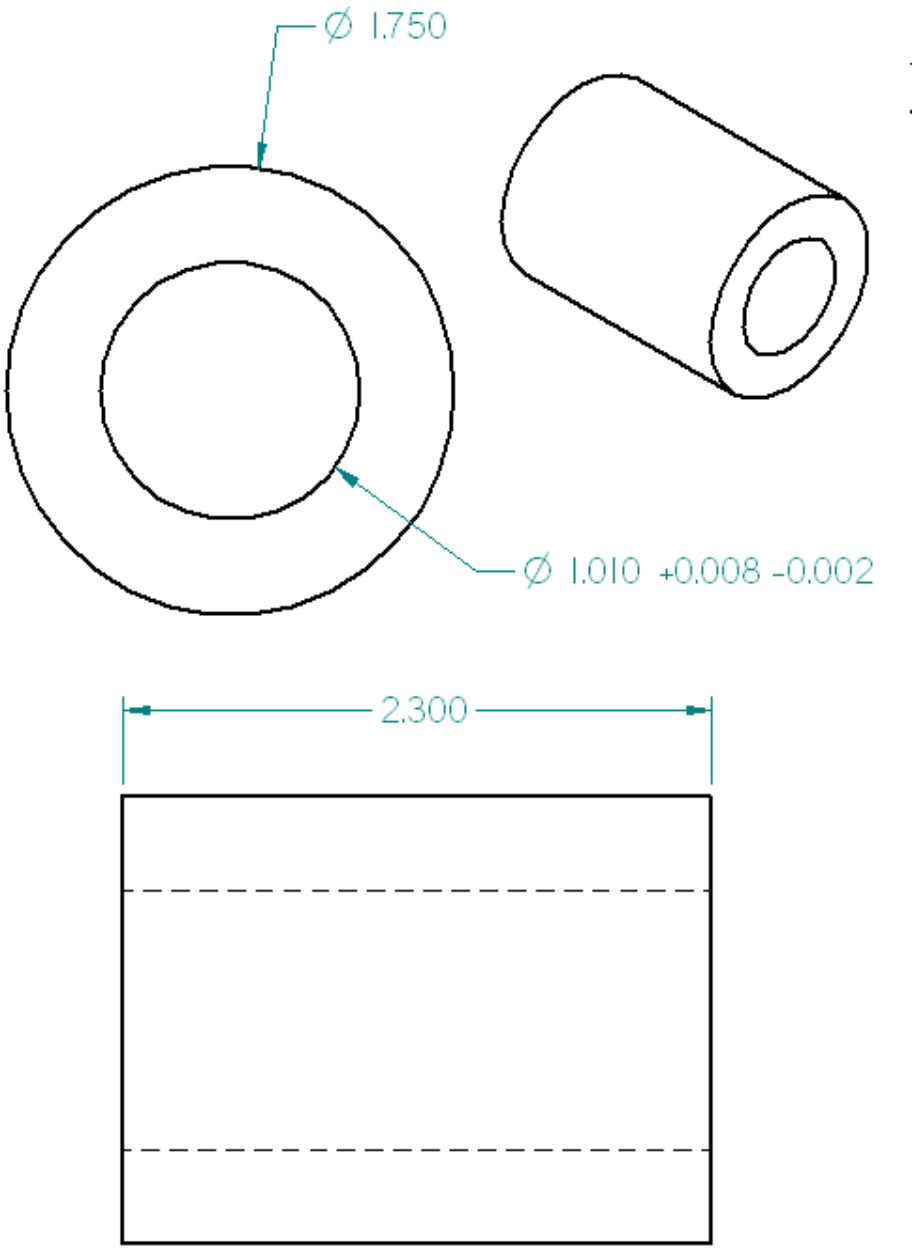

Figure C.4: Permanent magnet

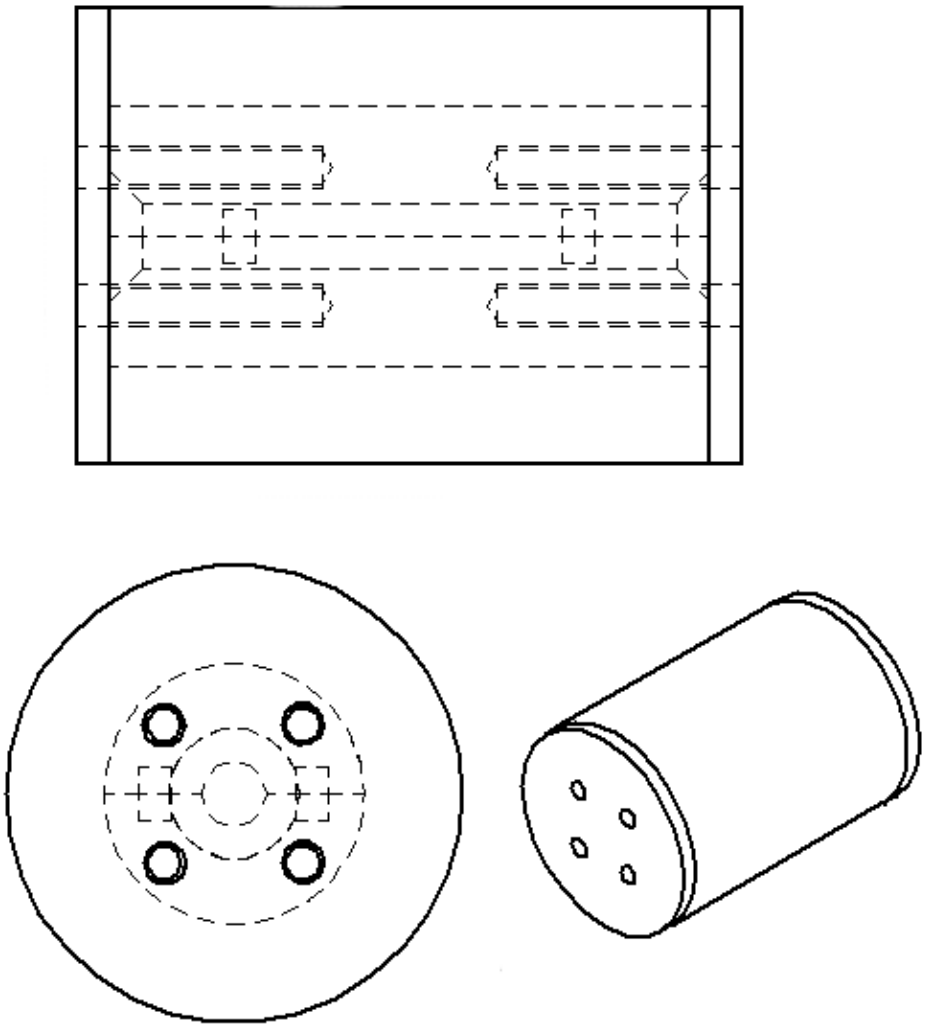

Figure C.5: Assembled magnetic mold

APPENDIX D

FEMM MOLD ANALYSIS

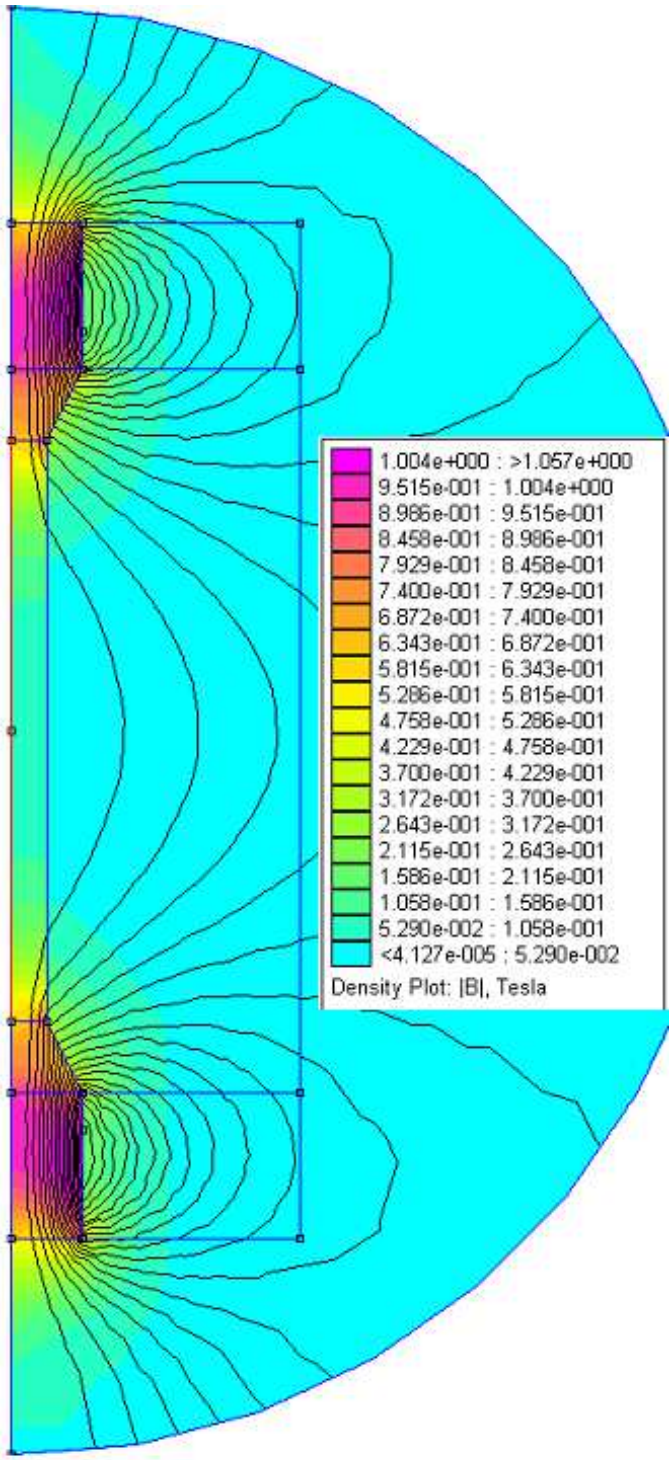

Figure D.1: Finite element analysis of induction for strong end magnet mold design

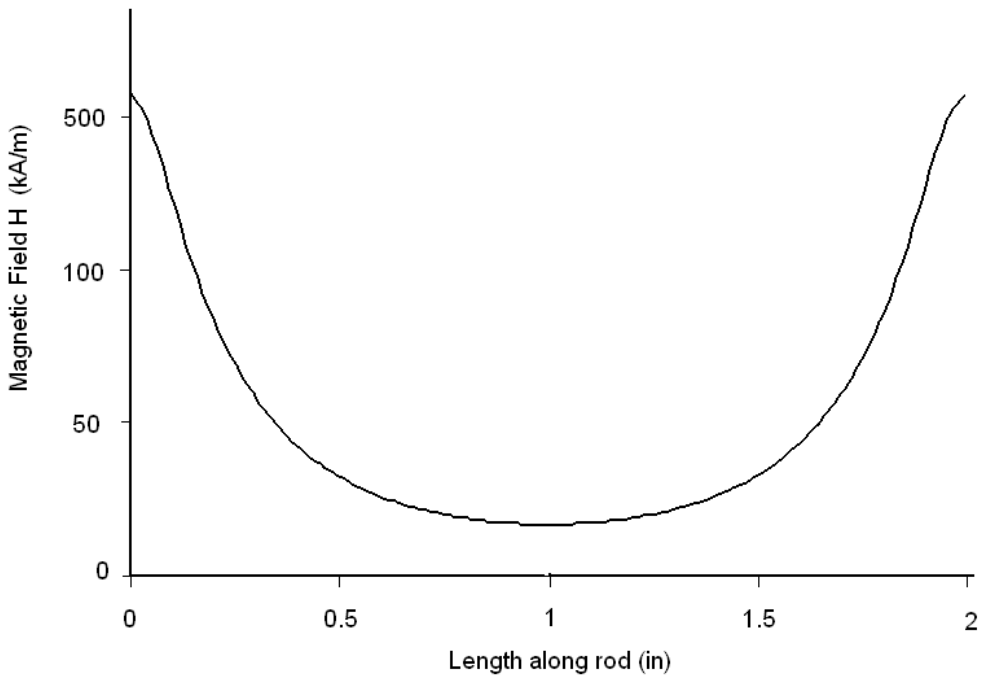

Figure D.2: Magnetic field distribution across composite rod for end magnet mold design

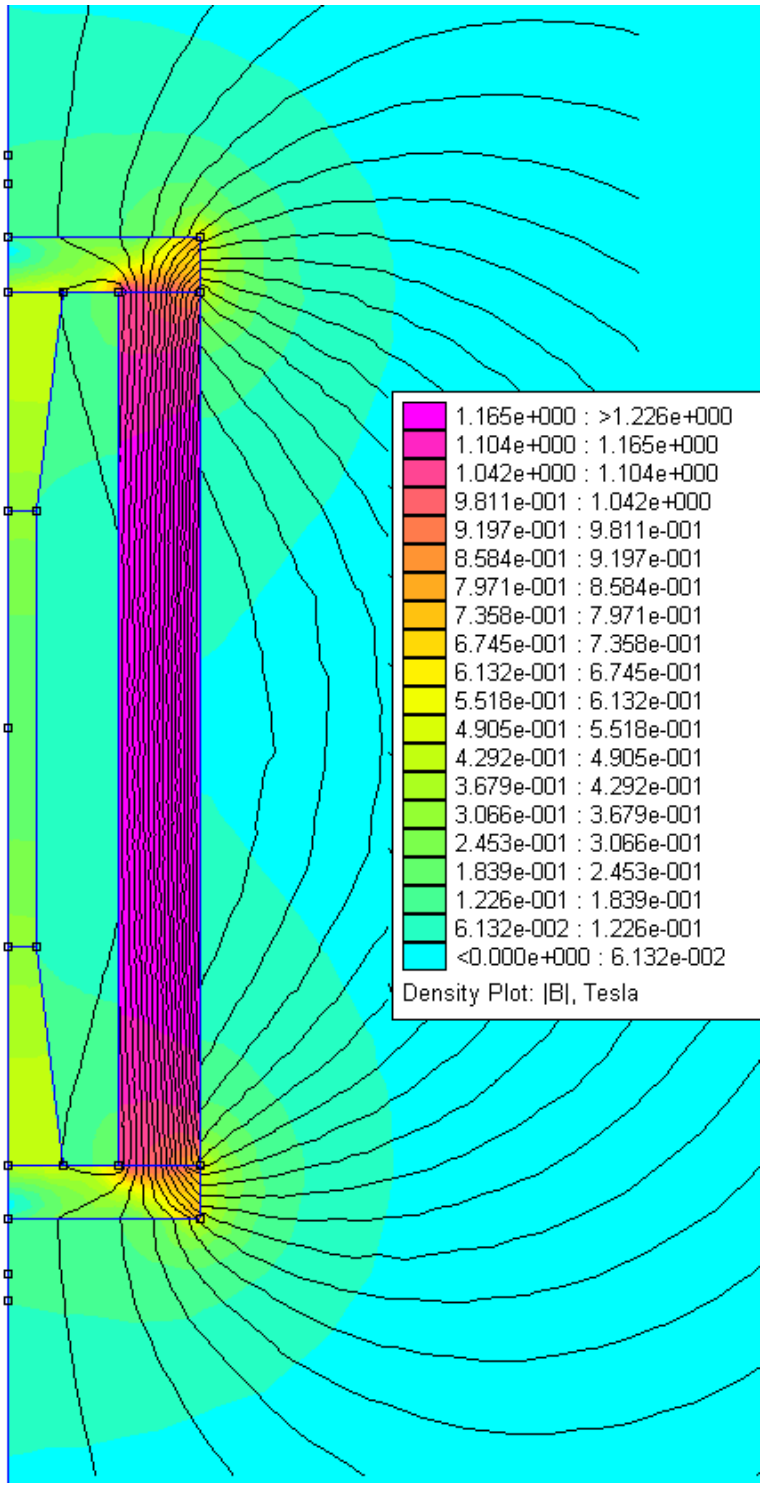

Figure D.3: Finite element analysis of induction for long cylindrical magnet mold design

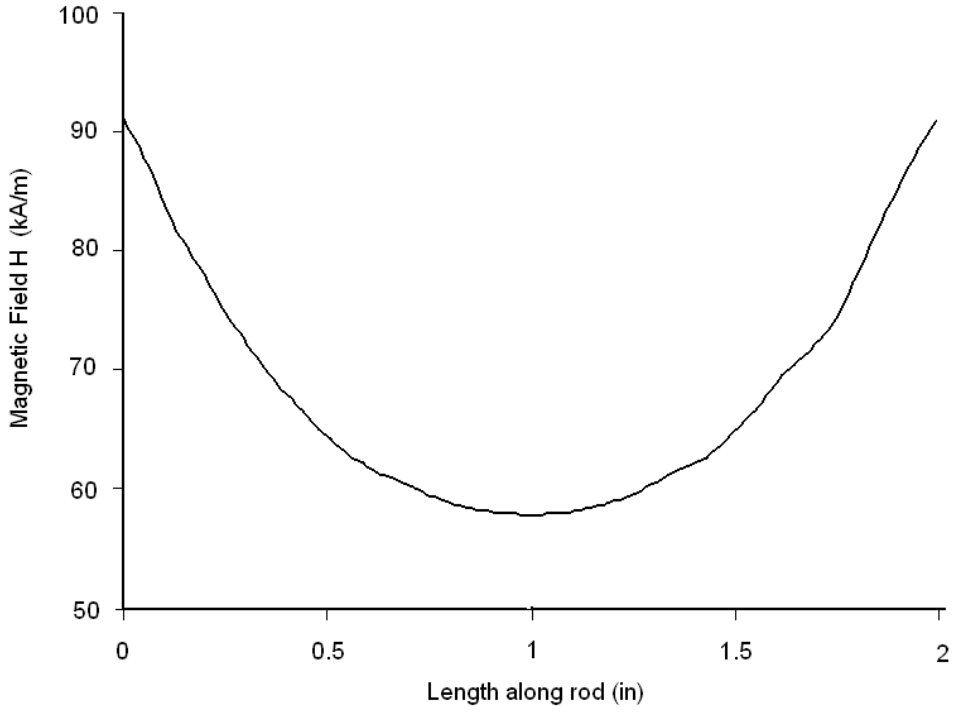

Figure D.4: Magnetic field distribution across composite rod for long cylindrical magnet mold design

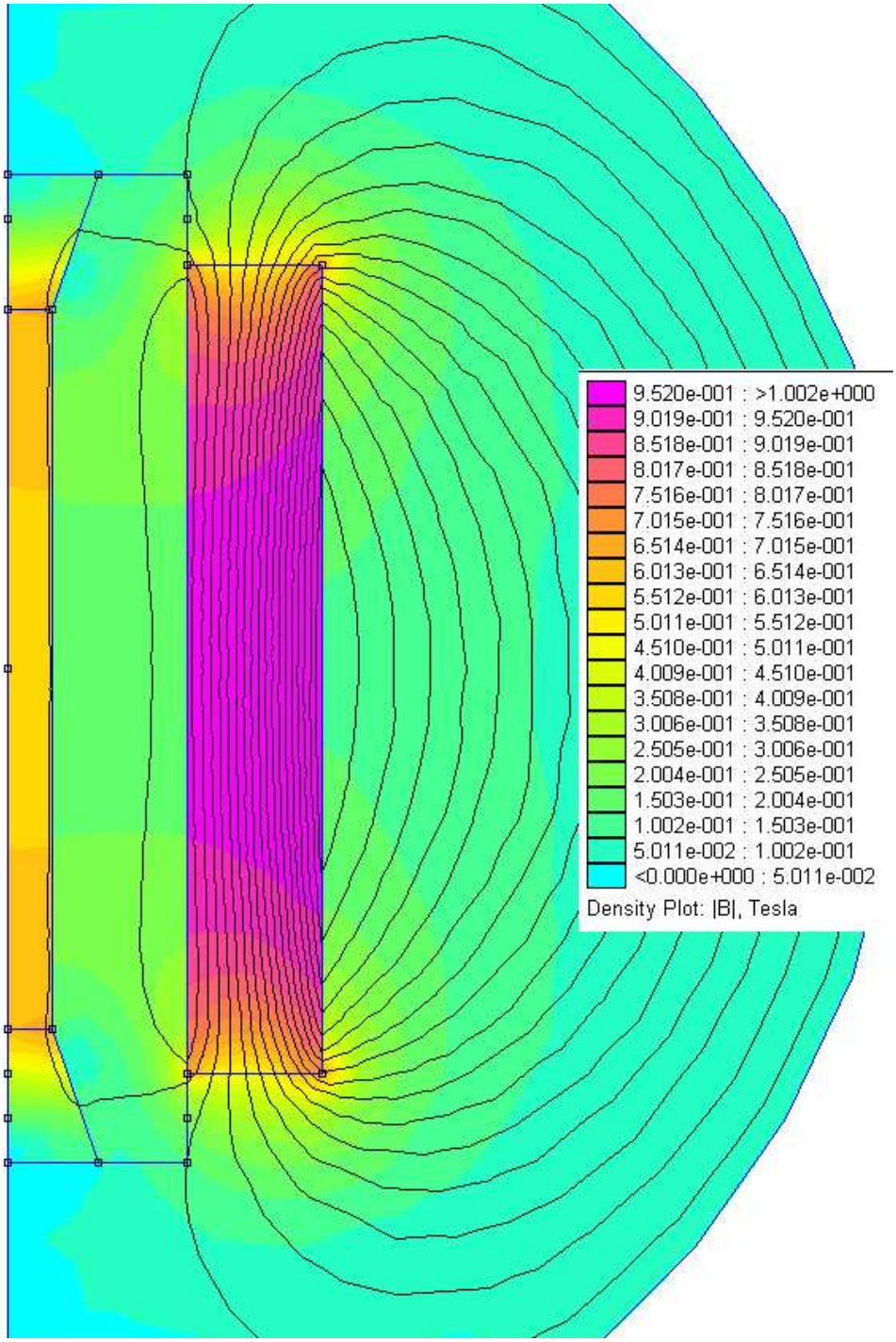

Figure D.5: Finite element analysis of induction for short cylindrical magnet mold design

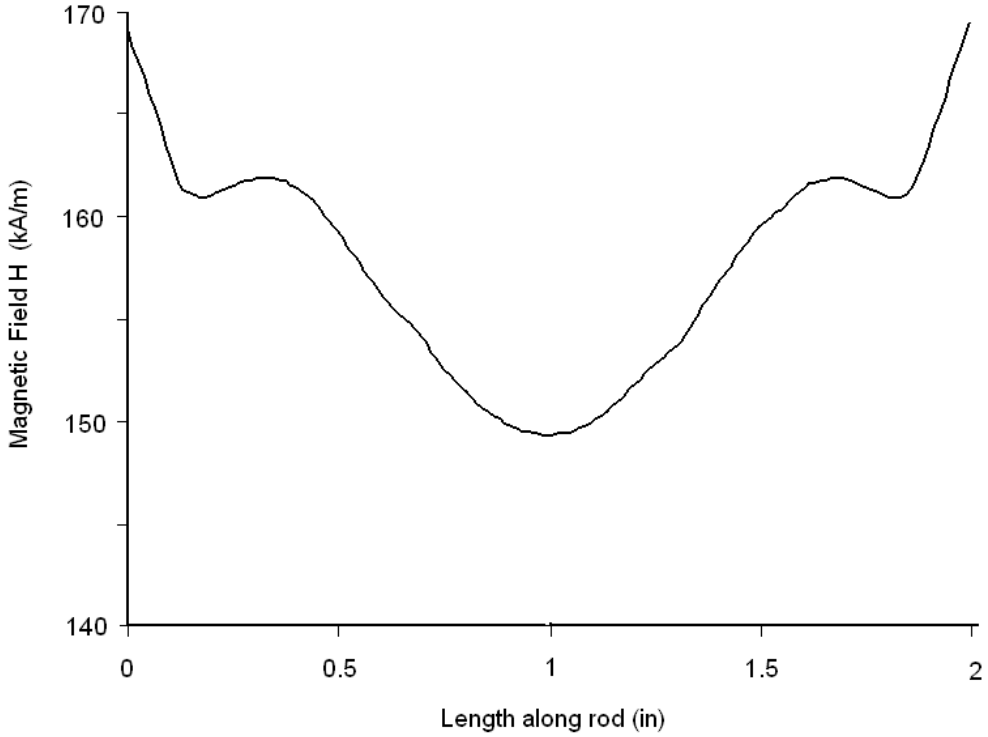

Figure D.6: Magnetic field distribution across composite rod for short cylindrical magnet mold design

BIBLIOGRAPHY

[1] W.D. Armstrong. "Nonlinear behavior of magnetostrictive particle actuated composite materials". *Journal of Applied Physics*, 87, no.6:3027–3031, 2000.

[2] N. Kurdiyeh Z.J. Guo B.W. Wang Busbridge, S.C. and A.R. Piercy. "Effect of elastic moduli of the matrix on the coupling of magnetostrictive composites". *IEEE Transactions on Magnetics*, 36, no.5:3235–3237, 2000.

[3] Butler A.C. Butler, J.L. and A.E. Clark. "Unidirectional magnetostrictive/piezoelectric hybrid transducer". *Journal of the Acoustical Society of America*, 88(1):7–11, 1990.

[4] J.L. Butler and A.E. Clark. "Hybrid piezoelectric and magnetostrictive acoustic wave transducer". In *US Patent No. 4,443,731*, 1984.

[5] Lindberg J.F. Butler, S.C. and F.T. Clark. "Hybrid magnetostrictive/piezoelectric Tonpilz transducer". *Ferroelectrics*, 187(1-4):163–174, 1996.

[6] S.C. Butler. "A broadband hybrid magnetostrictive/piezoelectric Tonpilz transducer". In *Undersea Defense Technology Conference"*, UDT Pacific 98, Sydney, Australia, 1998.

[7] S.C. Butler and F.A. Tito. "A broadband hybrid magnetostricitive/piezoelectric transducer array". In *2000 Proceedings of OCEANS MTS/IEEE*, volume 3 of *Proc. OCEANS MTS/IEEE*, pages 1469–1475, 2000.

[8] Frederick T. Calkins. *Design, analysis, and modeling of giant magnetostrictive transducers*. PhD thesis, Iowa State Univeristy, Ames, IA, 2003.

[9] Tord Cedell. *"Magnetostrictive materials and selected applications"*. Department of Production and Materials Engineering, Lund,Sweeden, 1995.

[10] Snyder J.E. Schwichtenberg C.R. Dennis K.W. Falzgraf D.K. McCallum R.W. Chen, Y. and D.C. Jiles. "Effect of elastic modulus of the matrix on magnetostrictive strain in composites". *Applied Physics Letters*, 74, no.8:1159–1156, 1999.

[11] Dapino M.J. Downey, P.R. "Extended frequency bandwidth and electrical resonance tuning in hybrid Terfenol-D/PMN-PT transducers in series". *Journal of Intelligent Material Systems and Structures*, in review.

[12] Patrick R. Downey. Hybrid pmn-pt/Terfenol-D broadband trnaducers in mechanical series configuration. Master's thesis, The Ohio State University, Columbus, OH, 2003.

[13] T.A. Duenas and G.P. Carman. "Experimental results for magnetostrictive composites. In *ASME International Mechanical Engineering Congress and Exposition*", Adaptive Structures and Material Systems, pages 63–71, 1998.

[14] T.A. Duenas and G.P. Carman. "Large magnetostrictive response of terfenol-d resin composites". *Journal of Applied Physics*, 87:4696–4701, 2000.

[15] T.A. Duenas and G.P. Carman. "Particle distribution study for low-volume fraction magnetostrictive composites". *Journal of Applied Physics*, 90:2433–2439, 2001.

[16] David Hall. *Dynamics and vibrations of magnetostrictice transduers*. PhD thesis, Iowa State University, Ames, IA, 1994.

[17] Busbridge S.C. Piercy A.R. Hudson, J. "Magnetomechanical coupling and elastic moduli of polymer-bonded Terfenol-D composites". *Journal of Applied Physics*, 83, no.11:7255–7257, 1998.

[18] F.V. Hunt. "Electroacoustics: the analysis of transduction, and its historical background". *American Institute of Physics for the Acoustical Society of America*, 1982.

[19] David Jiles. *"Introduction to Magnetism and Magnetic Materials"*. Chapman and Hall, New York, 1995.

[20] Lars Kvarnsjo. *"On characterization, modeling, and application of highly magnetostrictive materials"*. Royal Institute of Technology, Stockholm,Sweeden, 1993.

[21] J.S. Abell L. Ruiz de Angulo and I.R. Harris. "Magnetostrictive properties of polymer bonded Terfenol-D". *Journal of Magnetism and Magnetic Materials*, pages 157–158, 1996.

[22] T. Cedell A.E. Clark J.B. Restorff L. Sandlund, M. Fahlander and M. Wun-Fogle. "Magnetostriction, elastic moduli, and coupling factors of composite Terfenol-D". *Journal of Applied Physics*, 75:5656–5658, 1994.

[23] Aayush Malla. Effect of composition on the magnetic and elastic properties of shape memory Ni-Mn-Ga. Master's thesis, The Ohio State University, Columbus, OH, 2003.

[24] Geoffrey P. McKnight. *[112] Oriented Terfenol-D composites*. PhD thesis, University of California Los Angeles, CA, 2003.

[25] G.P. McKnight and G.P. Carman. "Energy absorption and damping in magnetostrictive composites". In *Materials Research Society Proceedings*, volume 604 of *Adaptive Structures and Material Systems*, pages 267–272, 2000.

[26] G.P. McKnight and G.P. Carman. "Large magnetostriction in Terfenol-D particulate composites with preferred [112] orientation". In *SPIE Smart Structures and Materials 2001*, volume 4333 of *Active Materials: Behavior and Mechanics*, pages 178–183, 2001.

[27] A.B. Flatau M.J. Dapino and F.T. Calkins. "Statistical anaysis of Terfenol-D material properties". *Journal of Intelligent Material Systems and Structures*, in review.

[28] M.J. Dapino P.R. Downey and R.C. Smith. "Analysis of hybrid PMN/Terfenol-D broadband transducers in mecahnical series configuration". In *Proceedings of SPIE Smart Structures and Materials*, volume 5049 of *Proc. SPIE*, pages 168–179, 2003.

[29] G.P. Carman S.W. Or, N. Nersessian. "Effect of combined magnetic bias and drive fields on dynamic magnetomechanical properties of Terfenol-D/epoxy 1-3 composites". *Journal of Magnetism and Magnetic Materials*, 262:L181–L185, 2003.

[30] L. Hsu T.A. Duenas and G.P. Carman. "Magnetostrictive composite material systems analytical/experimental". In *MRS Proceedings: Advances in Smart Materials*, Fundamentals and Applications, 1996.